Ground-Water Flow in the Surficial Aquifer System and Potential Movement of Contaminants from Selected Waste-Disposal Sites at Naval Station Mayport, Florida

By Keith J. Halford

U.S. GEOLOGICAL SURVEY

Water-Resources Investigations Report 97-4262

Prepared in cooperation with the

Southern Division,
Naval Facilities Engineering Command,
U.S. Navy

Tallahassee, Florida
1998

U.S. DEPARTMENT OF THE INTERIOR
BRUCE BABBITT, Secretary

U.S. GEOLOGICAL SURVEY
Thomas J. Casadevall, Acting Director

For additional information write to:

District Chief
U.S. Geological Survey, WRD
Suite 3015
227 North Bronough Street
Tallahassee, FL 32301

Copies of this report can be purchased from:

U.S. Geological Survey
Branch of Information Services
Box 25286
Federal Center
Denver, CO 80225

CONTENTS

FIGURES

TABLES

VERTICAL DATUM AND TRANSMISSIVITY

Sea level: In this report, "sea level" refers to the National Geodetic Vertical Datum of 1929 (NGVD of 1929)—a geodetic datum derived from a general adjustment of the first-order level nets of both the United States and Canada, formerly called Sea Level Datum of 1929.

Transmissivity: The standard unit for transmissivity is cubic foot per day per square foot times foot of aquifer thickness [$(ft^3/d)/ft^2$]ft. In this report, the mathematically reduced form, foot squared per day (ft^2/d), is used for convenience.

Ground-Water Flow in the Surficial Aquifer System and Potential Movement of Contaminants from Selected Waste-Disposal Sites at Naval Station Mayport, Florida

By Keith J. Halford

Abstract

Ground-water flow through the surficial aquifer system at Naval Station Mayport near Jacksonville, Florida, was simulated with a two-layer finite-difference model as part of an investigation conducted by the U.S. Geological Survey. The model was calibrated to 229 water-level measurements from 181 wells during three synoptic surveys (July 17, 1995; July 31, 1996; and October 24, 1996). A quantifiable understanding of ground-water flow through the surficial aquifer was needed to evaluate remedial-action alternatives under consideration by the Naval Station Mayport to control the possible movement of contaminants from sites on the station.

Multi-well aquifer tests, single-well tests, and slug tests were conducted to estimate the hydraulic properties of the surficial aquifer system, which was divided into three geohydrologic units—an S-zone and an I-zone separated by a marsh-muck confining unit. The recharge rate was estimated to range from 4 to 15 inches per year (95 percent confidence limits), based on a chloride-ratio method. Most of the simulations following model calibration were based on a recharge rate of 8 inches per year to unirrigated pervious areas.

The advective displacement of saline pore water during the last 200 years was simulated using a particle-tracking routine, MODPATH, applied to calibrated steady-state and transient models of the Mayport peninsula. The surficial aquifer system at Naval Station Mayport has been modified greatly by natural and anthropogenic forces so that the freshwater flow system is expanding and saltwater is being flushed from the system. A new MODFLOW package (VAR1) was written to simulate the temporal variation of hydraulic properties caused by construction activities at Naval Station Mayport. The transiently simulated saltwater distribution after 200 years of displacement described the chloride distribution in the I-zone (determined from measurements made during 1993 and 1996) better than the steady-state simulation.

The advective movement of contaminants from selected sites within the solid waste management units to discharge points was simulated using MODPATH. Most of the particles were discharged to the nearest surface-water feature after traveling less than 1,000 feet in the ground-water system. Most areas within 1,000 feet of a surface-water feature or storm sewer had traveltimes of less than 50 years, based on an effective porosity of 40 percent.

Contributing areas, traveltimes, and pathlines were identified for 224 wells at Naval Station Mayport under steady-state and transient conditions by back-tracking a particle from the midpoint of the wetted screen of each well. Traveltimes to contributing areas that ranged between 15 and 50 years, estimated by the steady-state model, differed most from the transient traveltime estimates. Estimates of traveltimes and pathlines based on steady-state model results typically were 10 to 20 years more and about twice as long as corresponding estimates from the transient model.

The models differed because the steady-state model simulated 1996 conditions when Naval Station Mayport had more impervious surfaces than at any earlier time. The expansion of the impervious surfaces increased the average distance between contributing areas and observation wells.

INTRODUCTION

Inorganic and organic priority contaminants defined by the U.S. Environmental Protection Agency (USEPA, 1988) have been detected in surface water, sediment, and ground-water samples collected near abandoned waste-disposal sites at Naval Station (NAVSTA) Mayport. Concern exists that such contaminants may move with the underlying ground water into the base drainage, St. Johns River, and surrounding salt marshes. As part of the Installation Restoration Program, NAVSTA Mayport is considering remedial-action alternatives to control the movement of contaminants from those sites that may otherwise discharge to the surface. This effort requires a quantifiable understanding of the response of ground-water flow to current conditions and to any future stresses imposed on the surficial aquifer system. Numerical simulation provides the most tractable way of achieving this level of understanding.

NAVSTA Mayport, located in northeast Duval County, Florida (fig. 1), provides all necessary support services for the surface fleet and aircraft stationed at or visiting Mayport. Industrial operations conducted at NAVSTA Mayport involve intermediate level maintenance for both ships and aircraft, and vehicle maintenance and repair. Any maintenance activities that can be conducted without putting a ship into dry-dock are considered intermediate (U.S. Department of the Navy, 1995). Wastes generated and disposed of at the station include waste oils, fuels, lubricants, solvents, paints, and general refuse associated with ship, aircraft, vehicle, and building maintenance activities (U.S. Department of the Navy, 1995). From 1942 to 1979, all wastes were disposed of in landfills on the station or wastes were burned at the site to reduce their volume. From 1979 to 1994, all burnable wastes were incinerated in a carbonaceous fuel boiler. From 1979 to 1985, the residual ash from the boiler, along with unburned debris, construction rubble, and large scrap materials were placed in onsite landfills (U.S. Department of the Navy, 1995).

The dissolved and degraded constituents of fuels, lubricants, and solvents (benzene, dichlorobenzene, toluene, acetone, napthalene, and trichloroethene) are the primary contaminants that may be transported by ground water at NAVSTA Mayport. The movement of these dissolved constituents is similar to the advective flow of the ground water, as the solubility of these contaminants is usually low and the concentrations are not great enough to significantly alter the density of the ground water. These dissolved constituents sorb to the porous media of aquifers and confining units, which retards the rate of travel, but does not alter the direction of travel.

Purpose and Scope

The purpose of this report is to present the results of a study to analyze and quantify ground-water flow in the surficial aquifer system at NAVSTA Mayport (fig. 1) and describe the advective potential for the movement of ground-water contaminants. This report includes ground-water-level data, a description of the geohydrologic framework, an estimate of the water budget, and an estimate of the ground-water discharge to surface-water features. Model simulations were used to evaluate the hydrologic feasibility of several alternative approaches to site remediation. Simulation results are based on a calibrated, three-dimensional finite-difference, ground-water flow model of the NAVSTA Mayport area. A transient model was developed to simulate the expansion of the freshwater aquifer beneath the Mayport peninsula over the last 200 years. Estimates of ground-water movement from existing and potential sites of contamination to their discharge points were determined using particle tracking (Pollock, 1994). The contributing areas for 224 observation wells were identified by back-tracking particles from the wetted well screens. Results of cross-sectional model simulations are presented to support the locations of lateral model boundaries and the application of a uniform-density based analysis to the solution of a variable-density flow problem.

Description of the Study Area

The study area is in northeastern Duval County at the mouth of the St. Johns River (fig. 1). Soils in the 3.5 square miles (mi^2) of non-marsh areas are fine sands with occurrences of shell or rock fragments (Stem and others, 1978). Most of the non-marsh areas

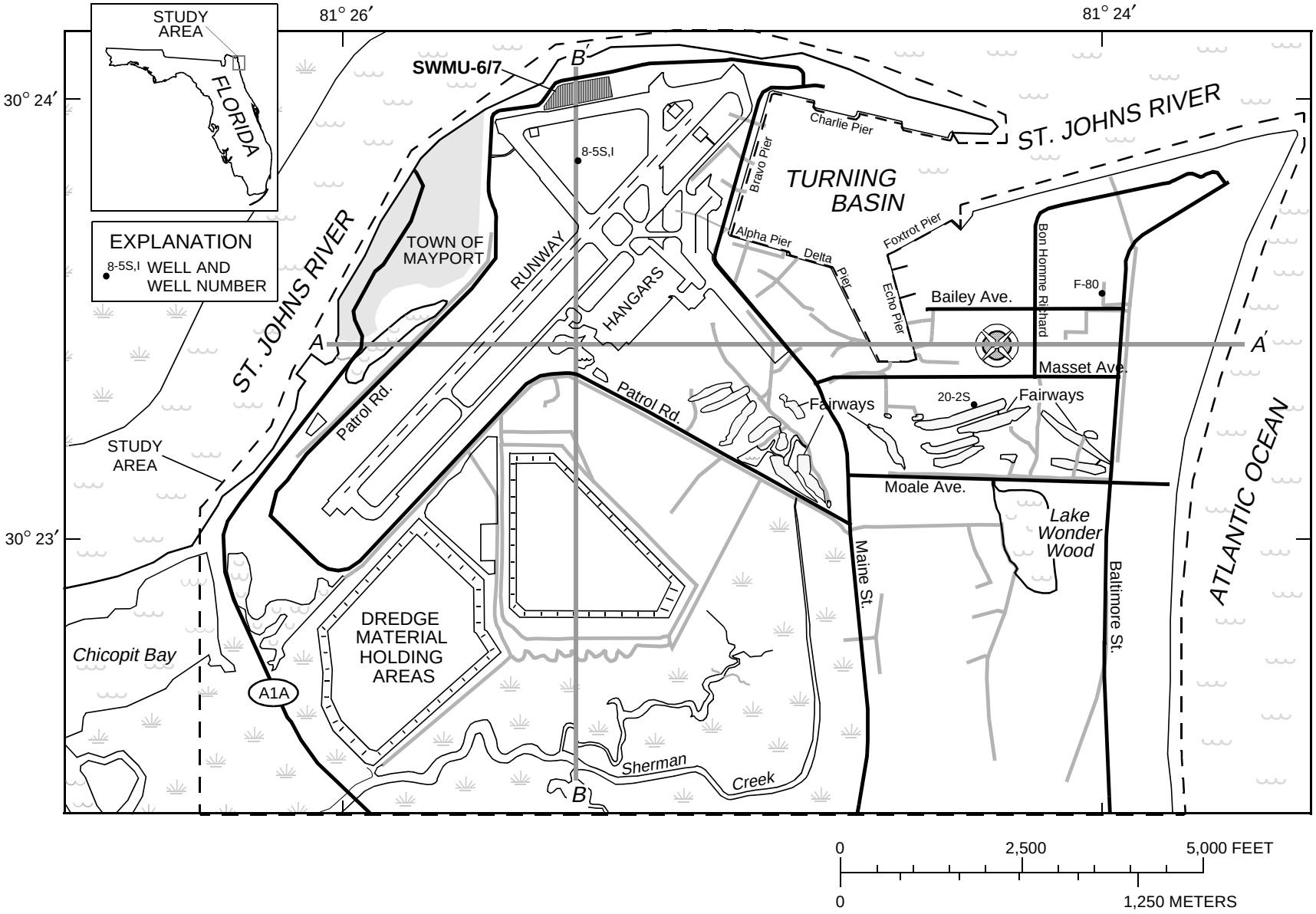

Figure 1. Map showing location of the study area, runways, dredge material holding areas, golf fairways and greens, SWMU-6/7, F-80 aquifer test and selected well sites, and traces of hydrogeologic sections shown in figure 9.

are covered with deposits of dredge material except for the town of Mayport, the area between Alpha-Delta piers and Maine St., and the southeastern part of the study area (fig. 1). Topographic relief is minimal and land-surface slopes generally are 0 to 5 percent (Stem and others, 1978). The soils are typically well drained and require supplemental irrigation to grow lawn grasses and ornamental plants (Stem and others, 1978).

The climate of Duval County is humid and subtropical. Average precipitation over the study area is about 52 inches per year (in/yr) with more than half falling from June to September (Owenby and Ezell, 1992). The yearly potential evaporation rate from the study area has been estimated to be 48 inches (in.) (Farnsworth and others, 1982, map 3). The average yearly temperature is 79 °F (Owenby and Ezell, 1992).

The geology and hydrology of the study area have been described in numerous reports as summarized in Spechler (1994), but most reports describe features at a county-wide scale and focus primarily on the Upper Floridan aquifer. Causey and Phelps (1978) described the extent and availability of water from the shallow-aquifer system in Duval County. The results of an aquifer test in the surficial aquifer system beneath NAVSTA Mayport are reported by Franks (1980). In addition to reporting the hydraulic characteristics, Franks (1980) describes the lithology to a depth of 100 feet (ft) below land surface near site F-80 shown in figure 1.

Acknowledgments

The author extends his appreciation to David Driggers, Southern Division Naval Facilities Engineering Command; Cheryl Mitchell, Staff Civil Engineering NAVSTA Mayport; Frank Lesene, ABB Environmental Services; and Larry Smith, ABB Environmental Services, for assistance provided during this study.

GEOHYDROLOGY

The geologic units of interest in the study area include sediments of Holocene to Miocene age that extend from land surface to the top of the Hawthorn Group about 50 ft below land surface (fig. 2). Previous investigators have defined this sequence as the surficial aquifer system (Spechler, 1994). The surficial aquifer system consists of fine-grained sands near the surface interspersed with thin (less than 1 ft) clay lenses and generally grades to a mixture of sand and coarse shell fragments from 30 to 50 ft below land surface (Franks, 1980). The base of the surficial aquifer system is the intermediate confining unit which, in the vicinity of NAVSTA Mayport, is a sequence of marine clays and discontinuous limestone stringers (Spechler, 1994). Thickness of the confining unit varies but averages about 350 ft.

Because this study is concerned with ground-water movement near land surface, the surficial aquifer system was further subdivided into three local geohydrologic units: the S-zone, the marsh-muck confining unit, and the I-zone (fig. 2). The S-zone consists of fine to medium sand with intermittent shell layers and clay lenses that are less than

Series	Formation	Lithology	Geohydrologic unit		Model layer
			Spechler (1994)	This report	
Holocene to Upper Miocene	Undifferentiated surficial deposits	Discontinuous sand, clay, and shell beds	Surficial aquifer system	S-zone	1
				Marsh-muck confining unit	--
				I-zone	2
Miocene	Hawthorn Group	Clay and interbedded phosphatic sands	Intermediate confining unit		--

Figure 2. Generalized geologic and geohydrologic units beneath NAVSTA Mayport. (Modified from Spechler, 1994.)

1 ft thick. The composition of the marsh-muck confining unit ranges from silty clays to dense, plastic clays and commonly includes a large fraction of organic material. The I-zone generally consists of well sorted sand and coarse shell fragments.

The S-zone consists mostly of dredge material and is more heterogeneous than the other two geohydrologic units. The distribution of clay, silt, sand, and shell deposited by dredging operations is generally more variable than the distribution of these materials by natural accretion. Most of NAVSTA Mayport is covered with at least 5 ft of dredge material. More than 30 ft of material is deposited in the dredge-material holding areas (U.S. Department of the Navy, 1995).

The geohydrologic framework within the study area was defined by mapping the base of the S-zone and the I-zone and the thickness of the marsh-muck confining unit. The depths of the two bases and the thickness of the confining unit were estimated from geologists' logs recorded for the more than 200 wells (fig. 3 and app. A) drilled as part of a remedial investigation (U.S. Department of the Navy, 1995). Control points were of sufficient areal density to permit estimates of the altitudes of the bases and the thickness of the marsh-muck confining unit by interpolation. Altitudes and thicknesses beneath the town of Mayport, in the marsh areas, and south of Lake Wonder Wood were extrapolated (figs. 4-6). The base of the S-zone usually is the contact between the buried saltmarsh areas and dredge material across much of the study area west of Maine St. (fig. 1) and typically is within 5 ft of sea level (fig. 4). The altitude of the base of the I-zone ranges from about 30 ft below sea level along the western edge of the study area to about 60 ft below sea level towards the center of the study area (fig. 5). The saturated thickness of the S-zone was estimated by subtracting the altitude of the base of the S-zone from the altitude of the average water table (fig. 7). The S-zone ranges from less than 5 ft in thickness between the southern Patrol Road and the runway to more than 20 ft in thickness near Lake Wonder Wood. The thickness of the I-zone was estimated by subtracting the altitude of the base of the I-zone and the thickness of the marsh-muck confining unit from the altitude of the base of the S-zone (fig. 8). The I-zone (fig. 8) is thickest between Patrol Road and the eastern dredge material holding area (fig. 1) and is thinnest near Lake Wonder Wood (fig. 1).

The marsh-muck confining unit is a significant geohydrologic feature that greatly retards the vertical movement of ground water where present (fig. 6). This unit is thickest beneath the southwestern runway. The marsh-muck confining unit occurs beneath most of NAVSTA Mayport (fig. 6) except in areas along the St. Johns River between the town of Mayport and Charlie pier, between Alpha-Delta piers and Moale Ave., and along the Atlantic Ocean (fig. 1). In addition to the controls shown, a geologist's log indicated that the marsh-muck confining unit was absent along the Atlantic Ocean about 1,000 ft south of the study area (Brown and others, 1984). The confining unit was assumed to be absent if less than 1 ft of clayey material was reported in the geologist's log (fig. 6).

Compositing the S-zone, the marsh-muck confining unit, and the I-zone thicknesses (figs. 6-8) defines a geohydrologic framework which forms the structure of the ground-water flow system. Flow path directions and rates are influenced by variations in the unit thicknesses and lateral extent of the geohydrologic units. The variations in thickness and altitude of the three geohydrologic units in the surficial aquifer system are shown in section in figure 9.

WATER BUDGET

The rate of ground-water movement and solute transport through the surficial aquifer system is governed largely by aquifer recharge. A water budget details the total amount of water available within the study area and can be used to constrain recharge rates estimated during model calibration. A water budget for the study area can be described by the following equation:

$$P + I + D - Q - ET = \Delta S \cong 0 , \qquad (1)$$

where

- P is precipitation, in inches per year;
- I is irrigation, in inches per year;
- D is deep leakage from the Upper Floridan aquifer to the surficial aquifer system, in inches per year;
- Q is stream discharge, in inches per year, which is composed of
  - Q_S surface runoff, in inches per year, and;
  - Q_B base flow, in inches per year;
- ET is evapotranspiration, in inches per year, and;
- ΔS is change in storage, in inches per year, and is assumed to be negligible over the long term.

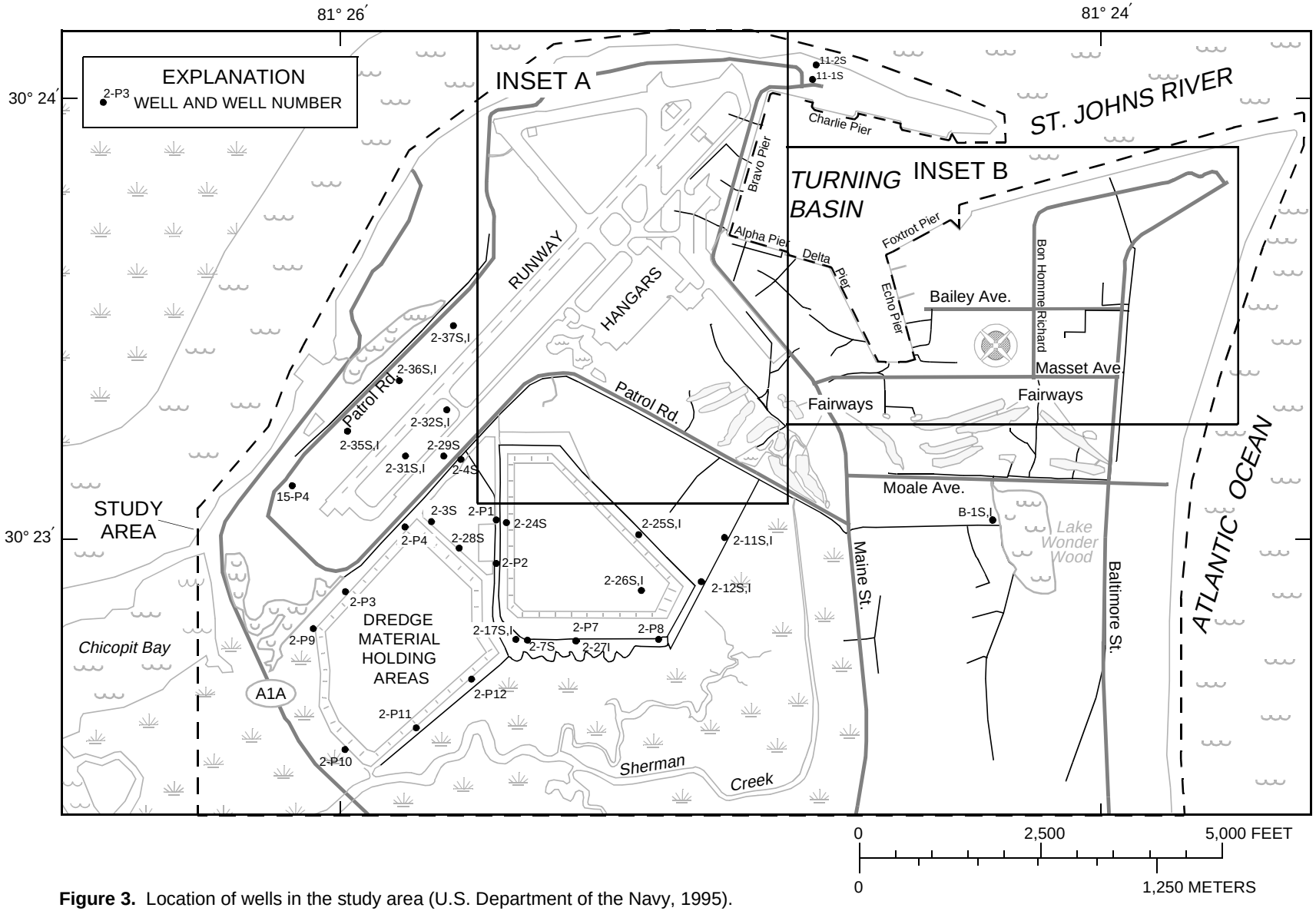

Figure 3. Location of wells in the study area (U.S. Department of the Navy, 1995).

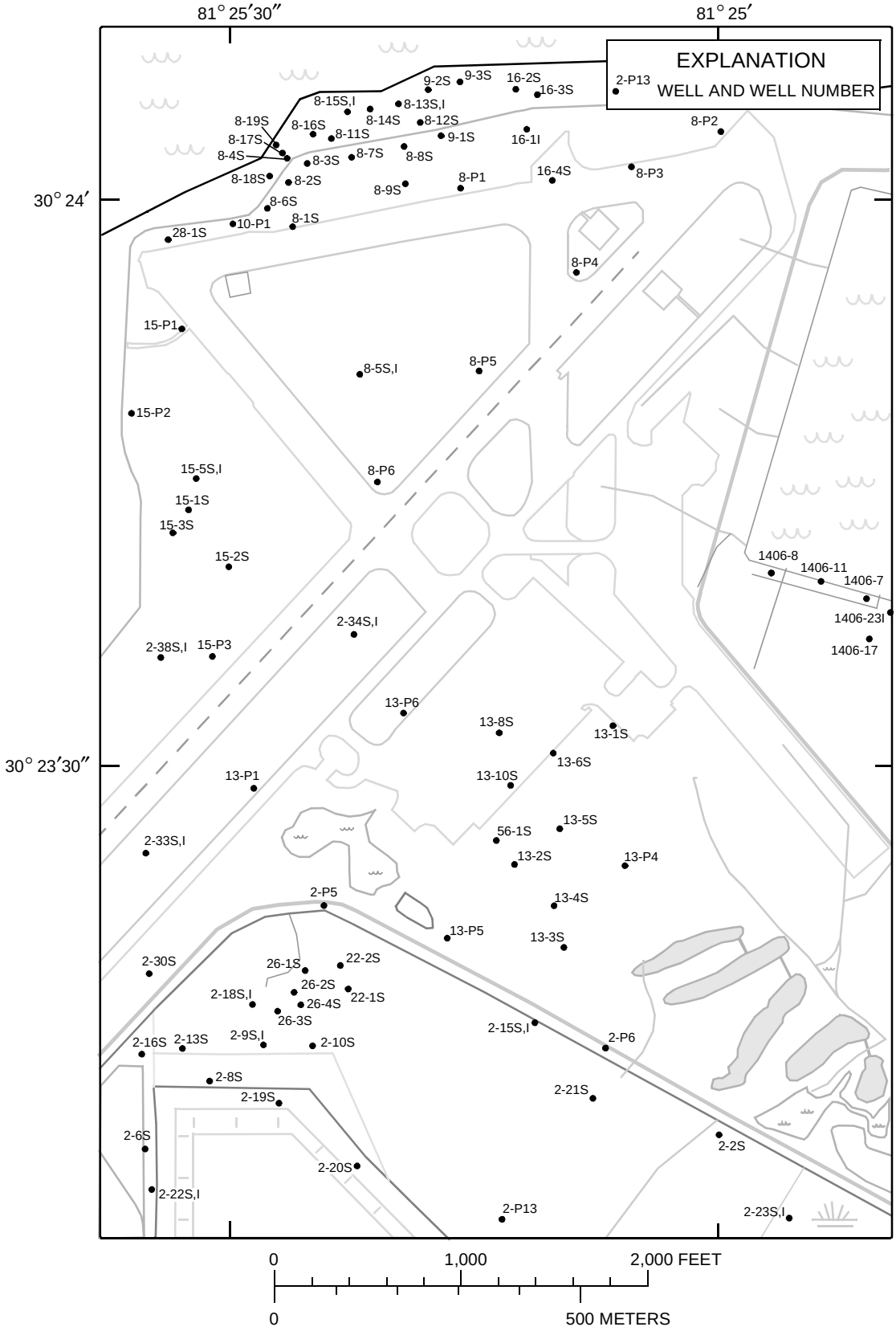

Figure 3. Inset A

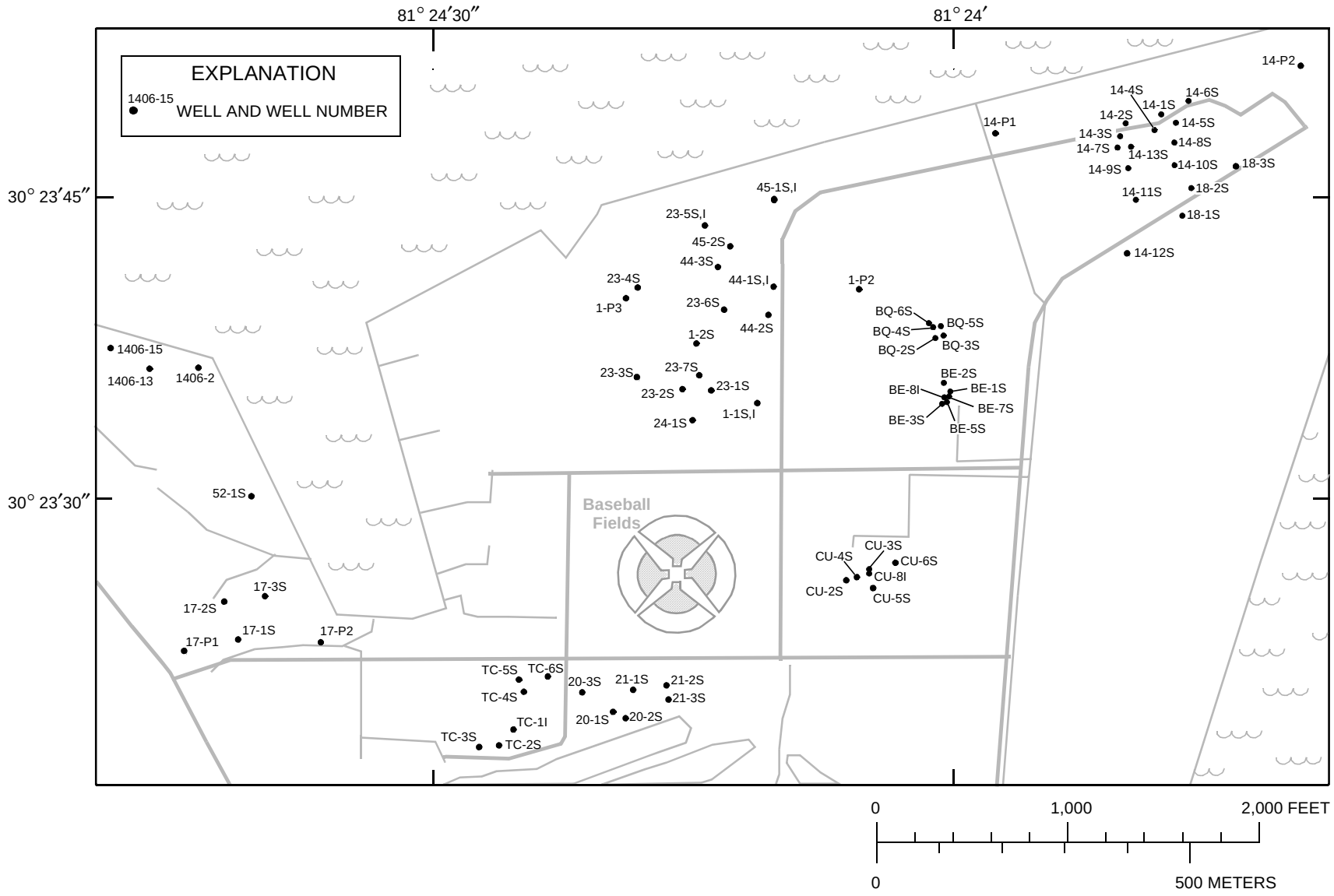

Figure 3. Inset B

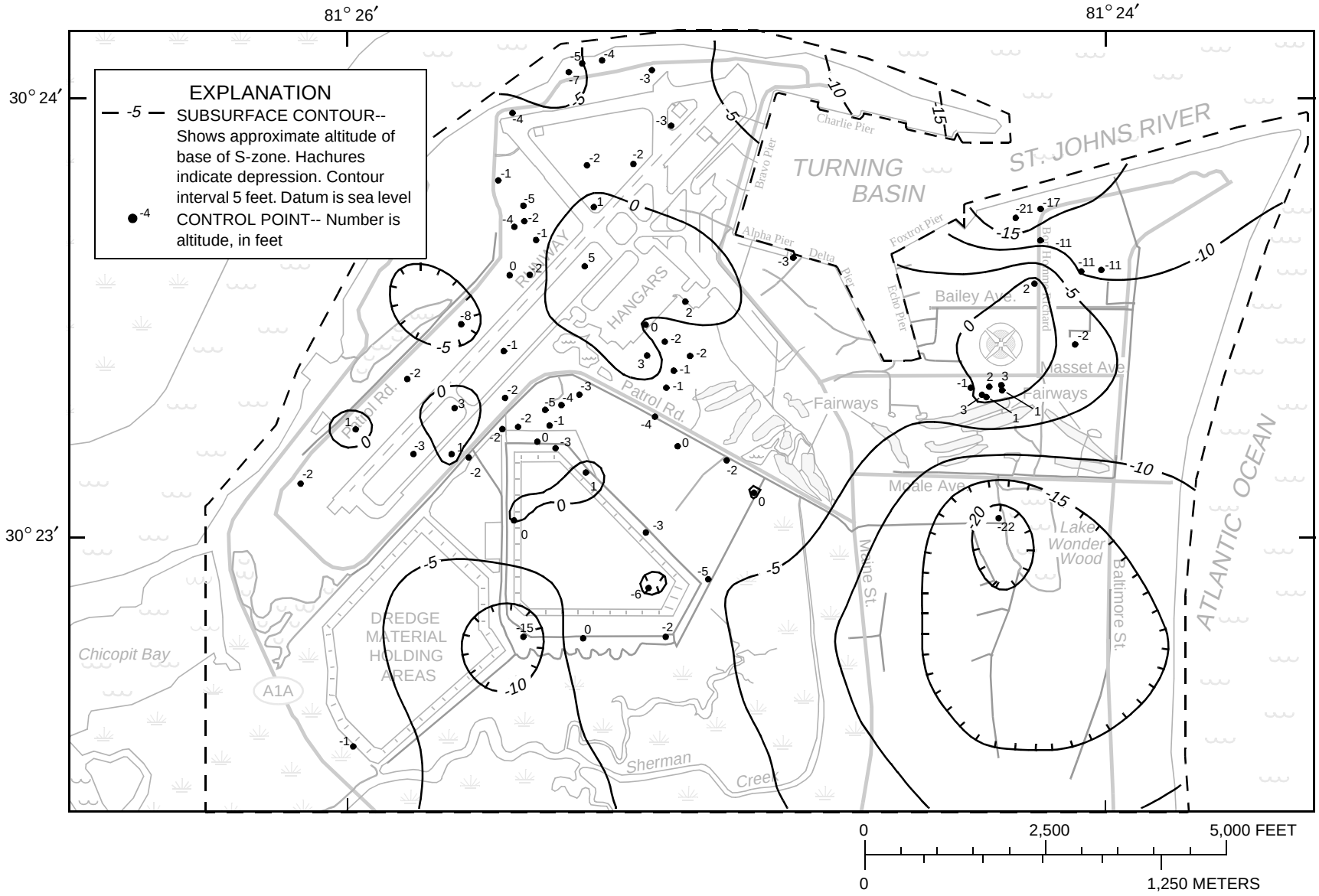

Figure 4. Altitude of base of the S-zone (layer 1).

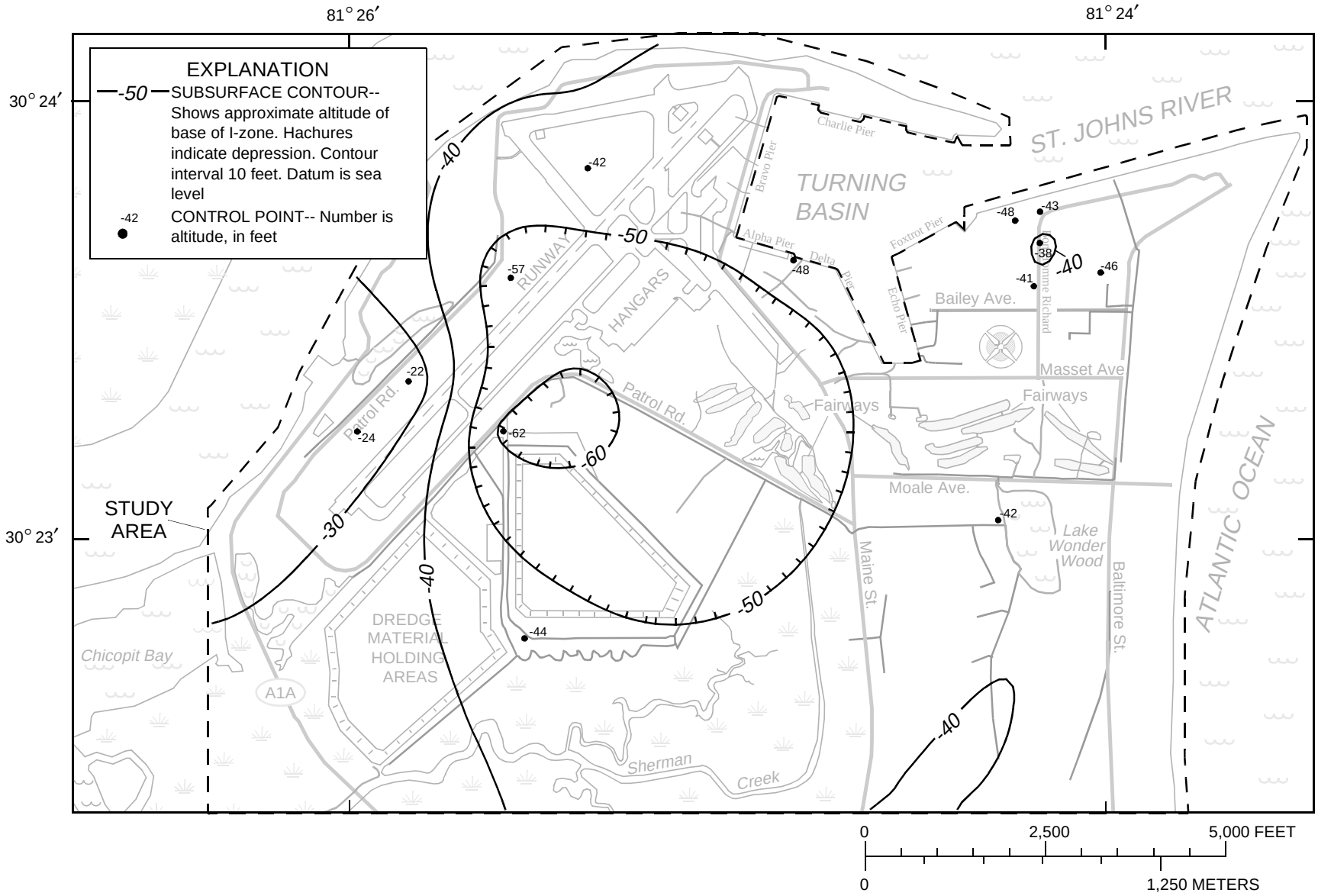

Figure 5. Altitude of base of the I-zone (layer 2).

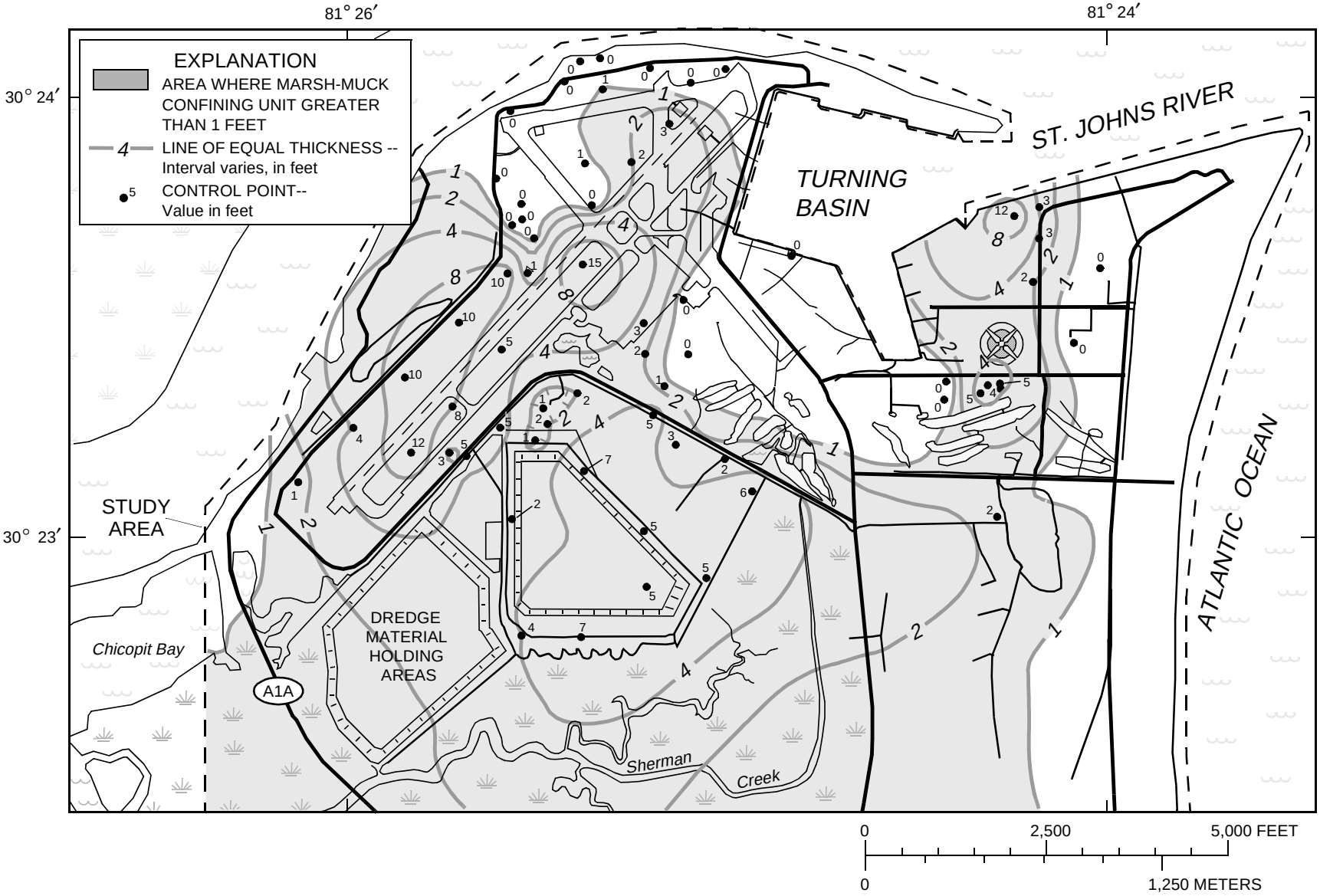

Figure 6. Thickness of the marsh-muck confining unit between the S-zone and the I-zone (between layers 1 and 2).

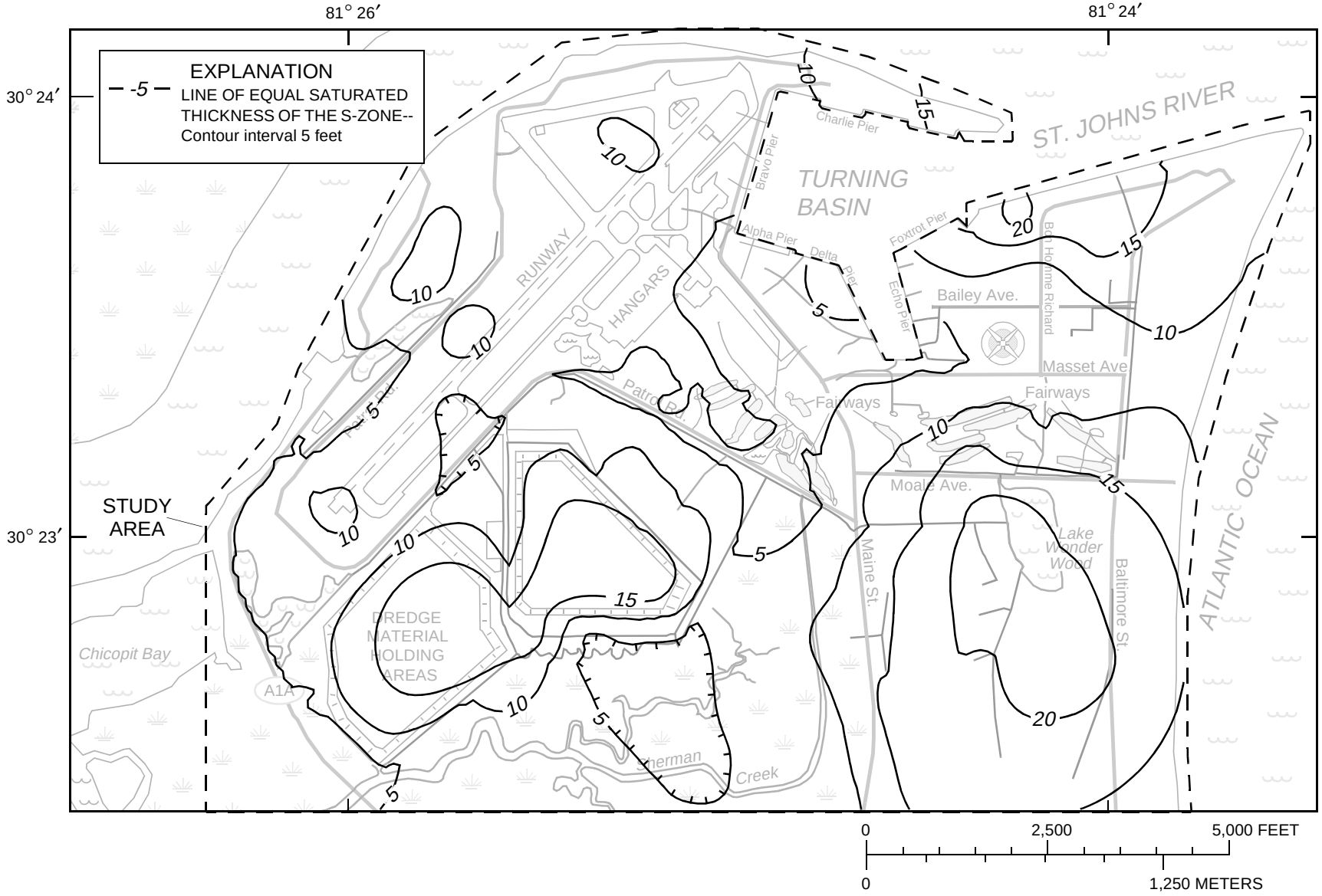

Figure 7. Average saturated thickness of the S-zone (layer 1) system.

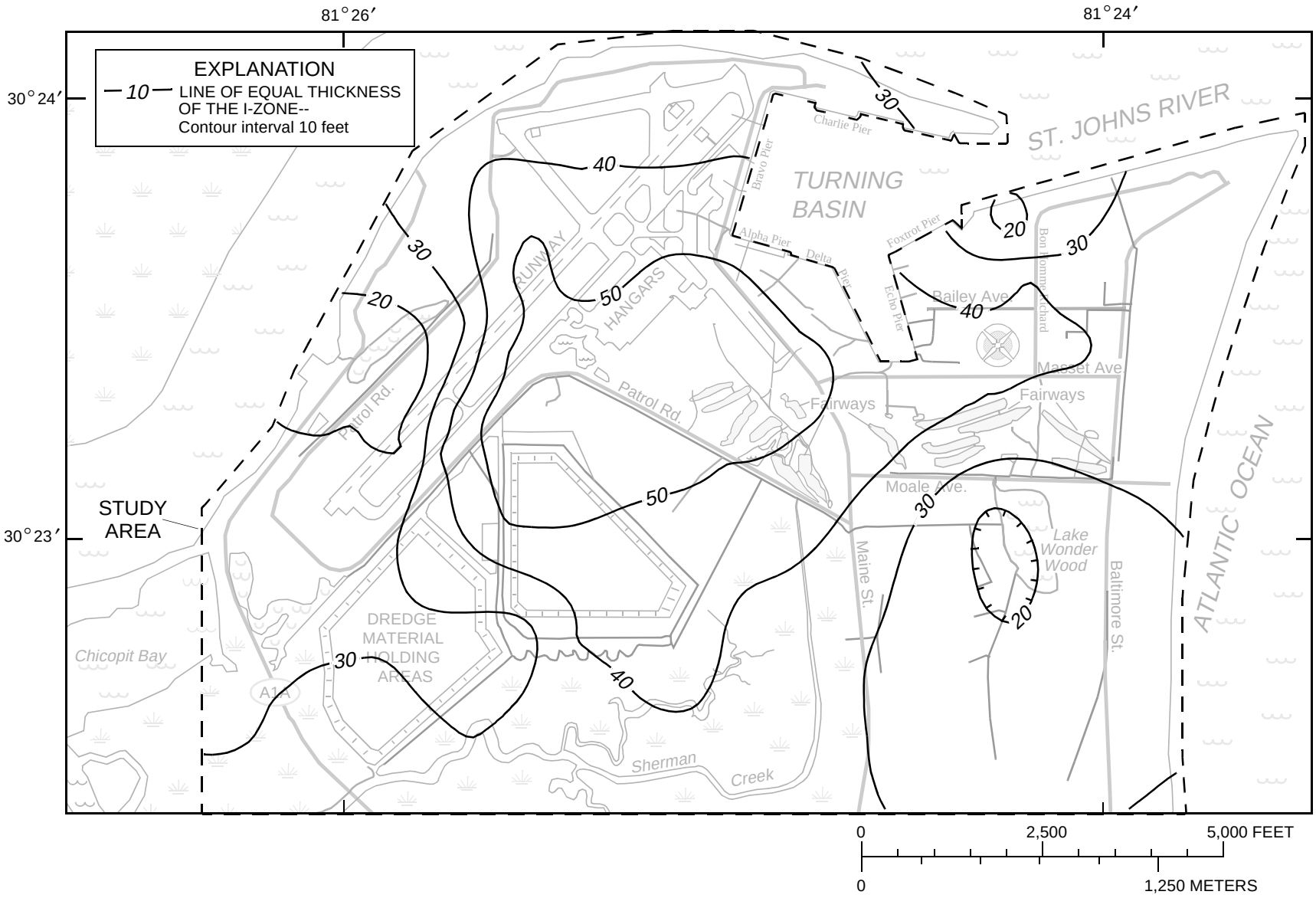

Figure 8. Thickness of the I-zone (model layer 2) in the surficial aquifer system.

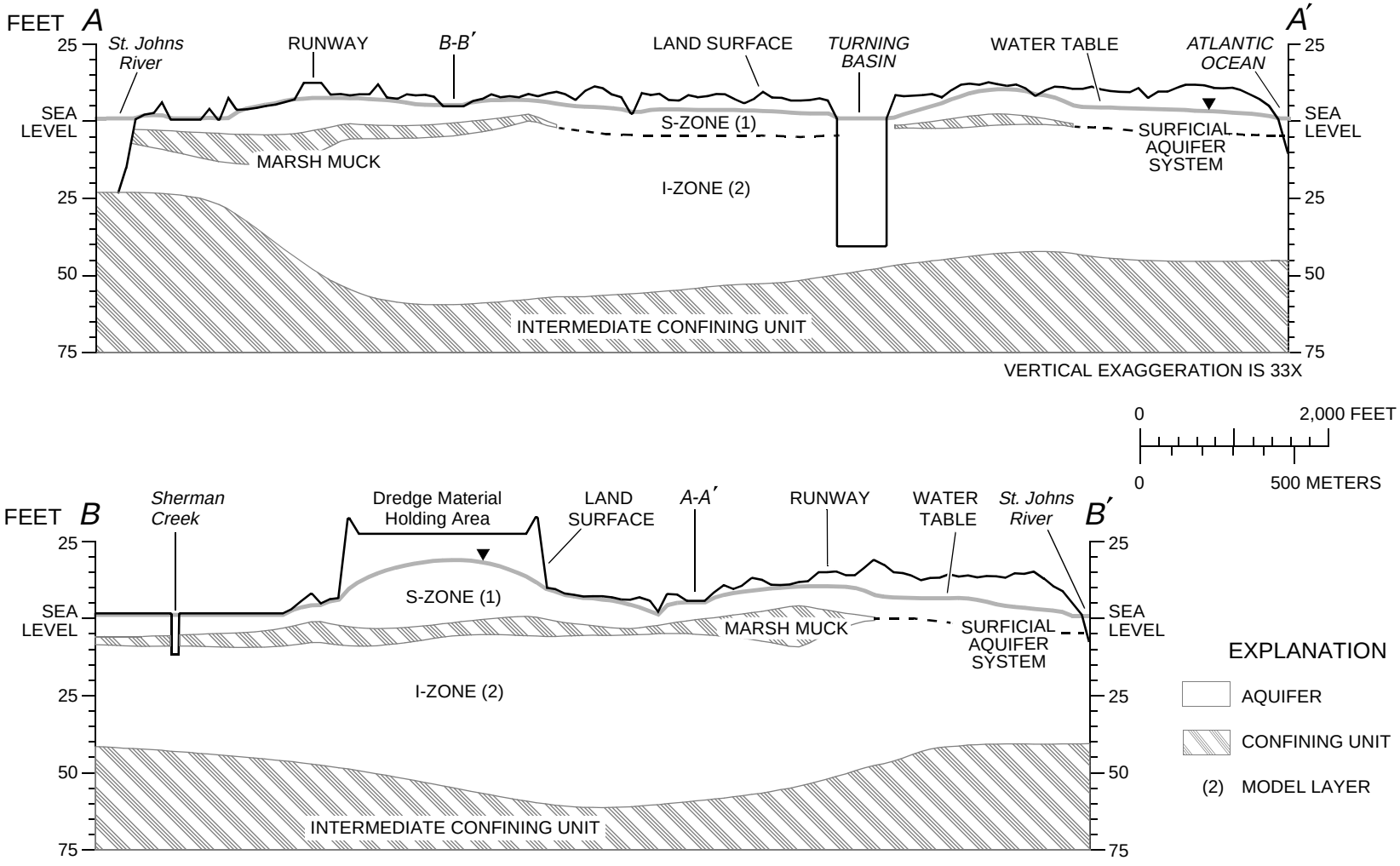

Figure 9. Generalized geohydrologic sections A-A′ and B-B′ in the study area. (Traces shown in Fig. 24).

Precipitation, irrigation, and deep leakage add water to the budget of the study area. Precipitation is the dominant and most variable source of water. The long-term average precipitation rate is about 51 in/yr (Owenby and Ezell, 1992). The average annual precipitation between 1992 and 1996 was 56 in/yr but the extremes during that same 5-year period ranged from 44 in. in 1996 to 68 in. in 1995 (fig. 10). The application of irrigation water pumped from the Upper Floridan aquifer and the public utility adds about 5 in/yr, in total, to the study area, but because of the localized nature of irrigation, application rates at individual sites are considerably higher than the average rate. Most of the irrigation in the study area is applied to the fairways and greens of the golf course (fig. 1) at rates between 150 and 300 in/yr. Other areas of intensive irrigation include the baseball fields, ornamental plants around most of the buildings constructed after 1980, and landscaped areas along Masset Ave. and Baltimore St. Deep leakage previously was estimated to be less than 0.5 in/yr (Krause and Randolph, 1989) and, for the purposes of this study, is not a significant component of the water budget.

Stream discharge and evapotranspiration remove water from the budget of the study area and are difficult to quantify at NAVSTA Mayport. Stream discharge generated within the study area cannot be measured directly because it is a very small component of the total surface-water movement. The evapotranspiration estimate typically is the residual that remains after summing all other components of the water budget and balances the budget. This approach assumes the other components are measurable. Micrometeorological methods provide a method of independently measuring evapotranspiration but are minimally accurate (only within about 10 percent of actual rates; Bidlake and others, 1993; Sumner, 1996). Pumpage is another typical discharge component of a ground-water budget but was not considered because none of the supply

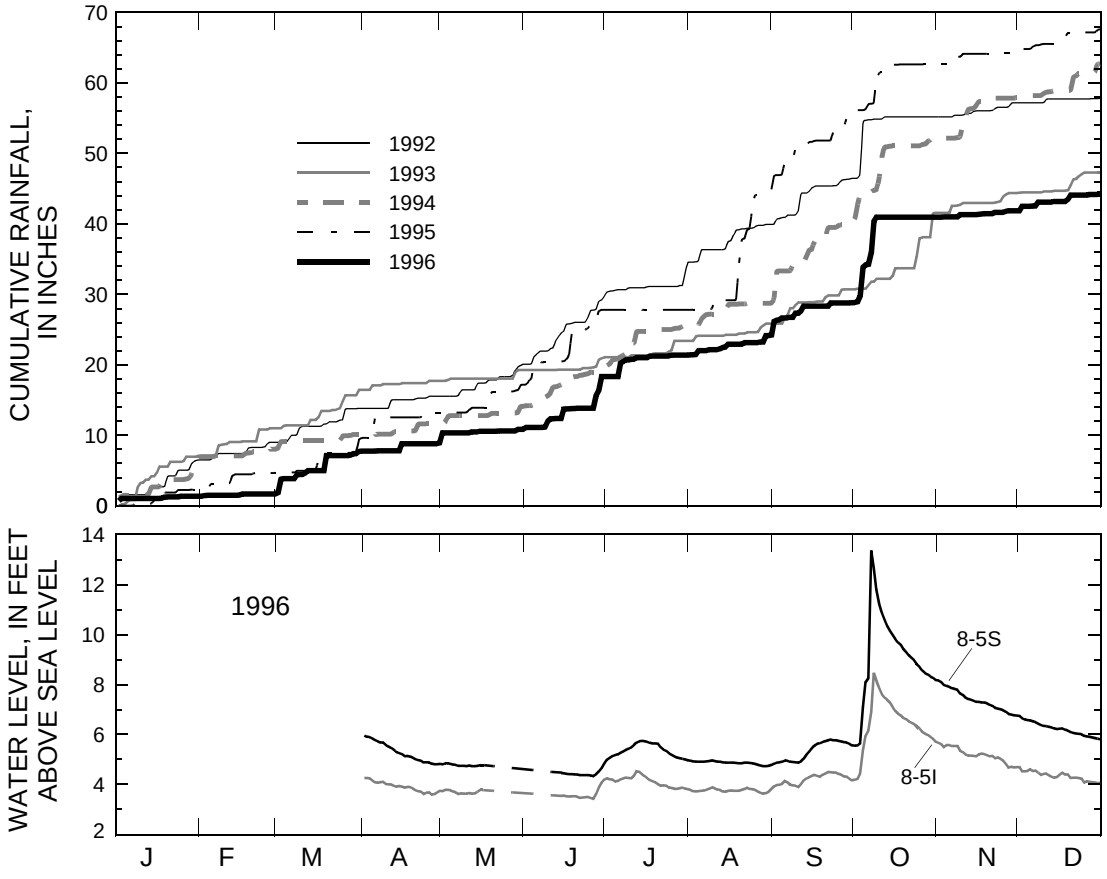

Figure 10. Annual cumulative rainfall for 1992 through 1996 and ground-water levels at wells 8-5S and 8-5I at NAVSTA Mayport during 1996.

wells in the study area extract water from the surficial aquifer system (U.S. Department of the Navy, 1995).

Measurement of stream discharge generated within the study area is obscured by discharge from the entire St. Johns River Basin (8,850 mi^2) passing through the study area (4 mi^2). In addition, tidal forcing generates large peak positive discharges in the St. Johns River that typically range from 100,000 to 140,000 cubic feet per second (ft^3/s) at Jacksonville Station 02246500 compared to an average discharge of about 6,100 ft^3/s (U.S. Geological Survey, 1996). Surface-water movement in Chicopit Bay, Sherman Creek, and the unnamed canals that drain Lake Wonder Wood and the golf course area along Patrol Road also is predominately influenced by tidal effects.

Although stream discharge generated within the study area cannot be measured directly, it can be extrapolated from a nearby basin. The average annual stream discharge from the study area can be approximated by the stream discharge from Pablo Creek at Jacksonville 02246828 which averaged about 19 in/yr between 1974 and 1996 (U.S. Geological Survey, 1996). The drainage area of Pablo Creek is 26 mi^2 and is about 5 miles (mi.) south of NAVSTA Mayport. The topography, land use, and climate of the Pablo Creek drainage are similar to those in the study area. If stream discharge is generated from the study area at a rate of 19 in/yr, then the annual mean stream discharge would be about 6 ft^3/s. This is about 0.1 percent of the annual mean stream discharge and about 0.004 percent of the typical peak discharge of the St. Johns River. Assuming that stream discharge is 19 in/yr, evapotranspiration from the study area would then be 37 in/yr to balance the water budget.

Recharge

Recharge (N) is the subcomponent of the water budget that drives ground-water flow through the surficial aquifer system (fig. 11) and can be defined as: $N = P - ET - Q_S$ or $N = Q - Q_S + D$. The surficial aquifer system is recharged when applied water exceeds evapotranspirative losses and overcomes capillary effects in the unsaturated zone. Surface runoff (Q_S) occurs when the infiltration capacity of the soil is exceeded and additional precipitation or applied irrigation water drains directly to local streams or depressions without infiltrating the subsurface (fig. 11). Of the water that crosses the water table, recharge (N) is the fraction that is not immediately extracted by evapotranspiration and moves downgradient. Discharge from the surficial

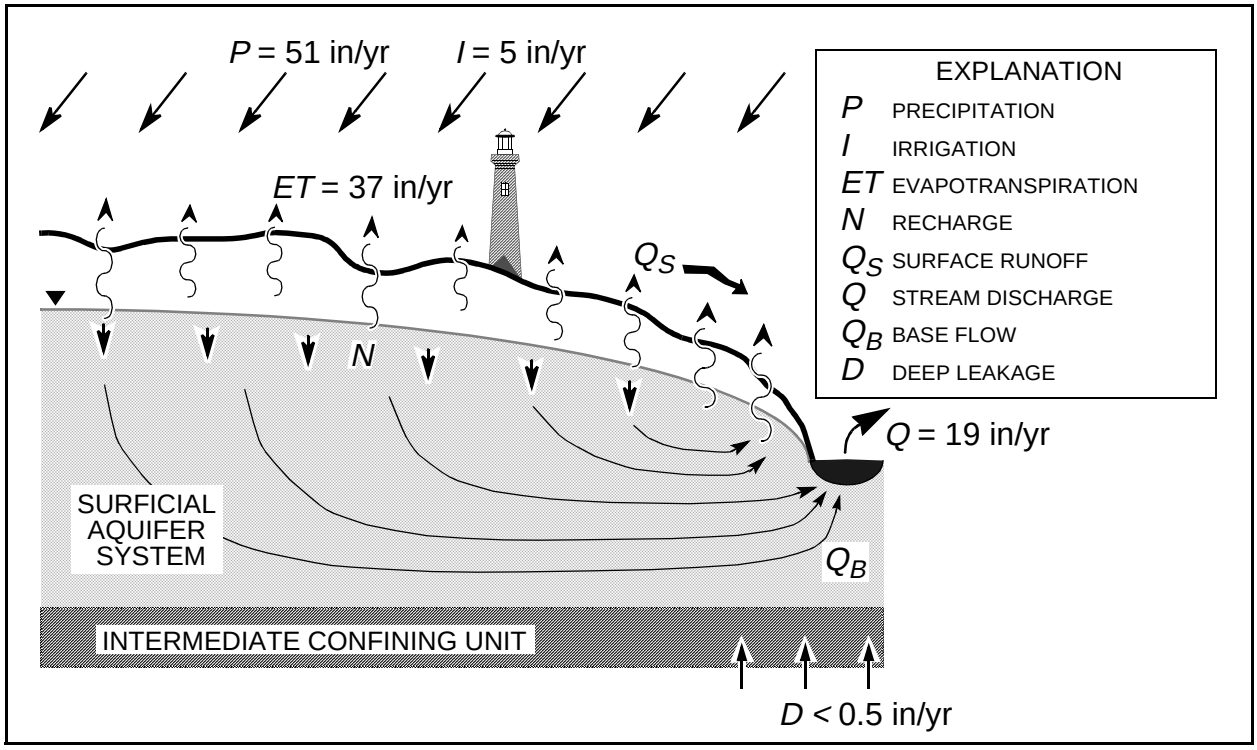

Figure 11. The water budget and its components within the study area.

aquifer system occurs as either evapotranspiration or stream discharge (fig. 11).

Recharge is practically impossible to measure directly or correlate to a measurable parameter, such as precipitation or stream discharge, owing to the complexity of interactions between evapotranspiration, the unsaturated zone, precipitation, surface runoff, and stream discharge. Recharge events that correspond with periods of intense rainfall (more than 4 in. over a 2- to 3-day period) are easily discernible by water-level responses in either the S-zone or I-zone of the surficial aquifer system (fig. 10). Effects from the majority of rainfall events are not as clearly reflected in the ground-water hydrographs, if at all (fig. 10).

Recharge usually is indirectly estimated as a calibration parameter in a ground-water flow model because of the complexity and interdependence of the controlling processes. Recharge rates have been estimated in this manner at NAS Jacksonville and NAS Cecil Field, about 15 and 35 mi west of NAVSTA Mayport, respectively. Recharge rates at NAS Jacksonville and NAS Cecil Field were estimated to be 7 in/yr (Davis and others, 1996) and 6 in/yr (Halford, 1998), respectively. Both of these estimates probably are biased below the actual recharge rates because differentially higher rates of riparian evapotranspiration were neglected in both studies.

Recharge Estimation by the Chloride Concentration Ratio Method

Recharge rates can be estimated by comparing the atmospherically deposited chloride concentration to the ground-water chloride concentration (Krulikas and Giese, 1995):

$$N = \left(\frac{Cl_{atmos}}{Cl_{GW}}\right)(P - Q_S), \qquad (2)$$

where

Cl_{atmos} is the concentration of the atmospherically deposited chloride, in milligrams per liter, which is the mass of chloride deposited by dry fall and wet fall divided by the precipitation during the collection period;

Cl_{GW} is the concentration of the chloride in ground water, in milligrams per liter; and

P-Q_S is precipitation minus surface runoff, in inches per year.

The chloride concentration ratio method assumes that chloride is a conservative constituent, the ground-water samples are from a recharge zone, the chloride concentration of the surface runoff is the same as in the water that infiltrates the ground, and the chloride concentration increase from Cl_{atmos} to Cl_{GW} is due to evapotranspiration alone, not a mineral fraction or connate water. Most of these assumptions are not overly restrictive and are met by the conditions at NAVSTA Mayport.

Conceptually, the chloride concentration ratio method is straightforward, but it is complicated by the spatial and temporal variability of the chloride concentration measurements. The concentration of atmospherically deposited chloride is not spatially uniform and can exhibit a high degree of annual variability (table 1), especially in a coastal setting. For example, the average atmospheric chloride concentration at National Atmospheric Deposition Program (NADP) station 100380 (located at the Kennedy Space Center, fig. 1) was 2.2 milligrams per liter (mg/L) between 1985 and 1994. However, the annual concentration would be expected to range from 1.5 to 3.0 mg/L within a 90 percent confidence interval. The confidence interval can be reduced from 1.5 mg/L to 0.5 mg/L by increasing the averaging period from 1 to 2 years. However, the confidence intervals are not quite comparable because they are based on small distributions of 10 and 5 samples, respectively.

Table 1. Annual atmospheric chloride deposition, ground-water chloride concentrations, and recharge estimate statistics for NAVSTA Mayport

[n, number of samples; mg/L, milligrams per liter; in/yr, inches per year]

Parameter	n	Minimum	Maximum	Average	Standard deviation	95 percent confidence limits	
						Lower	Upper
Cl_{atmos}, mg/L[a] 1-year average	10	1.7	2.7	2.2	0.37	1.5	3.0
Cl_{atmos}, mg/L[a] 2-year average	5	2.1	2.4	2.2	.13	2.0	2.5
Cl_{GW}, mg/L[b]	22	7	20	14	4	6	22
ln(Recharge)[c]	220	1.28	2.92	1.98	.35	1.29	2.67
Recharge, in/yr	220	4	19	7	--	4	14

[a] Estimates are extrapolated from the 1985 to 1994 precipitation measurements at NADP/NTN station 100380 (located at the Kennedy Space Center) and adjusted to the combined wet and dry amount by the dry-fall:wet-fall ratio of 0.42 estimated for Florida by Baker (1991).

[b] Chloride concentrations determined from samples collected during January 1993 (U.S. Department of the Navy, 1995).

[c] Recharge estimate statistics are based on a 1-year averaging period of the atmospheric chloride deposition data. Infiltration was assumed to be 44 in/yr (precipitation + irrigation - stream discharge + recharge).

Ground-water chloride measurements are more spatially variable than atmospheric chloride measurements (table 1), partly because the depth of samples and, hence, the traveltime from the point of recharge to the sampled well can significantly vary. The rate of infiltration through the unsaturated zone also affects opportunities for the enrichment of chloride in ground water and depends on the thickness of the zone, antecedent conditions, and the porosity of the unsaturated media. Accordingly, the time period sampled is dependent on the well construction, the rate and frequency of recharge events, and the porosity. The time period sampled affects the magnitude and uncertainty of the Cl_{atmos} estimate used to estimate the recharge rate. Where the aquifer is homogeneous, the traveltime through the unsaturated zone is negligible, and the aquifer is thick relative to the length of the well screen, the time period sampled by shallow wells in a recharge area can be approximated by:

$$\Delta t_{Sample} = \frac{L_{Screen}}{N}\theta, \qquad (3)$$

where

L_{Screen} is the contributing screen length, in feet;
N is the recharge rate, in feet per year; and
θ is the effective porosity, dimensionless.

As equation 3 shows, determining the time period sampled is difficult because it is dependent on the estimate of annual recharge rates. The time periods sampled at NAVSTA Mayport typically range from 0.3 to 6 years based on contributing screen lengths ranging between 3 and 8 ft, recharge rates between 6 and 12 in/yr (0.5 and 1 foot per year (ft/yr)), and effective porosities between 10 and 40 percent.

Chloride concentrations in water from most of the observation wells at NAVSTA Mayport cannot be used to estimate the ground-water recharge rate, except for chloride concentrations in samples from wells in the vicinity of well 8-5S and Solid Waste Management Unit-6/7 (SWMU-6/7). The chloride concentration in these areas represents mostly atmospheric sources because it is part of the older upland areas and has been flushed by freshwater recharge many times. The chloride deposition rate east of Maine St. (fig. 1) is largely unknown because the area is recharged by a mixture of precipitation and unmetered irrigation from Upper Floridan supply wells and the public utility. The ground-water chloride concentrations in the hangar areas, along the southwest runway, and in the areas south of the Patrol Road are elevated (as much as 25,000 mg/L) and are indicative of the incomplete flushing of a recently reclaimed salt marsh.

A recharge rate of 7 in/yr (table 1) was estimated using an average of 22 ground-water chloride measurements (14 mg/L) made during January 1993 (U.S. Department of the Navy, 1995) at 14 wells in the vicinity of well 8-5S and SWMU-6/7. These 14 wells were considered appropriate for use in the analyses because the primary land cover is unirrigated grasses. The annual atmospheric chloride deposition rate was extrapolated from NADP station 100380. An average atmospheric deposition rate of 2.24 mg/L corresponds to most of the time periods sampled by the wells. Infiltration was assumed to be 44 in. during 1992 based on the total precipitation (58 in.) minus the surface discharge from Pablo Creek (21 in.) plus the recharge at NAS Jacksonville (7 in.).

Recharge rates estimated using the chloride concentration ratio method are associated with a large uncertainty. For example, if all of the assumptions of the method are met and the infiltration rate is known, the recharge rate can range from 4 to 15 in/yr based on a 95 percent confidence interval (table 1). A reduction of the confidence interval to 50 percent still yields a range in recharge rates from 5 to 9 in/yr.

The water-budget analysis and recharge rate estimates provide a general idea of how much water passes through the surficial aquifer system, but cannot indicate what fraction of flow passes through the S-zone or the I-zone of the surficial aquifer system. The direction and velocity of the movement of contaminants from specific sites are also not determined through a water-budget analysis. A ground-water flow model is needed to address these more specific questions.

SIMULATION OF GROUND-WATER FLOW IN THE SURFICIAL AQUIFER SYSTEM

A three-dimensional numerical model was used to quantitatively analyze ground-water flow and the advective transport of contaminants through the surficial aquifer system. The McDonald and Harbaugh (1988) modular finite-difference model (MODFLOW) was used to simulate flow in the surficial aquifer system and to solve the governing equation:

$$\nabla \cdot (Kb\nabla h) + q + (P - Q_S) - ET = S\frac{\partial h}{\partial t} \quad , \quad (4)$$

where

∇ is del, the vector differential operator;
K is hydraulic conductivity, in feet per day;
b is thickness, in feet;
h is hydraulic head, in feet;
q is a source or sink, in feet per day;
P-Q_S is precipitation minus surface runoff, in feet per day;
ET is evapotranspiration, in feet per day;
S is storage coefficient in confined aquifers and the specific yield in unconfined aquifers, dimensionless; and
t is time, in days.

Description of the Ground-Water Flow Model

To implement a finite-difference model, the study area was discretized into a rectangular grid of cells by row and column. The active model grid covered an area of about 4.4 mi^2 and was divided into 107 rows of 152 columns (fig. 12). Uniform, square cells that measured 100 ft on a side were used throughout the simulated area. Of the 32,528 model cells, 8,126 cells were inactive beyond the study area and in areas covered by the St. Johns River, the turning basin, and the Atlantic Ocean.

The grid was oriented along a north-south axis for convenience. Neither a majority of known stresses or boundary conditions were aligned along any particular axis. No measurements of anisotropy were available and a lateral anisotropy ratio of 1:1 was used for simulation. Values of aquifer and confining-unit hydraulic properties were assigned to the center of each cell, defined as a node, by interpolation from observed point values.

The model was vertically discretized into two layers to simulate the S-zone and I-zone of the surficial aquifer system (fig. 9). Vertical impedance to flow within the surficial aquifer system was simulated by assigning leakance values at each cell between model layers. The leakance is the average vertical hydraulic conductivity of the aquifer or confining unit material between nodes divided by the vertical distance between corresponding nodes in adjacent model layers and is in units of feet per day per foot (d^{-1}). Leakage between the S-zone and the I-zone primarily is controlled by the thickness of the marsh-muck confining unit in areas where the confining unit is more than 1 ft thick. Vertical movement of water was assumed to be controlled by the vertical hydraulic conductivity of the aquifer where the confining unit is 1 ft thick or less.

Hydraulic Characteristics

Multi-well aquifer tests, single-well aquifer tests, and slug tests were conducted at NAVSTA Mayport to estimate the hydraulic properties of the surficial aquifer system. The lateral hydraulic conductivities estimated by these tests were the final values used in the ground-water flow model. Because there is no pumpage from the surficial aquifer and the surface-water features are tidally influenced, ground-water discharge could not be independently quantified and the lateral hydraulic conductivity distribution could not be reasonably estimated by model calibration.

An aquifer test consists of applying a known stress to an aquifer; measuring the change in water level, drawdown or recovery, due to that stress; and inferring the hydraulic properties of the aquifer. For the multi-well and the single-well aquifer tests, the aquifer was stressed by pumping at a constant, known rate. The principal difference between the multi-well tests and the single-well tests is the measurement of drawdowns in observation wells in addition to the pumped well. For slug tests, the aquifer was stressed by removing a known volume from a well and measuring the water level recovery.

Lateral hydraulic conductivity estimates from multi-well tests are considered most representative of aquifer hydraulic characteristics because the amount of water exchanged and, therefore, the volume of aquifer affected usually are greater than during slug tests or single-well tests. The median volumes removed during the multi-well, single-well, and slug tests at NAVSTA Mayport were about 900, 40, and 0.4 gallons (gal), respectively. Hydraulic conductivity estimates generally are averaged over a greater volume of aquifer by the inclusion of drawdown measurements from several observation wells. An increased number of observation well locations also increases the uniqueness of hydraulic conductivity estimates, even when fitting the test data to more complex models that account for unconfined conditions and vertical flow within the aquifer.

In addition to multi-well aquifer tests, single-well tests and slug tests were used to estimate lateral hydraulic conductivities. Although the multi-well aquifer tests provide the most representative estimates

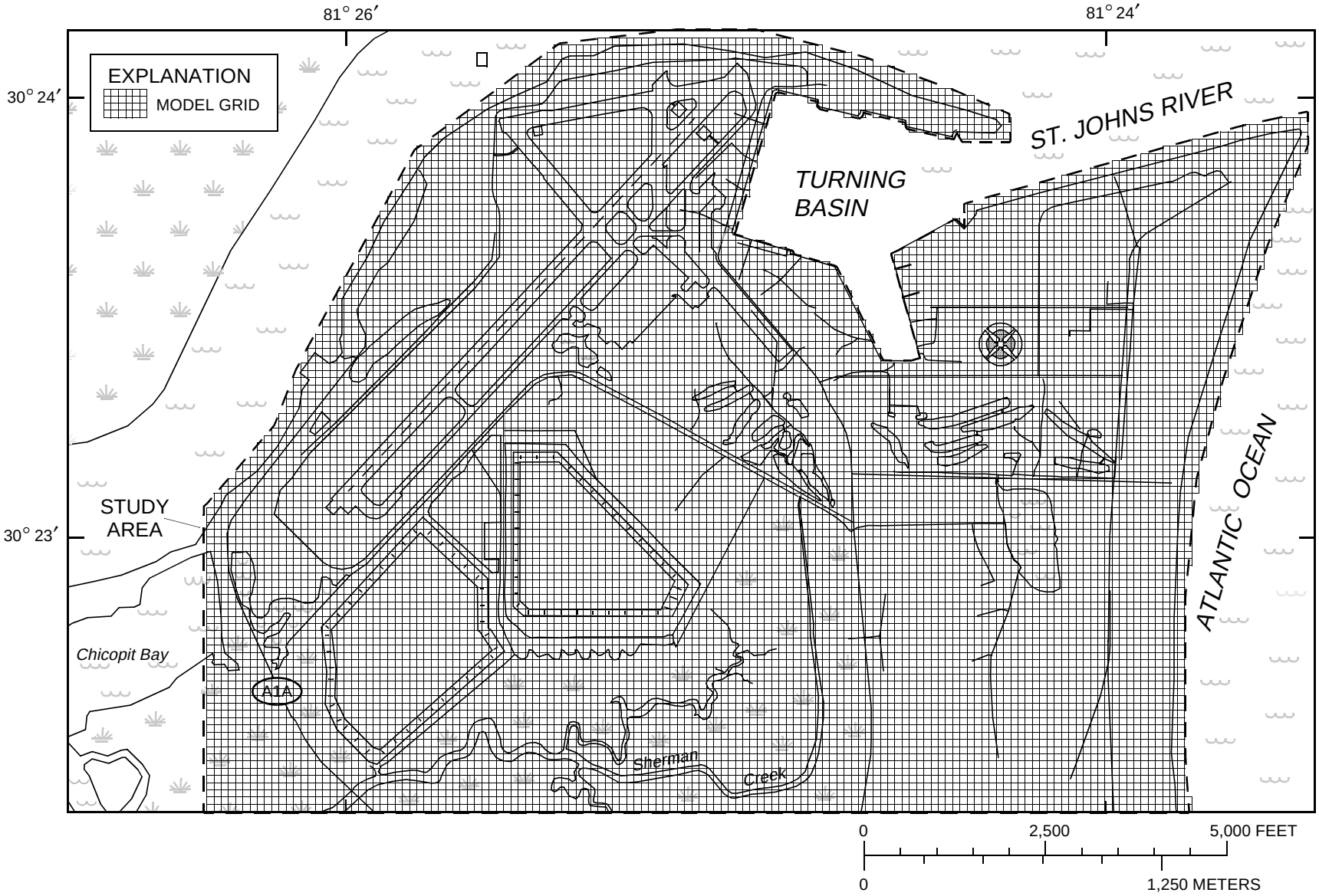

Figure 12. Active model grid.

of lateral hydraulic conductivity estimates, the single-well tests and slug tests can be executed in less time and at a lower cost than the multi-well aquifer tests. About 15 to 20 single-well tests were conducted and analyzed in the same amount of time it took to conduct one multi-well aquifer test at NAVSTA Mayport. Although greater uncertainty is associated with estimates based on data collected during single-well tests and slug tests, the improved efficiencies associated with these tests facilitate an increase in spatial coverage and provide a better description of the spatial variability of the lateral hydraulic conductivity.

Lateral hydraulic conductivities were estimated from the multi-well aquifer tests by fitting a model to the measured drawdowns. The appropriate flow model was dictated by the geology and ground-water flow conditions at the site and the configuration of the pumped well and observation wells. The drawdown response in a single, confined aquifer can be described by the analytical Theis (1935) model. The Theis model was used to analyze the drawdown in well 8-3 which was affected by a nearby sump screened across both the S-zone and the I-zone (table 2). Most of the other multi-well aquifer tests were better described by the numerical model VS2DT (Lappala and others, 1987; Healy, 1990) that accounts for an unconfined aquifer and vertical flow within the aquifer. Six of the multi-well aquifer tests were analyzed by fitting results computed with a variably saturated, radially symmetric, numerical model, VS2DT, to the measured drawdowns (Halford, 1997). Aquifer tests conducted at wells B-1S and B-1I were analyzed with a three-dimensional MODFLOW model to account for the asymmetric effects of Lake Wonder Wood and a nearby drainage canal.

Where the marsh-muck confining unit was about 1 ft thick or less at the test site, the aquifer-test model (either VS2DT or MODFLOW) spanned both the S-zone and the I-zone of the surficial aquifer system. The entire vertical section was simulated for these tests to avoid prescribing boundary conditions within the section. Where the marsh-muck confining unit was more than 1 ft thick, vertical leakage across the confining unit was generally ignored.

Lateral hydraulic conductivity estimates were constrained in all aquifer test analyses by assuming that one value could characterize the entire thickness of either the S-zone or the I-zone at the test site.

Table 2. Lateral and vertical hydraulic conductivity estimates determined from multi-well aquifer tests

[Well locations are shown in figure 3; ft/d, feet per day; gpm, gallons per minute; ft, feet; <, less than; --, not applicable]

Well identifier[a]	Lateral hydraulic conductivity (K_{XY}), ft/d			Vertical hydraulic conductivity (K_Z), ft/d	Vertical anisotropy (K_Z/K_{XY})	Flow rate, gpm	Test duration hour:minute	Maximum drawdown, ft	Initial wetted screen, ft	Aquifer thickness, ft	Marsh-muck confining unit thickness, ft
	Multi-well	Single well[b]	Slug test[c]								
2-17S	8	15	11	8	1	4.6	6:45	4.0	9	18	4
2-38S	80	135	65	12 < 0.002[f]	0.15	5.0	2:15	3.5	10	6	10
8-3S[d]	15	--	--	--	.13	1.0	5:00	--	25	40	0
13-5S	13	33	--	13	1	1.9	7:15	4.0	9	7	1
20-2S	27	35	27	10	0.38	1.7	5:30	2.4	8	8	4
B-1S[e]	30	41	--	--	--	5.4	6:00	3.0	9	24	2
BE-7S	32	58	--	3	.09	4.5	3:10	2.3	8	49	0
B-1I[e]	70	--	--	< 1[f]	--	5.4	6:00	1.2	5	18	2
F-80I[g]	34	48	--	2	.07	20	5:00	12.2	10	49	0

[a] Suffix denotes zone tested.

[b] All single-well tests were analyzed with no more than the first hour of drawdown data.

[c] Lateral hydraulic conductivity estimates from slug tests were reported in U.S. Department of the Navy (1995).

[d] Aquifer was stressed by a 4-ft diameter sump with 25 ft of screen. The drawdown response was simulated with the Theis (1935) solution. Vertical anisotropy was determined by a nearby test in the unsaturated zone. An unspecified air flow rate was induced near the water table (about 7 ft below land surface) and six drawdowns were measured at 10, 20, and 30 ft from the pumped well and 2 and 4 ft below land surface. The maximum drawdown was equivalent to 0.58 ft of water and the compressibility effects of air could be ignored.

[e] Observed drawdowns were fitted to a three-dimensional model that accounted for the effects of Lake Wonder Wood and a nearby canal. The model was simulated with the MODFLOW code.

[f] Maximum vertical hydraulic conductivity of the marsh-muck confining unit at test sites. Based on both the S-zone and I-zone tests.

[g] Aquifer test was performed in 1979 and originally reported by Franks (1980).

Estimates of vertical hydraulic conductivity across the marsh-muck confining unit or within the S-zone were similarly constrained. Preliminary results of aquifer tests in vertically adjacent zones were applied iteratively until "best fit" results were achieved for tests in both zones (table 2).

The single-well aquifer tests were analyzed with the Cooper-Jacob (1946) approximation of the Theis solution. The Cooper-Jacob model of aquifer response can be described by a straight line on a plot of drawdown as a function of the logarithm of time. Lateral hydraulic conductivity (K) values are estimated from flow rate and drawdown measurements by:

$$K = \frac{2.3 Q_{Pump}}{4\pi b s_{\log cycle}}, \qquad (5)$$

where

Q_{Pump} is the rate the well is pumped, in cubic feet per day;

b is the thickness of the aquifer, in feet; and

$s_{\log cycle}$ is the measured rate of drawdown increase, in feet per log-cycle.

For all of the aquifer tests conducted at NAVSTA Mayport, the drawdowns observed in the pumped wells increased semi-logarithmically after the initial well-bore effects dissipated. Using equation 5, a lateral hydraulic conductivity estimate was determined at most of the single-well aquifer test sites (table 3). The limited drawdown data could have been fitted to more sophisticated models but no more than one hydraulic characteristic could have been reasonably estimated.

Although the Cooper-Jacob method provides a simple method of analysis, many of the inherent assumptions of the method are not met or are only partially satisfied at NAVSTA Mayport because a leaky confining unit is present and the surficial aquifer system is unconfined. The combined result of neglecting these factors was that lateral hydraulic conductivity estimates based on single-well tests, K_{single}, were consistently greater than corresponding estimates based on multi-well tests, K_{multi} (table 2).

Table 3. Lateral hydraulic conductivity estimates determined from single-well aquifer tests

[Well locations are shown in figure 3; gpm, gallons per minute; ft, feet; --, not applicable]

Well identifier[a]	Lateral hydraulic conductivity, ft/d			Flow rate, gpm	Test duration hour:minute	Maximum drawdown, ft	Initial wetted screen, ft	Aquifer thickness, ft	Marsh-muck confining unit thickness, ft
	Corrected single-well [b]	Single well	Slug test [c]						
2-32S	58	98	--	1.9	0:09	1.0	7	6	7
2-34S	28	48	--	2.1	0:08	2.4	6	6	14
2-35S	9	15	--	1.2	2:45	6.2	7	7	5
2-36S	15	25	54	3.5	0:06	4.9	9	6	10
2-37S	1	2	--	1.8	0:04	3.0	10	13	10
8-5S	2	4	1.2	0.7	0:06	3.6	9	7	1
15-P2	5	9	5.5	2.0	0:07	2.3	10	50	0
16-4S	34	58	--	1.8	0:16	0.8	4	10	1
23-3S	6	11	2	1.8	0:18	5.1	8	9	5
23-5S[d]	7	12	9	2.0	0:15	.8	8	21	11
23-7S	8	14	1.5	.9	0:16	3.0	8	6	4
CU-4S	5	8	--	1.8	0:14	1.0	6	49	0
1-1I	9	16	--	4.6	0:11	5.0	5	41	2
2-11I	55	92	--	4.6	0:13	2.4	5	44	6
2-12I	47	79	45	5.0	0:15	2.4	5	42	5
2-17I	72	120	93	4.3	2:35	4.6	5	25	4
2-18I	13	22	29	4.8	5:00	2.2	5	58	1
2-23I	49	83	--	4.5	0:21	2.4	5	48	6
2-32I	14	25	--	4.8	0:07	1.0	5	40	7
2-34I[e]	--	--	--	.6	0:07	26.0	5	45	14
2-35I	10	18	--	4.8	6:15	4.0	5	21	5
2-36I	70	117	46	4.8	0:13	2.0	5	13	10
2-37I	3	5	--	1.8	0:12	2.6	5	28	10
2-38I	.6	1.1	1.4	2.4	2:00	19.0	5	46	10
8-5I	14	24	--	4.6	0:11	3.3	5	40	1
16-1I	56	95	--	4.5	0:15	1.9	5	42	0
23-5I	1.1	2	1.3	1.6	0:18	7.8	5	17	11
CU-8I	15	26	--	4.0	0:17	2.9	5	49	0

[a] Suffix denotes zone tested.

[b] The single-well lateral hydraulic conductivity estimates were corrected by equation 6.

[c] Lateral hydraulic conductivity estimates from slug tests were reported in U.S. Department of the Navy (1995).

[d] Pumped for 15 minutes but only the first minute was analyzed due to proximity of St. Johns River.

[e] Specific capacity was less than 0.02 gallon per minute per foot.

A log-log graph of K_{multi} versus K_{single} suggests a linear relation exists between the logarithms of the two variables (fig. 13), which can be described by:

$$K_{Multi} = 0.53 K_{Single}^{1.03}. \qquad (6)$$

Equation 6 adequately corrects the initial estimates from single-well aquifer tests, as indicated by the regression coefficient ($r^2 = 0.89$), and is considered to provide the best estimate of lateral hydraulic conductivity at NAVSTA Mayport. The corrected values of lateral hydraulic conductivity from the single-well tests were used in the calibrated model (table 3).

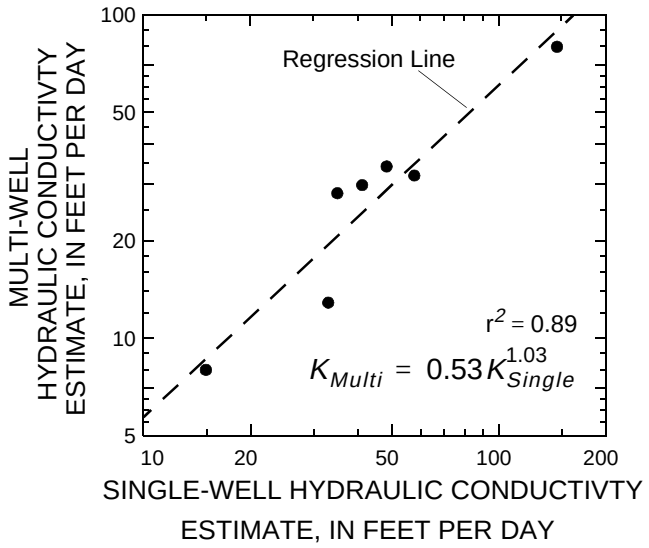

Figure 13. Relation between lateral hydraulic conductivity values estimated by single-well tests and multi-well tests.

Additional lateral hydraulic conductivity estimates at NAVSTA Mayport were determined from slug tests (U.S. Department of the Navy, 1995), 59 in the S-zone and 5 in the I-zone (table 4). The slug tests were analyzed by the Bouwer and Rice (1976) method which empirically corrects for the effects of partially penetrating wells in an unconfined aquifer.

Table 4. Lateral hydraulic conductivity estimates determined from slug tests

[Lateral hydraulic conductivity in feet per day; all other values in feet; <, less than; well locations are shown in figure 3]

Well identifier[a]	Lateral hydraulic conductivity[b]	Initial wetted screen	Aquifer thickness	Marsh-muck confining unit thickness
1-P1	20	5	18	3
1-P2	25	5	15	1
1-P3	18	8	14	7
2-18S	5	10	8	1
2-22S	7	10	6	3
2-25S	3	10	18	5
2-26S	10	10	18	5
2-31S	29	10	9	11
2-33S	34	10	9	5
2-P11	8	4	7	2
2-P2	8	5	11	3
2-P4	13	5	10	4
2-P5	6	5	6	2
2-P6	6	5	2	3
2-P8	5	5	5	5
2-P9	18	5	9	1
8-4S	7	6	43	0
8-6S	2	7	44	0
8-7S	2	7	44	0
8-8S	1.0	6	8	< 1
8-P2	7	5	44	0
8-P3	0.8	5	45	< 1
8-P4	10	7	10	3
13-8S	45	10	7	5
13-P1	18	5	8	5
13-P4	16	5	61	0
13-P5	1.3	5	4	3
14-3S	13	9	47	0
14-4S	10	9	47	0
14-5S	11	8	47	0
14-6S	11	9	47	0
14-7S	8	9	47	0
14-8S	11	8	47	0
14-9S	8	9	47	0
14-10S	18	9	47	0
14-11S	21	9	48	0
14-12S	14	6	48	0
14-13S	9	9	47	0
14-14S	13	9	47	0
14-P1	12	5	47	0
14-P2	22	5	46	0
15-1S	3	9	9	1
15-P3	6	10	9	3
16-2S	5	7	43	0
17-P2	23	5	51	0
18-1S	14	8	48	0
18-2S	9	8	47	0
18-3S	17	8	47	0
23-1S	2	9	8	3
23-2S	1.0	10	8	4
23-4S	5	9	15	8
23-6S	3	7	12	5
24-1S	2	10	8	3
44-1S	5	7	14	3
44-2S	1.0	6	12	3
44-3S	5	7	17	7
45-2S	8	8	19	9
56-1S	36	10	5	3
CU-5S	6	6	47	0
2-15I	12	10	50	5
2-25I	50	5	46	5
2-31I	9	5	23	11
2-33I	7	5	49	5
15-5I	15	5	55	0

[a] Suffix denotes zone tested.

[b] Lateral hydraulic conductivity estimates were reported in U.S. Department of the Navy (1995).

Lateral hydraulic conductivity estimates based on slug test results are reported to be within 25 percent of actual value (Bouwer and Rice, 1976) under ideal conditions, but the discrepancy is expected to be greater in practice.

Lateral hydraulic conductivity values were estimated using results from pumping tests and slug tests at 15 wells. Values based on the pumping tests and slug tests ranged from 0.4 to 80 feet per day (ft/d) and from 1.2 to 93 ft/d, respectively. The geometric averages of the two sets of estimates are the same (10 ft/d) but the median discrepancy between any two estimates was about 50 percent of the greater estimate. The maximum discrepancies between values at a single site resulted from tests at wells 23-7S and 2-36S. The slug test underestimated the single-well test results at 23-7S by a factor of 4 (1.5 ft/d compared to 7 ft/d), and overestimated the single-well test results at 2-36S by a factor of 4 (54 ft/d compared to 13 ft/d).

The areal distribution of lateral hydraulic conductivity in the S-zone (layer 1) and the I-zone (layer 2) were estimated by kriging the log of the test estimates of hydraulic conductivity. Ordinary kriging was used to interpolate and extrapolate from the test site locations (point values) to the model nodes because it provides the best linear, unbiased estimate (Isaaks and Srivastava, 1989). Ordinary kriging can be used because no spatial trends exist in the log-hydraulic conductivity values of either the S-zone or the I-zone.

Spatial interpolation by kriging is based on the internal structure of the data set (autocorrelation). This structure, if present, is examined by plotting the squared difference in measured values, γ_{ij}, against the distance between locations i and j. A scatter plot of γ_{ij} as a function of distance will show a general increase in γ_{ij} as pairs become further apart. An overall structure, however, is hard to determine because of the variability which exists at any given point (Isaaks and Srivastava, 1989).

An underlying internal structure is made more apparent by averaging γ_{ij} over intervals (lags) to obtain:

$$\gamma(h) = \frac{1}{2N(h)} \sum_{(i,j)|h_{ij} \approx h} (Y_i - Y_j)^2 \quad , \qquad (7)$$

where

h is the average distance between log-hydraulic conductivity values in an interval;
$N(h)$ is the number of pairs in an interval; and
Y is a measured log-hydraulic conductivity value.

A plot of $\gamma(h)$ versus h produces an empirical variogram (fig. 14). Variograms of log-hydraulic conductivity differences showed little uncertainty (nugget effect) associated with the measured values relative to the variance of Y in either the S-zone or the I-zone (fig. 14). For about the first 1,000 to 1,500 ft, $\gamma(h)$ increased rapidly with distance. Beyond about 4,000 ft, $\gamma(h)$ remained near the variance of Y in both the S-zone and the I-zone which was 0.25 and 0.62 log $(ft/d)^2$, respectively (fig. 14). The variability in γ_{ij} as a function of data pair orientation was not considered because the available data were insufficient to define anisotropic variograms.

Exponential variograms (fig. 14) provide the functional form of the relation between $\gamma(h)$ and distance. The empirical variograms of Y in the S-zone and the I-zone were approximated by:

$$\tilde{\gamma}_{ij} = \sigma^2 \left(1 - \exp\frac{-3h}{a}\right) \quad , \qquad (8)$$

where

σ^2 is the variance of log-hydraulic conductivity, in log $(ft/d)^2$, and
a is the range, in feet.

Range is the primary variogram parameter that affects kriging estimates. As range increases, more measured values influence the estimate. Both the S-zone and the I-zone exponential variograms were defined by a range of 3,000 ft.

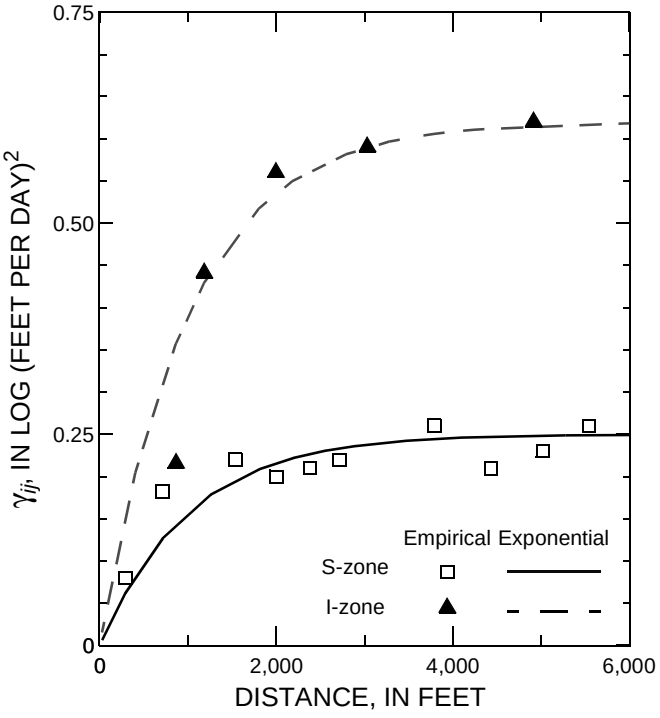

Figure 14. Empirical and exponential variograms of log hydraulic conductivity in the S-zone (layer 1) and the I-zone (layer 2).

Kriging estimates for each model node were generated from a weighted linear combination of the point estimates of log-hydraulic conductivity. The weights were determined by solving the kriging system of equations that minimizes the estimation error, subject to the constraints of unbiasedness (Isaaks and Srivastava, 1989). When solving the kriging system of equations, the exponential variogram placed more emphasis on measurements (point values) that were closer to a node location.

The hydraulic conductivity distribution of the S-zone (layer 1) was kriged from 79 measurements (7 multi-well aquifer tests, 13 single-well tests, and 59 slug tests) and the S-zone exponential variogram (fig. 14). Many measurements were along the runways and north of the golf course (fig. 15). A few measurements were near the dredge material holding areas; no measurements were available south of Lake Wonder Wood. Three principal areas of relatively low hydraulic conductivity in the S-zone were identified near SWMU-6/7, between the hangars and the eastern dredge material holding area, and north of the baseball fields (fig. 15).

The hydraulic conductivity distribution of the I-zone (layer 2) was kriged from 23 point estimates from 2 multi-well aquifer tests, 15 single-well tests, 5 slug tests, and a specific capacity test. The specific capacity test was less than 0.02 gallons per minute per foot (gal/min)/ft at well 2-34I and a hydraulic conductivity of 0.1 ft/d was assigned to this site. The I-zone exponential variogram (fig. 14) described the spatial structure of the lateral hydraulic conductivity measurements. Most of the measurements were near the runways and around the eastern dredge material holding area (fig. 16). There were no measurements beneath the golf course areas, along the Atlantic Ocean, or south of Lake Wonder Wood. Two areas of relatively low hydraulic conductivity in the I-zone were identified near the center of the runways and near Foxtrot pier (fig. 16).

The transmissivity (T) distribution of the I-zone (layer 2) was used in place of the hydraulic conductivity distribution in the flow model because the thickness of the I-zone is not a function of the water table. The transmissivity distribution of the I-zone was calculated by multiplying the lateral hydraulic conductivity distribution (fig. 16) by the corresponding thickness for layer 2 (fig. 8).

The initial areal distribution of leakance between layers 1 and 2 was defined by the presence or absence of the marsh-muck confining unit. Where the marsh-muck confining unit was 1 ft thick or greater (fig. 6), the marsh-muck confining unit was assumed to control the vertical movement of water. The initial leakance estimate for these areas was calculated by dividing the preliminary estimate of vertical hydraulic conductivity of the confining unit (0.001 ft/d) by the thickness of the marsh-muck confining unit (fig. 6). The vertical hydraulic conductivity of the aquifer was assumed to control the vertical movement of water where the marsh-muck confining unit was less than 1 ft thick (fig. 6). The initial leakance estimate for areas where the marsh-muck confining unit was thin or missing was calculated by multiplying the lateral hydraulic conductivity of the S-zone (fig. 15) by the vertical anisotropy determined from multi-well test results (table 2) and dividing it by the average internode distance between layers 1 and 2 (30 ft). A vertical anisotropy of $K_Z/K_{XY} = 0.1$ was applied consistently and is the rounded average of the non-unity values listed in table 2.

Different vertical leakances were assigned beneath Sherman Creek and Lake Wonder Wood. Sherman Creek is about 10 ft deep at SR A1A and was dredged between 1969 and 1972 from south of the dredge material holding areas to the canal along Patrol Road (fig. 1). Because the marsh-muck confining unit was assumed to be breached along the length of Sherman Creek, the leakance beneath the creek was arbitrarily set 1,000 times greater than the leakance of the surrounding marsh-muck confining unit in order to simulate the breach. Lake Wonder Wood, created between 1960 and 1965, was dredged to about 20 ft below sea level, and is well connected with the I-zone. Leakance below the lake was estimated during model calibration.

Tidal Effects and Surface-Water Features

The dominant surface-water features surrounding NAVSTA Mayport are the St. Johns River and the Atlantic Ocean along the northern and eastern edges, respectively (fig. 1). Both features are deep, tidally-influenced, saltwater bodies that communicate directly with the S-zone and the I-zone of the surficial aquifer system. The typical tidal range is about 6 ft but can be as much as 10 ft (U.S. Department of the Navy, 1995). The average stage of the St. Johns River and the Atlantic Ocean near NAVSTA Mayport is about 1 ft above sea level.

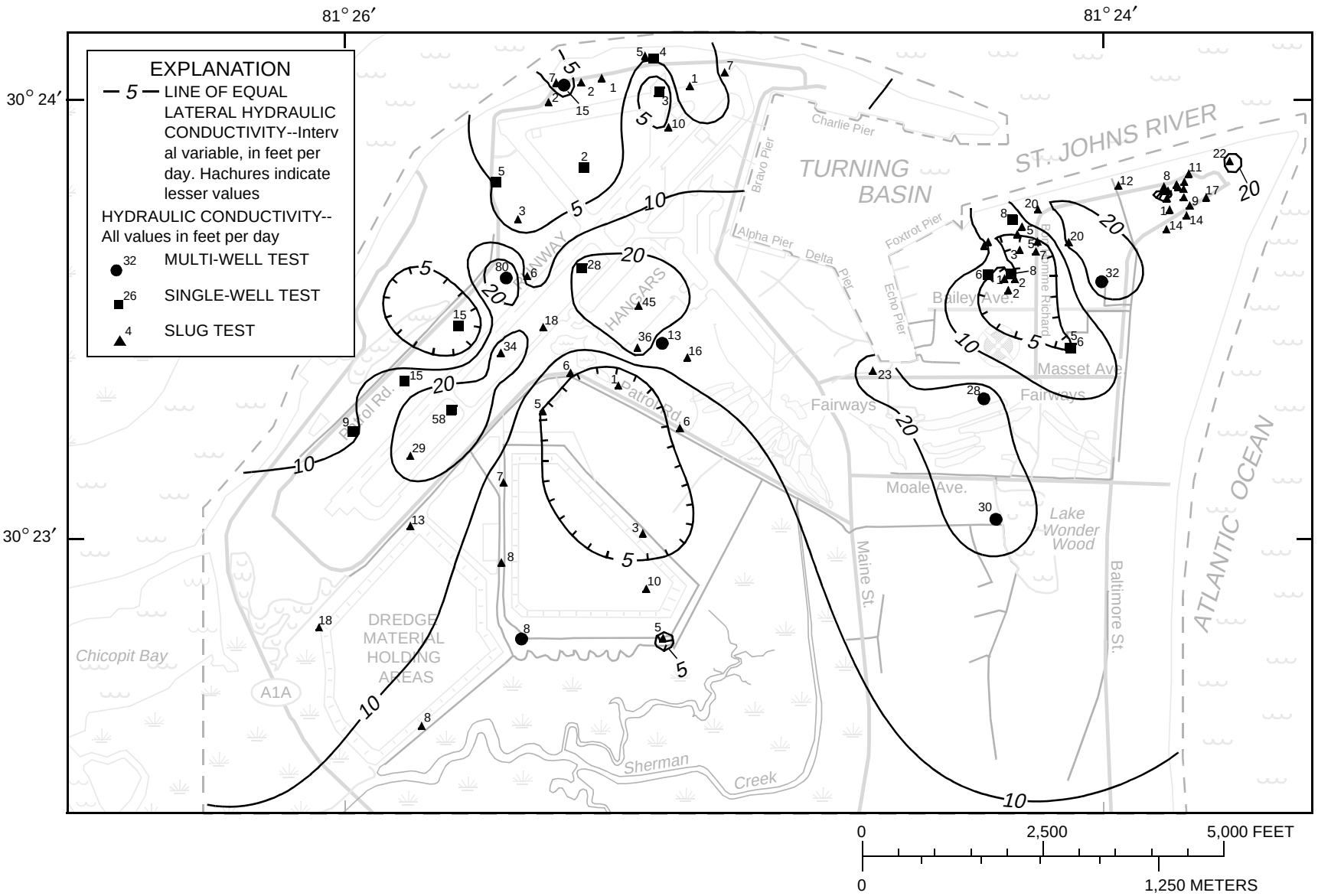

Figure 15. Lateral hydraulic conductivity of the S-zone (layer 1).

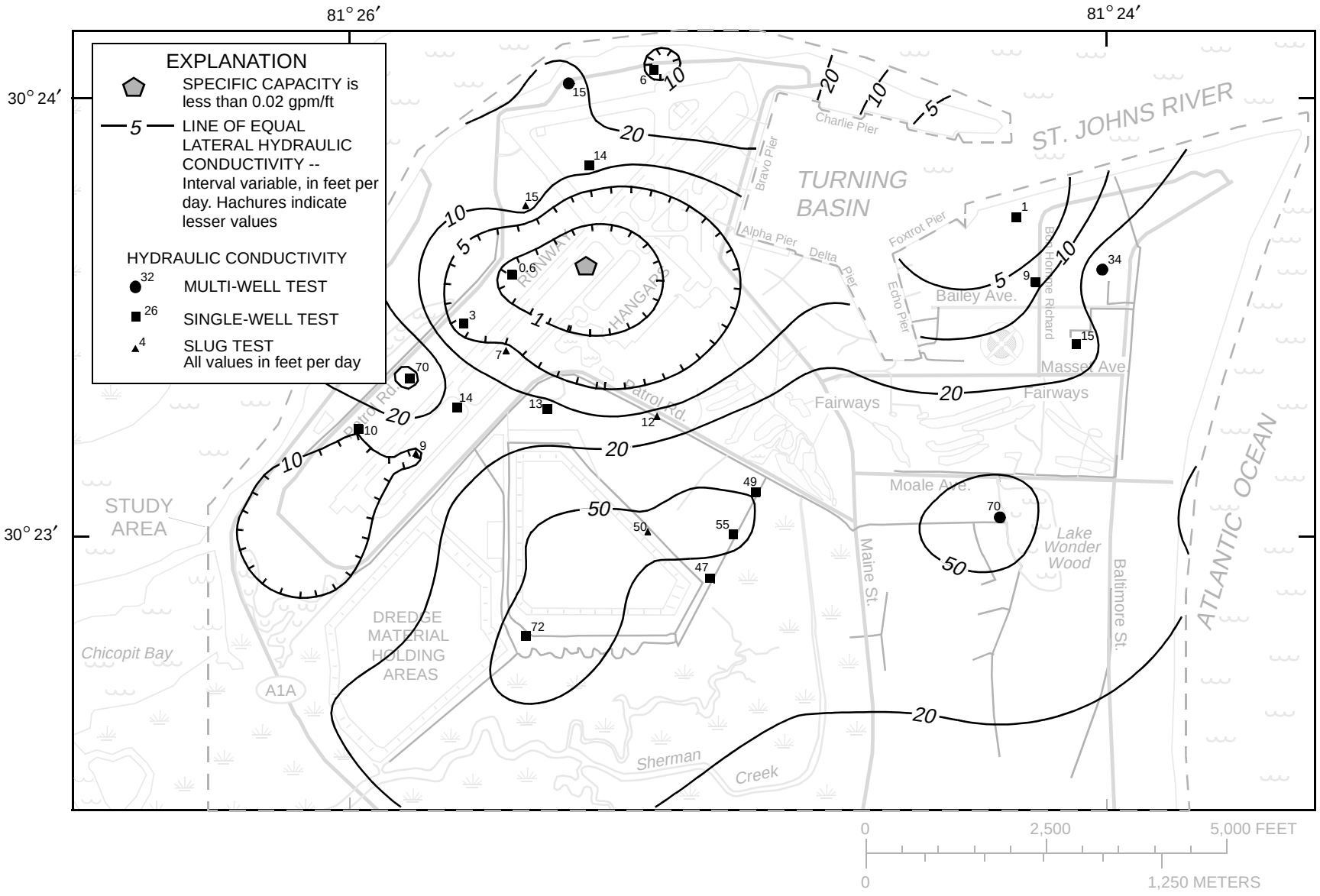

Figure 16. Lateral hydraulic conductivity of the I-zone (layer 2).

Chicopit Bay, Sherman Creek, and the unnamed canals that drain Lake Wonder Wood and the golf course area along Patrol Road also are tidally-influenced. The tidal range varies from about 6 ft at Sherman Creek and SR A1A to about 2 ft at the far reaches of the unnamed canals that drain Lake Wonder Wood and the golf course area along Patrol Road. The average stage of these features is also about 1 ft above sea level.

Measurable tidal effects propagate throughout most of the surficial aquifer system (fig. 17). Within 200 ft of the St. Johns River, vertical tidal displacements of 0.5 ft or more were observed in the S-zone near SWMU-6/7 and in the I-zone east of the turning basin. Tidal displacements decreased away from the shoreline but were still measurable in wells 8-5S and 8-5I by the runways and near the F-80 aquifer test site (fig. 17). East of the dredge material holding area and west of Lake Wonder Wood, ground-water displacements of more than 0.1 ft were responses to tidal fluctuations in the adjacent canals, not in the St. Johns River or the Atlantic Ocean (fig. 17).

The tidal displacement data can be used to independently evaluate the lateral hydraulic conductivity of the surficial aquifer system. If the tidal displacements do not significantly change the saturated thickness, then an analytical solution that describes the displacements in a one-dimensional, confined aquifer due to tidal forcing (Cooper and others, 1964) can be described by:

$$\Delta h_{Tide} = \frac{h_0}{2} e^{-x\sqrt{\frac{\pi S}{t_0 Kb}}} \sin\left(2\pi\frac{t}{t_0} - x\sqrt{\frac{\pi S}{t_0 Kb}}\right) , \quad (9)$$

where

h_0 is the amplitude of the tidal signal, in feet;
x is the distance from the tidal signal, in feet;
t_0 is the period of the tidal cycle, in days (about 0.52 day or 12.5 hours); and
t is the elapsed time since the beginning of a tidal cycle.

Equation 9 shows that the amplitude of water-level displacement in a given well is a function of the distance from the tidal signal and of the aquifer diffusivity, *Kb/S*.

Hydraulic characteristic estimates imposed by equation 9 tend to be qualitative because the appropriate specific yield or storage coefficient is unknown and can vary over three orders of magnitude or more. Specific yield estimates from multi-well aquifer tests of the S-zone ranged from 0.04 to 0.12 at clean sites and was about 0.004 near SWMU-6/7, where free product occurs at the water table. Storage coefficient estimates from multi-well tests of the I-zone ranged from 3×10^{-4} to 6×10^{-4}. Quantitative analysis is further complicated by the vertical transmission of the tidal signal between the I-zone and S-zone which causes diffusivity estimates from equation 9 to reflect a composite storage coefficient for both zones.

Relative differences between lateral and vertical hydraulic conductivity can be inferred between sites if the spatial variability of specific yield and storage coefficient are assumed to be minimal. Average diffusivities in the areas near wells 8-5S, 8-5I, and the F-80 aquifer test site (fig. 17) are about 500,000 feet squared per day (ft^2/d) based on an attenuation of the tidal amplitude to about 0.01 of the source and distances of between 1,000 and 1,500 ft (table 5). The differences in tidal displacements in the S-zone and I-zone at these three sites suggest that the vertical hydraulic conductivity near wells 8-5S and 8-5I is much less than near the F-80 aquifer-test site (fig. 17). The diffusivity of the area between the southwestern end of the runway and the St. Johns River is about 100,000 ft^2/d which suggests the transmissivity of the surficial aquifer system in this area should be about five times less than near well 8-5I or the F-80 aquifer-test site.

Vertical ground-water displacements were greater in the S-zone than in the I-zone east of the dredge material holding area and west of Lake Wonder Wood because the tidal signal originated in the adjacent canals (fig. 17). The vertical displacement in the I-zone at these sites probably was the result of the loading effect of the canals on the marsh-muck confining unit. The similar range of displacement in the S-zone and I-zone east of the dredge material holding area suggests that the leakance between the two zones is less in this area than west of Lake Wonder Wood.

Tidal fluctuation affects ground-water movement but does not affect the average ground-water flow rate or direction. Tidal fluctuation increases the potential for dispersion when the maximum tidally driven component of flow is greater than the topographically driven component of lateral ground-water flow. In areas near the shoreline, flow paths and dispersion are increased because shallow flow paths can be reversed and deeper flow paths along the freshwater/saltwater interface oscillate. Away from the shoreline and canals, the maximum

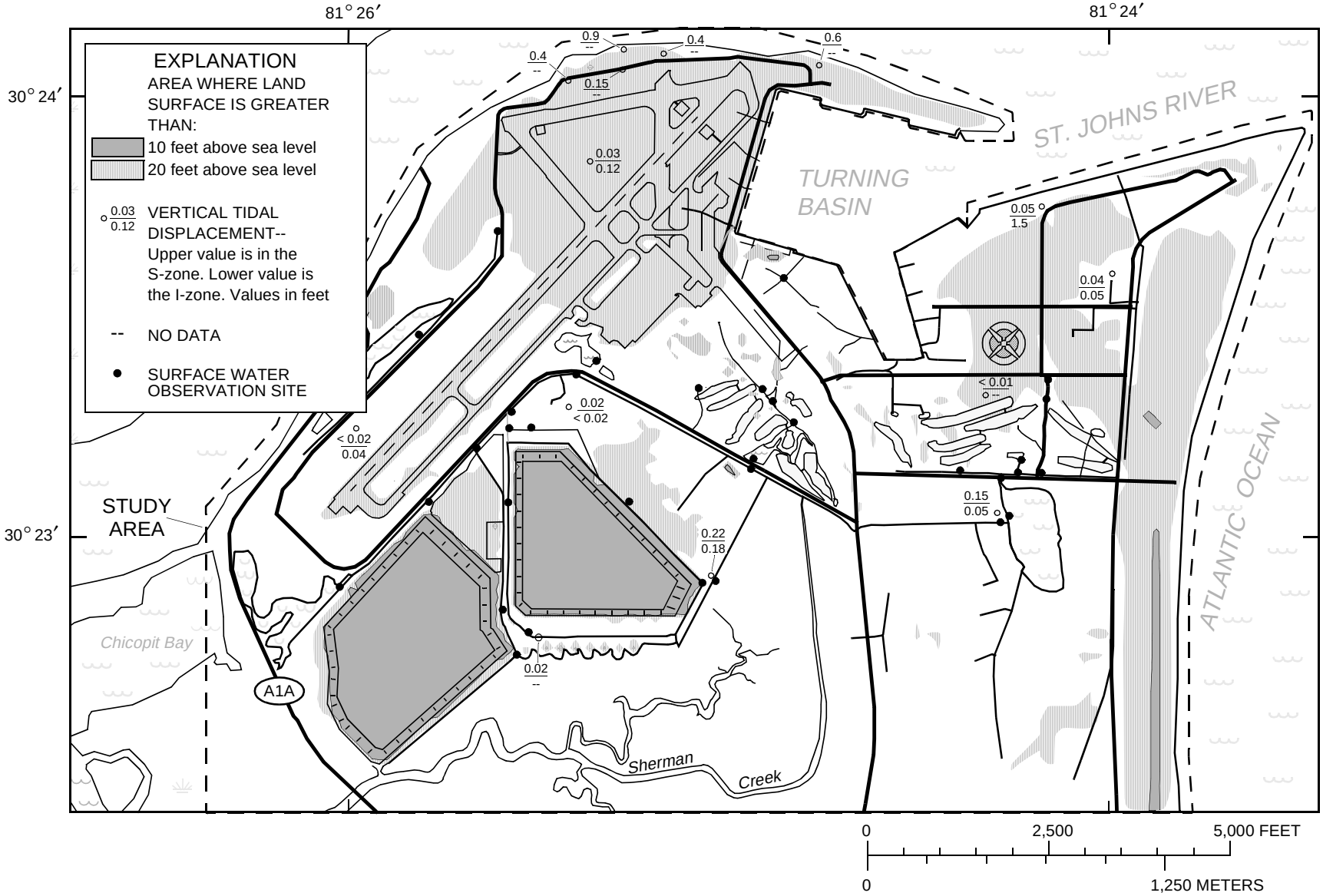

Figure 17. Generalized land surface altitudes in the study area, surface-water observation sites, and vertical tidal displacement measurement sites.

tidally driven component of velocity is small relative to the topographically driven component of lateral ground-water flow, thus producing a periodic increase and decrease in the ground-water flow rate but not lengthening the flow path.

Interaction between the S-zone (layer 1) of the surficial aquifer system and the St. Johns River and the Atlantic Ocean was simulated by specified heads at a stage of 1 ft above sea level. Tidal fluctuations were not simulated. Interaction between the I-zone (layer 2) and the St. Johns River and the Atlantic Ocean was simulated using drains with high conductances. This interaction could have been simulated with specified heads instead of drains and, as such, could add water to the volumetric budget. This additional water would account for the flow of saltwater along the freshwater/saltwater interface but would not be part of the freshwater flow system. The outlet head at each drain node was set to 1.75 ft (the average stage of the St. Johns River and the Atlantic Ocean plus the differential hydrostatic head between 30 ft columns of seawater and freshwater). The length of the column, 30 ft, represents the typical depth to the middle-to-upper I-zone below the St. Johns River and the Atlantic Ocean. This approximation of the freshwater/saltwater interface adequately simulates the freshwater flow system (app. B).

The distribution and altitude of surface-water features controls the direction and rate of ground-water flow in the surficial aquifer system. The distribution of surface-water features was determined from aerial photographs and plans of NAVSTA Mayport (C. Mitchell, Staff Civil Engineer Mayport, U.S. Navy, written commun., 1996). The elevations of the canals, creeks, lakes, and ponds were interpolated from the surveyed elevations at the surface-water observation sites shown in figure 17. The base of storm sewers typically was about 5 ft below land surface.

Table 5. Amplitude, phase shift, and wavelength of tidal signals in a one-dimensional, confined aquifer with different diffusivities driven by a source with a 1-foot amplitude

[Diffusivity: upper value is amplitude, in feet; lower value is the difference in phase in hours:minutes, assuming a 12.5-hour cycle]

Distance from source, in feet	Diffusivity, *Kb/S*, in feet squared per day				
	10,000	50,000	100,000	500,000	1,000,000
50	0.293 2:26	0.577 1:05	0.678 0:46	0.841 0:20	0.884 0:14
100	0.086 4:53	0.333 2:11	0.460 1:32	0.707 0:41	0.782 0:29
250	0.002 12:12	0.064 5:27	0.143 3:51	0.420 1:43	0.541 1:13
500	0.000 11:55	0.004 10:55	0.021 7:43	0.176 3:27	0.293 2:26
1,000		0.000 9:21	0.000 2:57	0.031 6:54	0.086 4:53
1,500				0.005 10:21	0.025 7:19
Wavelength, in feet	256	572	809	1,810	2,560

Interaction between the surficial aquifer system and the canals, creeks, marshes, storm sewers, lakes and ponds was simulated by river nodes. The simulated flow rate in or out of the aquifer at a river node was defined by:

$$Q_B = C_{RB}(H_{RIVER} - H_{AQUIFER}) \quad , \qquad (10)$$

where

C_{RB} is the hydraulic conductance of the riverbed, in feet squared per day;

H_{RIVER} is the average stage of the river or lake, in feet; and

$H_{AQUIFER}$ is the head in the aquifer beneath the river, in feet.

Equation 10 only applies if $H_{AQUIFER}$ is greater than or equal to the assigned elevation of the bottom of the surface-water feature.

A riverbed conductance of 100,000 ft^2/d was used for all river nodes and was not estimated. The results of model simulations of similar aquifer conditions at Cecil Field NAS (Halford, 1998) indicated that model results would not be sensitive to changes in riverbed conductance. The ground-water flow model at Cecil Field NAS was insensitive to increasing riverbed conductance and estimates of riverbed conductance were highly correlated with estimates of lateral hydraulic conductivity of the surficial aquifer, a more sensitive parameter than the riverbed conductance. This result implies that surface-water interaction is controlled by the hydraulic conductivity of the surficial aquifer rather than the riverbed conductance; model calibration at NAVSTA Mayport was conducted accordingly.

All canals, creeks, marshes, storm sewers, lakes and ponds shown in figure 1 were represented in the model. A total of 3,197 river nodes was assigned to layer 1 of which 2,222 simulated the marsh in the southwestern part of the study area. The river bottom elevation for all canals, creeks, marshes, and storm sewers was set equal to the river stage to ensure all

simulated reaches were either gaining or inactive. For the lakes and ponds, the river bottom was set far below the altitude of the water surface so water could be gained or lost from these features.

Ground water is diffusely discharged in areas between the southwestern runway and the St. Johns River, northeast of the dredge material holding areas, and over much of the golf course. These diffuse discharge areas can shrink or expand depending on the frequency and intensity of rainfall or irrigation events. All land areas not occupied by a visible surface-water feature were simulated as drains with high conductances and outlet heads set at land surface. If the water table rises to land surface, the drains behave as specified heads and simulate the removal of water from the S-zone (layer 1); otherwise they have no effect. Conceptually, the drain nodes simulated the effects of relatively high evapotranspiration and ground-water discharge in these areas.

Boundary Conditions

Proper representation of model boundary conditions is one of the most important aspects in the simulation of an aquifer system. Model boundaries are assigned to represent the actual hydrologic boundaries as accurately as possible. If model boundaries are generalized, they are placed far enough away from the influence of hydrologic stresses in the model area to minimize their influence on simulation results.

The upper boundary, layer 1, is the water table and is represented in MODFLOW as a free surface except where the water table intersects land surface. Six zones of spatially uniform recharge rates were applied to this boundary in all simulations (fig. 18). The predominant areas were unirrigated, pervious surfaces. The dredge material holding areas were differentiated from the other unirrigated recharge areas because they are elevated (fig. 17) and have diked perimeters that impede surface runoff (fig. 9). Areas identified as golf-course irrigation were assigned only to the fairways and greens (fig. 18). The underflow recharge areas are those where water moves beneath impervious surfaces and enters into storage after recharge events. This water then is later released from storage as drainage. The flux across the water table was not uniform in each area due to rejection of water where the water table was near or at land surface.

The lower model boundary is the contact between the surficial aquifer system and the intermediate confining unit and is simulated as a no-flow boundary. The potential flow across this boundary is upward from the Upper Floridan aquifer to the surficial aquifer system because of the upward gradient between the two aquifers. The potentiometric surface of the Upper Floridan beneath NAVSTA Mayport is about 25 to 30 ft above sea level (Halford and others, 1993) and water levels in the surficial aquifer system typically range from 1 to 10 ft above sea level.

The lateral model boundaries in both layers 1 and 2 are no-flow boundaries that coincide with surface-water features. The northern and eastern edges of the study area lie within the St. Johns River and the Atlantic Ocean, respectively. Two-thirds of the southern boundary and the western boundary pass through marsh along Sherman Creek and Chicopit Bay (fig. 1). Flow does not cross these boundaries because no hydraulic gradient exists transverse to the boundaries. The eastern one-third of the southern boundary crosses the coastal ridge perpendicularly (fig. 17). This divide constitutes a no-flow boundary because water flows parallel to the boundary. The boundary along the turning basin perimeter is a no-flow boundary because the retaining walls beneath the piers are made of two layers of interlocking sheet pile with a grout fill (U.S. Department of the Navy, 1995) and are assumed to be impervious except where breached by storm sewers.

Model Calibration

Calibration is the attempt to reduce the difference between model results and measured data by adjusting model input. Calibration was accomplished in this study by adjusting input values of vertical hydraulic conductivity and recharge until an acceptable calibration criterion was achieved. The "goodness" or improvement of the calibration is based on the differences between simulated and measured ground-water levels and stream discharges. Simulated water levels and discharges from a calibrated, deterministic ground-water model commonly depart from measured water levels and discharges, even after a diligent calibration effort. The discrepancy between model results and measurements (model error) commonly is the cumulative result of simplification of the conceptual model, grid scale, and the difficulty in obtaining sufficient measurements to account for all of the spatial variation in hydraulic properties and recharge throughout the model area.

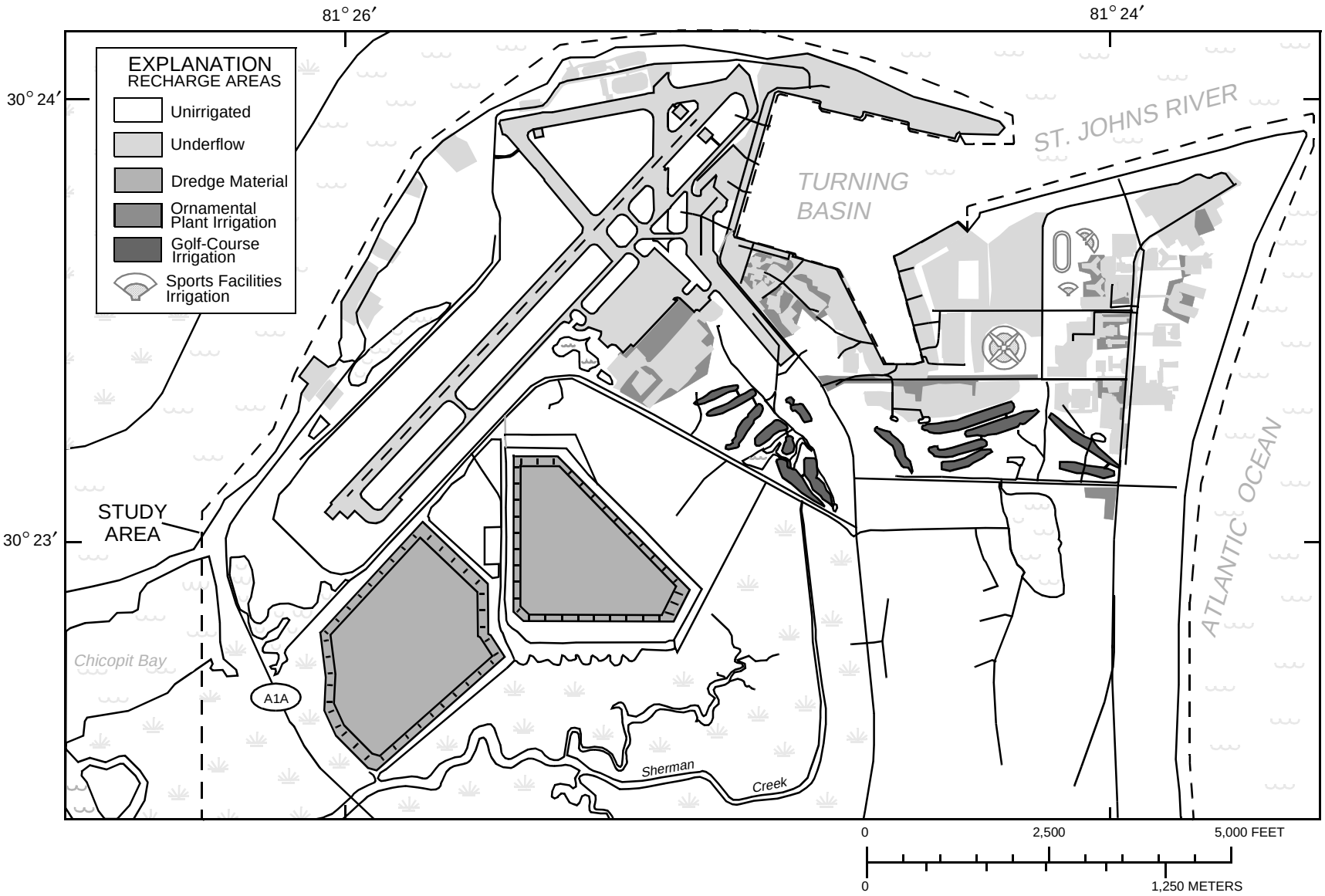

Figure 18. Recharge area delineation based on recharge source.

The ground-water flow model was calibrated to 229 water-level measurements from 181 wells. Water-level data were obtained from three synoptic surveys conducted during July 17, 1995, to October 24, 1996. Synoptic water-level measurements were affected by factors not accounted for by the model. Some water-level measurements near SWMU-6/7 were rejected for calibration purposes because of obvious tidal effects. Other water-level measurements along the periphery of the western dredge material holding area were not used due to discretization effects and steep gradients in close proximity to a drainage feature. The synoptic surveys were treated as independent "snapshots" of the ground-water system taken at various times (Halford, 1998).

The data from these surveys were fitted to the simpler steady-state equation:

$$\nabla \bullet (Kb\nabla h) + q + N' = 0 \quad , \tag{11}$$

where

N' is the effective recharge rate during a given survey, in feet per day, which is the summation of precipitation, surface runoff, evapotranspiration, and water released from storage and can be summarized by

$$N' = (P - Q_o) - ET - S_y \frac{\partial h}{\partial t} \, . \tag{12}$$

Although the effective recharge rates, N', estimated for each synoptic survey period are not estimates of the average recharge rate, estimates obtained during extreme conditions can bracket the average recharge rate (Halford, 1998).

Some stresses must be known to calibrate a model if both recharge rates and hydraulic conductivities are simultaneously adjusted. When the use of equation 11 is appropriate, the stresses and recharge rates are proportional to the hydraulic conductivity. Usually, the lateral and vertical hydraulic conductivities are estimated when calibrating ground-water flow models of a surficial aquifer system. Commonly, stream discharge during baseflow conditions is assumed to represent the recharge rate to the aquifer during a specified period. At NAVSTA Mayport, ground-water discharge from the surficial aquifer system is an insignificant and unmeasureable contribution (less than 10 ft^3/s) relative to the tidal flow (more than 100,000 ft^3/s).

In a coastal setting like the one at NAVSTA Mayport, a successful calibration strategy is based on knowing the lateral hydraulic conductivity distributions of the flow zones and estimating recharge rates during model calibration. Ground-water flow rates estimated with this approach are not dependent on the quality of stream discharge measurements and assumptions about baseflow. Instead, the accuracy of flow-rate estimates is dependent on the quality of lateral hydraulic conductivity estimates.

Calibration improvement was determined by decreases in the sum-of-squares (SS) error which is defined by

$$SS = \sum_{k=1}^{nwl} [(\hat{h}_k - h_k) w_k]^2 \quad , \tag{13}$$

where

$\hat{h}_k$ is the $k^{\underline{th}}$ simulated water level, in feet;
h_k is the $k^{\underline{th}}$ measured water level, in feet;
nwl is the number of water-level comparisons; and
w_k is the $k^{\underline{th}}$ weight which was subjectively used to reduce the bias towards periods with more water levels. Weights of 1, 2, and 4 were applied to observations in synoptic-survey periods 1, 2, and 3 which had 180, 40, and 9 observations, respectively.

Although the sum-of-squares error serves as the objective function, root-mean-square (RMS) error is reported instead because RMS error is more directly comparable to actual values and serves as a composite of the average and the standard deviation of a set. Root-mean-square error is related to the sum-of-squares error by

$$RMS = \sqrt{\frac{SS}{nwl}} \quad . \tag{14}$$

Because measured water levels rarely coincide with the center of a cell, simulated water levels were interpolated laterally to points of measurement from the centers of surrounding cells. Simulated water levels were interpolated because they were assumed to be part of a continuous distribution. Vertical interpolation was not considered because of the discontinuity and associated refraction of potential fields from an aquifer across a confining unit.

Parameter Estimation

Model calibration is facilitated by a parameter estimation program (Halford, 1992). The parameter estimation process is initialized by using the model to establish the initial differences between simulated and measured water levels. These differences, or residuals, are then minimized by the parameter estimation program. To implement parameter estimation, the sensitivity coefficients (the derivatives of simulated water level change with respect to parameter change) are calculated by the influence coefficient method using the initial model results (Yeh, 1986). Each parameter is changed a small amount and MODFLOW is used to compute new water levels for each perturbed parameter. The current arrays of sensitivity coefficients and residuals are used by a quasi-Newton procedure (Gill and others, 1981, p. 137) to compute the parameter changes that should improve the model. The model is updated to reflect the latest parameter estimates and a new set of residuals is calculated. The entire process of changing a parameter in the model, calculating new residuals, and computing a new value for the parameter is continued iteratively until model error or model-error change is reduced to a specified level or until a specified number of iterations are made (Halford, 1992).

Logs of the parameters are estimated because vertical hydraulic conductivities are usually log-normally distributed (Domenico and Schwartz, 1990). Log-parameters also are better behaved from a numerical perspective because the estimates are restricted to positive values and are scaled to some degree. Log-recharge rates also are used, thus ensuring that all estimated values of N' are positive.

Sixteen parameters (table 6) were used as global multipliers that changed the value of either vertical hydraulic conductivity or effective recharge rates by a fixed amount throughout specific zones. The initial values of vertical hydraulic conductivity in the marsh-muck confining unit were derived directly from

Table 6. Initial, calibrated, and alternative values of parameters estimated to calibrate the model

[ft/d, feet per day; in/yr, inches per year; ft, feet]

Estimated parameter	Initial	Calibrated	l-zone transmissivity[a]	
			Halved	Doubled
K_Z/K_{XY} aquifer, dimensionless	0.1	0.05	0.03	0.06
K_Z marsh-muck confining unit, ft/d	.001	.0003	.0001	.001
K_Z Lake Wonder Wood[b], ft/d	.1	.02	.02	.02
$N'_{unirrigated}$, period 1, in/yr	10	8.2	5.5	12.2
$N'_{Golf\text{-}Course}$, period 1, in/yr	10	69	69	74
$N'_{Dredge\ Material}$, period 1, in/yr	10	21	21	21
$N'_{Underflow}$, periods 1 and 3, in/yr	.1	.8	.7	.8
$N'_{Sports\ Facilities}$, periods 1and 3, in/yr	10	46	40	64
$N'_{Ornamental\ Plant\ Irrigation}$, in/yr	10	18	13	26
$N'_{unirrigated}$, period 2, in/yr	10	5.8	3.9	7.9
$N'_{Golf\text{-}Course}$, period 2, in/yr	10	59	57	63
$N'_{Dredge\ Material}$, period 2, in/yr	10	13	12	12
$N'_{Sports\ Facilities}$, period 2, in/yr	10	25	24	33
$N'_{Underflow}$, period 2, in/yr	.1	1.2	1.1	1.3
$N'_{unirrigated}$, period 3, in/yr	10	14.1	8.8	24
$N'_{Golf\text{-}Course}$, period 3, in/yr	10	114	117	113
Weighted RMS error, in ft	1.82	.76	.78	.83

[a] The calibrated parameter estimates were used as initial estimates for both alternative models. The initial weighted RMS errors of the halved and doubled models were 1.20 and 1.11 feet, respectively.

[b] The vertical leakance below Lake Wonder Wood was estimated by dividing this value by the thicknesses shown in figure 6.

the multi-well test results. An initial effective recharge rate of 10 in/yr was used for all three synoptic-survey periods. Final parameter estimates were not sensitive to the initial parameter estimates.

The unweighted minimum, maximum, average, and RMS errors of the calibrated model were -2.78, 1.92, 0.00, and 0.82 ft, respectively. A more detailed listing of the error statistics by layer and synoptic-survey period is provided in table 7. The greater number of water-level measurements available during synoptic-survey period 1 did not overly bias model calibration toward that period (table 7). The water-level residuals did not exhibit any apparent trend across the study area during any of the synoptic-survey periods (figs. 19-20). Simulated potentiometric surfaces and water-level residuals are only shown for synoptic-survey period 1 because the distribution of residuals is similar in all periods.

Simulated water levels for the three synoptic-survey periods approximated the measured levels throughout the approximately 12-ft range observed in the study area (fig. 21). The measured water level range from 1 to 13 ft above sea level is similar to the simulated water level range from 1 to 20 ft above sea level in the surficial aquifer system. Water levels probably are greater than 13 ft above sea level towards the centers of the dredge material holding areas, but no wells existed to measure water levels. The water-level residuals were normally distributed and 78 percent of the simulated water levels were within 1 ft of the measured water levels.

Although the model can simulate the ground-water flow system beneath NAVSTA Mayport fairly well, there are a few areas where model results may be deficient. The simulated water table south of the runway and north of the western dredge material holding area is 2 to 3 ft less than the measured water table, probably because lateral hydraulic conductivity of the S-zone was overestimated (note the residuals of -3 and -2 ft in fig. 19). The simulated potentiometric surface of the I-zone is about 2 ft less than the measured surface near Baltimore St. and Masset Ave. (fig. 20). These differences could indicate that either the recharge rate in this area was underestimated or the transmissivity between this area and the Atlantic Ocean was overestimated.

Estimated parameters were not highly correlated (table 8). Recharge from golf course irrigation and sports facilities irrigation during synoptic-survey period 2 was the most highly correlated pair of parameters (0.72). The vertical anisotropy of the aquifer, K_Z/K_{XY}, was somewhat correlated (-0.69) with the effective recharge rate of the unirrigated areas for period 3. Very little correlation existed between the vertical anisotropy of the aquifer and any of the other recharge rate estimates during periods 1 and 2 (table 8), during which many more water levels were measured.

Table 7. Water-level error statistics by layer and synoptic-survey period from calibrated Mayport model results

[$N'_{unirrigated}$, effective recharge rate estimate; in/yr, inches per year; n, number of samples; maximum, minimum, average, and RMS in feet]

Zone (Layer)	SYNOPTIC-SURVEY PERIOD														
	(1) July 17, 1995 $N'_{unirrigated}$ = 8.2 in/yr					(2) July 31, 1996 $N'_{unirrigated}$ = 5.8 in/yr					(3) October 24, 1996 $N'_{unirrigated}$ = 14.1 in/yr				
	Minimum	Maximum	Average	RMS	n	Minimum	Maximum	Average	RMS	n	Minimum	Maximum	Average	RMS	n
S (1)	-2.78	1.92	0.02	0.86	156	-1.84	1.26	-0.04	0.74	29	-2.23	0.75	-0.35	1.10	7
I (2)	-1.67	1.03	.02	.65	24	-1.62	.47	-.15	.64	11	-.08	-.08	-.08	.08	2
All	-2.78	1.92	.02	.84	180	-1.84	1.26	-.07	.71	40	-2.23	.75	-.29	.97	9
Composite water level statistics for all periods											-2.78	1.92	.00	.82	229

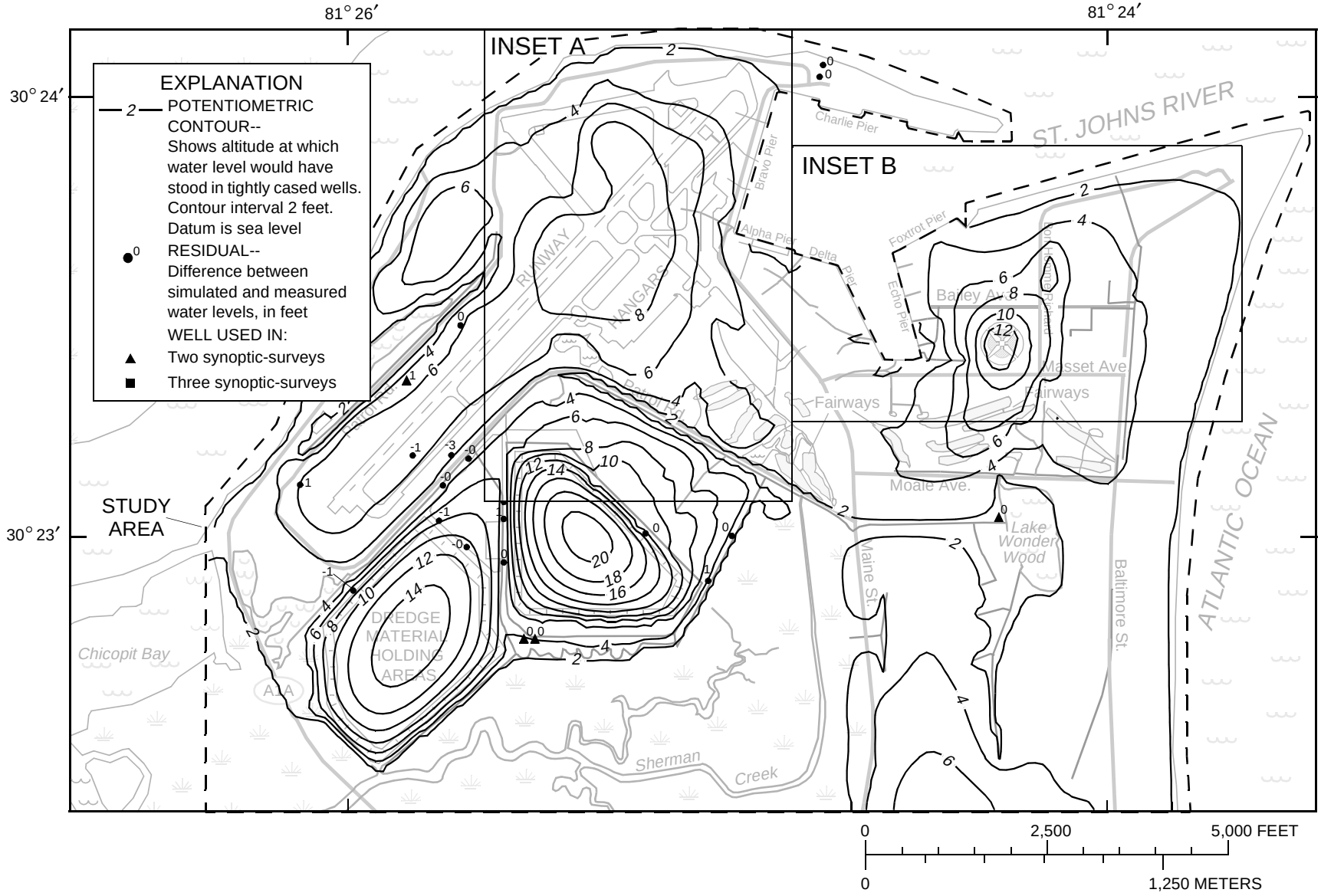

Figure 19. Simulated potentiometric surface of the S-zone (layer 1) on July 17, 1995.

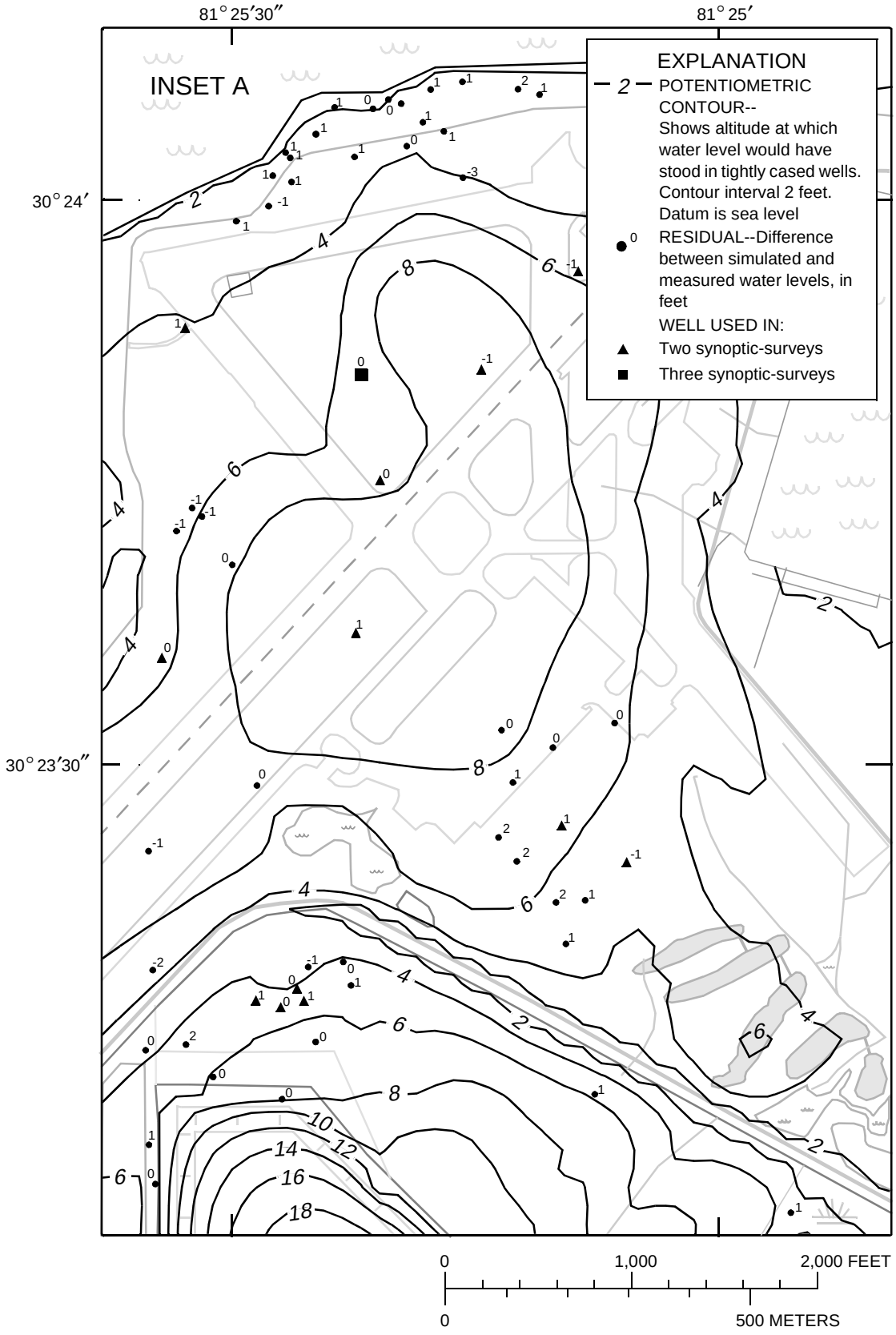

Figure 19. Inset A.

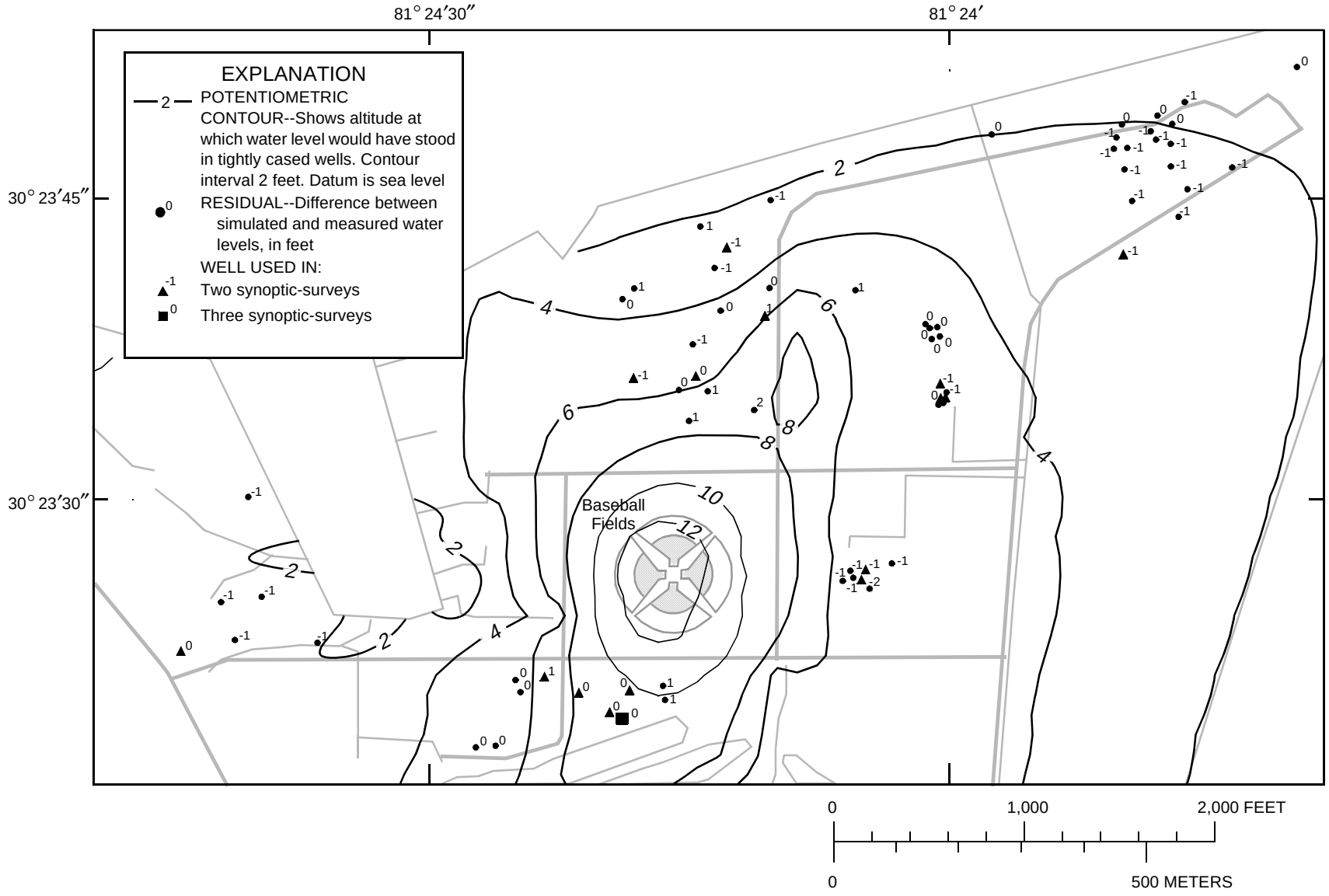

Figure 19. Inset B.

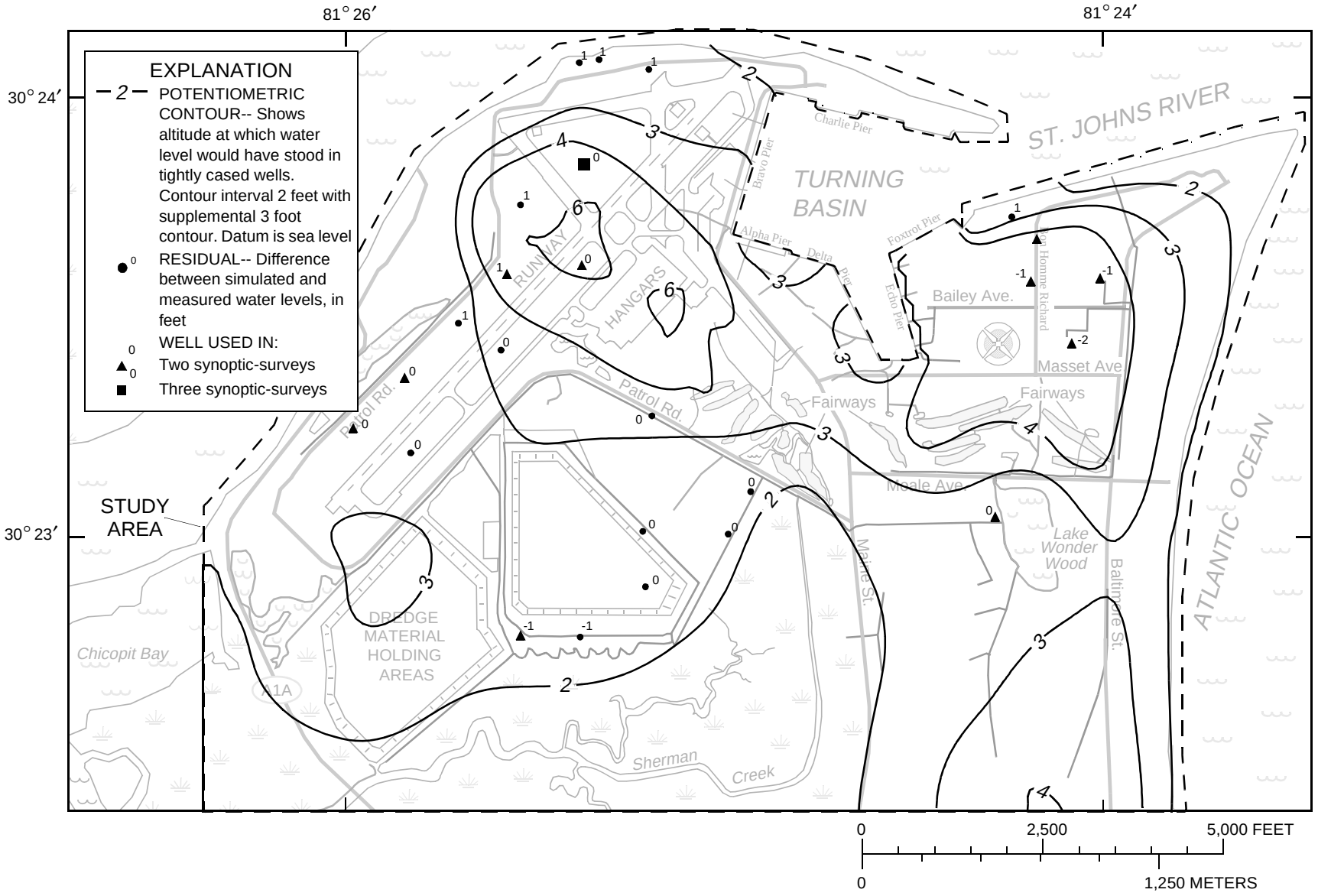

Figure 20. Simulated potentiometric surface of the I-zone (layer 2) on July 17, 1995.

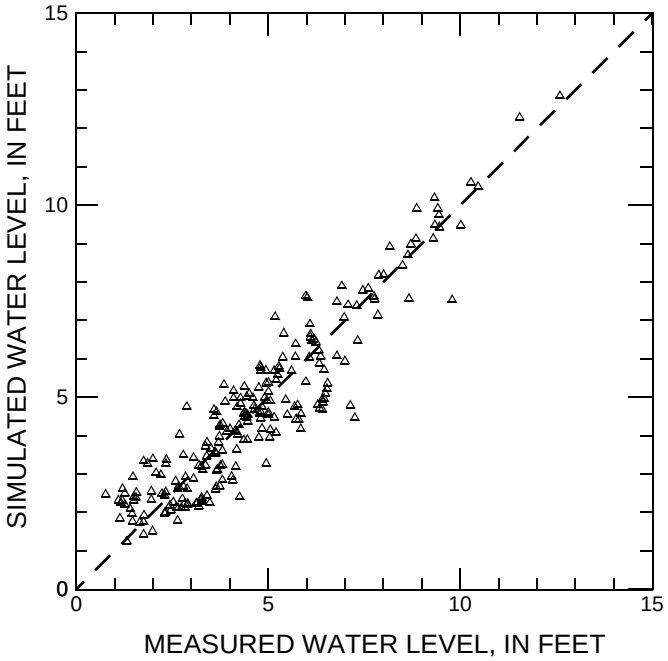

Figure 21. Simulated and measured water levels for the calibrated model.

Sensitivity Analysis

To determine how model parameters affected simulation results, each estimated parameter (except for K_Z Lake Wonder Wood) was varied independently from 0.2 to 5 times their calibrated value. This range was greater than the uncertainties associated with the parameters, but provided a more complete perspective on parameter sensitivity. Model sensitivity was described in terms of weighted RMS error. The sensitivity of model results to changing one parameter while all others are held at their calibrated values is shown in figure 22. Model error was determined to be most sensitive to changes in effective recharge rates to the unirrigated and golf-course irrigation areas and the vertical anisotropy of the aquifer. The model was least sensitive to changes in the effective recharge rate of the underflow areas and was more sensitive to overestimation of this parameter (fig. 22).

Although the lateral hydraulic conductivity distributions of the S-zone (layer 1) and the I-zone (layer 2) were not changed during model calibration,

Table 8. Correlation coefficients between parameters from the calibrated model
[--, not applicable]

Estimated parameters	Correlation coefficients, $\rho_{i,j}$																
$N'_{unirrigated}$, period 3	1.00	--	--	--	--	--	--	--	--	--	--	--	--	--	--	--	--
$N'_{unirrigated}$, period 1	0.00	1.00	--	--	--	--	--	--	--	--	--	--	--	--	--	--	--
$N'_{unirrigated}$, period 2	.00	0.00	1.00	--	--	--	--	--	--	--	--	--	--	--	--	--	--
$N'_{Golf\text{-}Course}$, period 2	.00	.00	0.18	1.00	--	--	--	--	--	--	--	--	--	--	--	--	--
$N'_{Golf\text{-}Course}$, period 1	.00	.14	.00	0.00	1.00	--	--	--	--	--	--	--	--	--	--	--	--
K_Z/K_{XY} aquifer	-.69	-.21	-.20	-.09	-0.08	1.00	--	--	--	--	--	--	--	--	--	--	--
$N'_{Golf\text{-}Course}$, period 3	.02	.00	.00	.00	.00	-0.02	1.00	--	--	--	--	--	--	--	--	--	--
$N'_{Ornamental\ Plant\ Irrigation}$	.01	.27	.29	.35	.26	-.22	0.10	1.00	--	--	--	--	--	--	--	--	--
$N'_{Dredge\ Material}$, period 1	.00	.10	.00	.00	.01	.00	.00	0.03	1.00	--	--	--	--	--	--	--	--
K_Z marsh-muck confining unit	-.31	-.04	.04	-.15	-.06	.19	-.04	.00	0.03	1.00	--	--	--	--	--	--	--
$N'_{Sports\ Facilities}$, periods 1and 3	.00	.29	.00	.00	.32	-.10	.13	.29	.00	-0.10	1.00	--	--	--	--	--	--
$N'_{Sports\ Facilities}$, period 2	.00	.00	.29	.72	.00	-.11	.00	.40	.00	-.12	0.00	1.00	--	--	--	--	--
$N'_{Underflow}$, period 2	.00	.00	.70	.28	.00	-.14	.00	.37	.00	-.03	.00	0.64	1.00	--	--	--	--
$N'_{Underflow}$, periods 1 and 3	.00	.57	.00	.00	.15	-.13	.00	.37	.02	-.14	.60	.00	0.00	1.00	--	--	--
K_Z Lake Wonder Wood	.00	-.09	-.13	-.18	-.14	.10	-.03	-.28	.00	.00	-.16	-.20	-.15	-0.10	1.00	--	--
$N'_{Dredge\ Material}$, period 2	.15	.00	.14	.02	.00	-.11	.00	.06	.00	.30	.00	.01	.08	.00	-0.01	1.00	--
$\rho_{i,j} = \frac{C_{i,j}}{\sqrt{C_{i,i}C_{j,j}}}$	$N'_{unirrigated}$, period 3	$N'_{unirrigated}$, period 1	$N'_{unirrigated}$, period 2	$N'_{Golf\text{-}Course}$, period 2	$N'_{Golf\text{-}Course}$, period 1	K_Z/K_{XY} aquifer	$N'_{Golf\text{-}Course}$, period 3	$N'_{Ornamental\ Plant\ Irrigation}$	$N'_{Dredge\ Material}$, period 1	K_Z marsh-muck confining unit	$N'_{Sports\ Facilities}$, periods 1and 3	$N'_{Sports\ Facilities}$, period 2	$N'_{Underflow}$, period 2	$N'_{Underflow}$, periods 1and 3	K_Z Lake Wonder Wood	$N'_{Dredge\ Material}$, period 2	
Normalized main diagonal $\sqrt{\frac{C_{i,i}}{C_{1,1}}}$	1.00	.47	.38	.34	.29	.29	.19	.19	.17	.17	.16	.14	.06	.06	.02	.01	

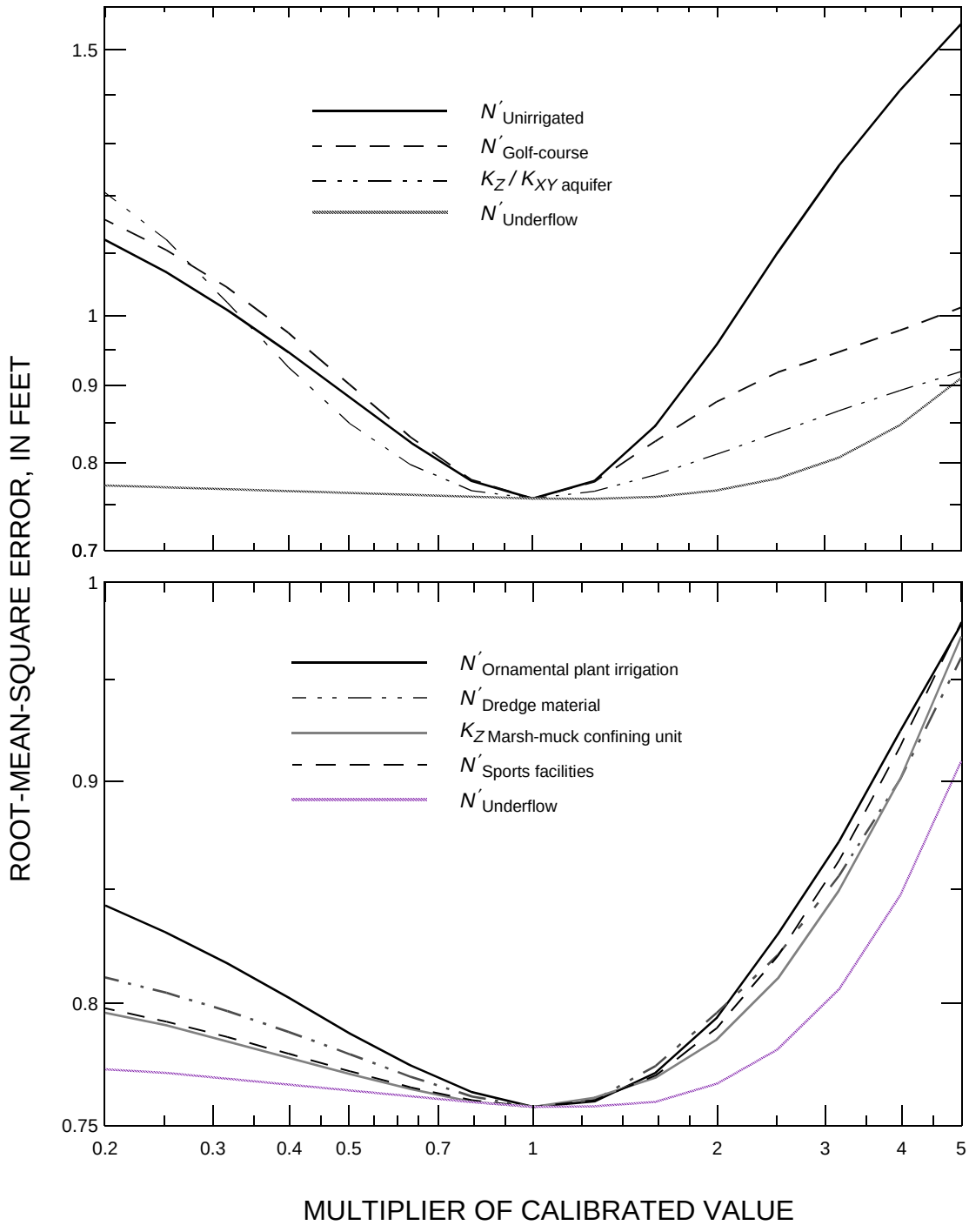

Figure 22. Model sensitivity to independent changes in selected calibration parameters.

estimates of these distributions affect effective recharge rate and vertical hydraulic conductivity estimates. These effects were investigated by estimating the same parameters listed in table 6 with two alternative models. The lateral hydraulic conductivity of the I-zone was assumed to be half of the best estimate for one alternative model and double the best estimate for the other alternative model. The lateral hydraulic conductivity of the I-zone was varied because it is less well known than the lateral hydraulic conductivity of the S-zone.

Effective recharge rates to the unirrigated areas and vertical hydraulic conductivity estimates of the alternative models differed most from the calibrated

model. Effective recharge rate estimates from the calibrated model decreased 33 percent in the halved model and increased 50 percent in the doubled model. The vertical hydraulic conductivity of the marsh-muck confining unit was decreased 70 percent in the halved model and increased by a factor of three in the doubled model. The RMS errors of the halved and doubled models, 0.78 and 0.83 ft, were slightly greater than the RMS error of the calibrated model, 0.75 ft. The alternative models show that a relatively small RMS error alone does not assure a well calibrated model and either some stresses or hydraulic conductivities must be known.

Estimation of the Average Recharge Rate

Instead of conceptualizing the effective recharge rates estimated for each synoptic survey period as volumetric rates, they can be thought of as measures of the energy release rate or discharge from the flow system during each period. Rising or declining water levels represent increasing or decreasing rates of discharge from the surficial aquifer system. Discharge rates increase even as the surficial aquifer system is recharged, analogous to the increase in discharge from a leaky bucket as it is filled.

The relation between water level and effective recharge rate (eq. 12) is expected to be linear and can be used to estimate the daily aquifer discharge rate. The effective recharge rates that were applied to the unirrigated areas for periods 1, 2, and 3 were regressed against the water levels in well 8-5I during the respective periods. The effective recharge rates were correlated with the water levels (fig. 23) and could be estimated on a daily basis using the hydrograph for well 8-5I (fig. 10).

The recharge rate over the period of water-level record (fig. 10) was 7.6 in/yr and was estimated by averaging the effective recharge rate (estimated from the relation in fig. 23). The recharge rate for 1996 was probably closer to 7 in/yr because the first 3 months of the year (without water-level record) were comparatively drier (fig. 10). The recharge rate over the last 36 years is probably closer to 8 in/yr because 1996 was a relatively dry year (44 in. compared to an average precipitation rate of 51 in/yr between 1961 and 1996).

The median recharge rate (6.6 in/yr) is lower than the average rate (7.6 in/yr) because recharge is not uniformly distributed throughout the year. Recharge events were of a smaller magnitude from

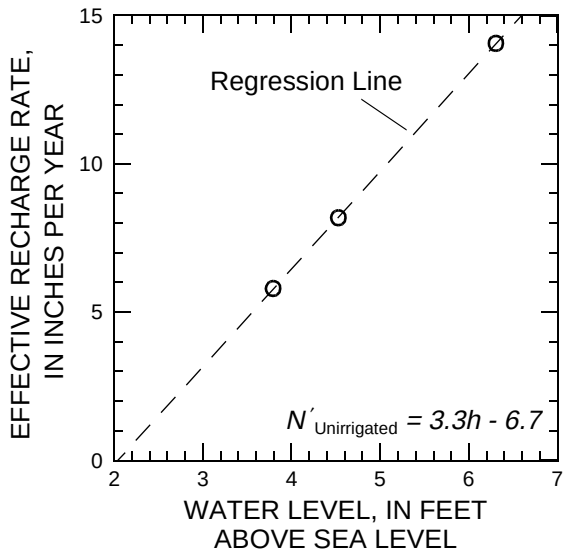

Figure 23. Relation between water levels measured in well 8-5I and effective recharge rate estimates for the unirrigated areas.

winter through early summer (fig. 10) and the daily effective recharge rate (estimated from the relation in fig. 23) ranged from about 5 to 8 in/yr during this period. Intense precipitation events in the fall produced effective recharge rates as great as 22 in/yr. The effective recharge rate remained greater than the average rate for almost 2 months after a 12-in. precipitation event in early October.

Ground-Water Flow during the Calibration Period

The analysis of ground-water flow and potential movement of contaminants within the surficial aquifer system was addressed using the calibrated model driven by the recharge rate distribution estimated for period 1. This recharge rate distribution was assumed to be representative of the average rate of water application to the surficial aquifer system because the recharge rate to the unirrigated areas was about 8 in/yr. The response of the ground-water system to recharge rates that are lower than average is discussed because the effective recharge rate on any given day is less than the average amount of recharge received during a year. Flow conditions related to higher-than-average recharge rates also are discussed because the locations of discharge points of ground-water flow paths and the rate of contaminant travel to those discharge locations vary according to changes in recharge rates.

The water table configuration is strongly influenced by drainage features. The simulated lateral flow direction in the S-zone commonly is perpendicular to the nearest drainage feature (fig. 19). One exception is in the area near well 8-5I, where the lateral flow direction is affected by the spatial variability in hydraulic conductivity and the predominant flow direction is downward. The simulated potentiometric surface of the I-zone is strongly influenced by the larger surface-water features (fig. 20).

Schematics of the simulated volumetric flow budgets for the three synoptic survey periods are presented in figure 24. The volumetric budget for period 1 is most representative of estimated average

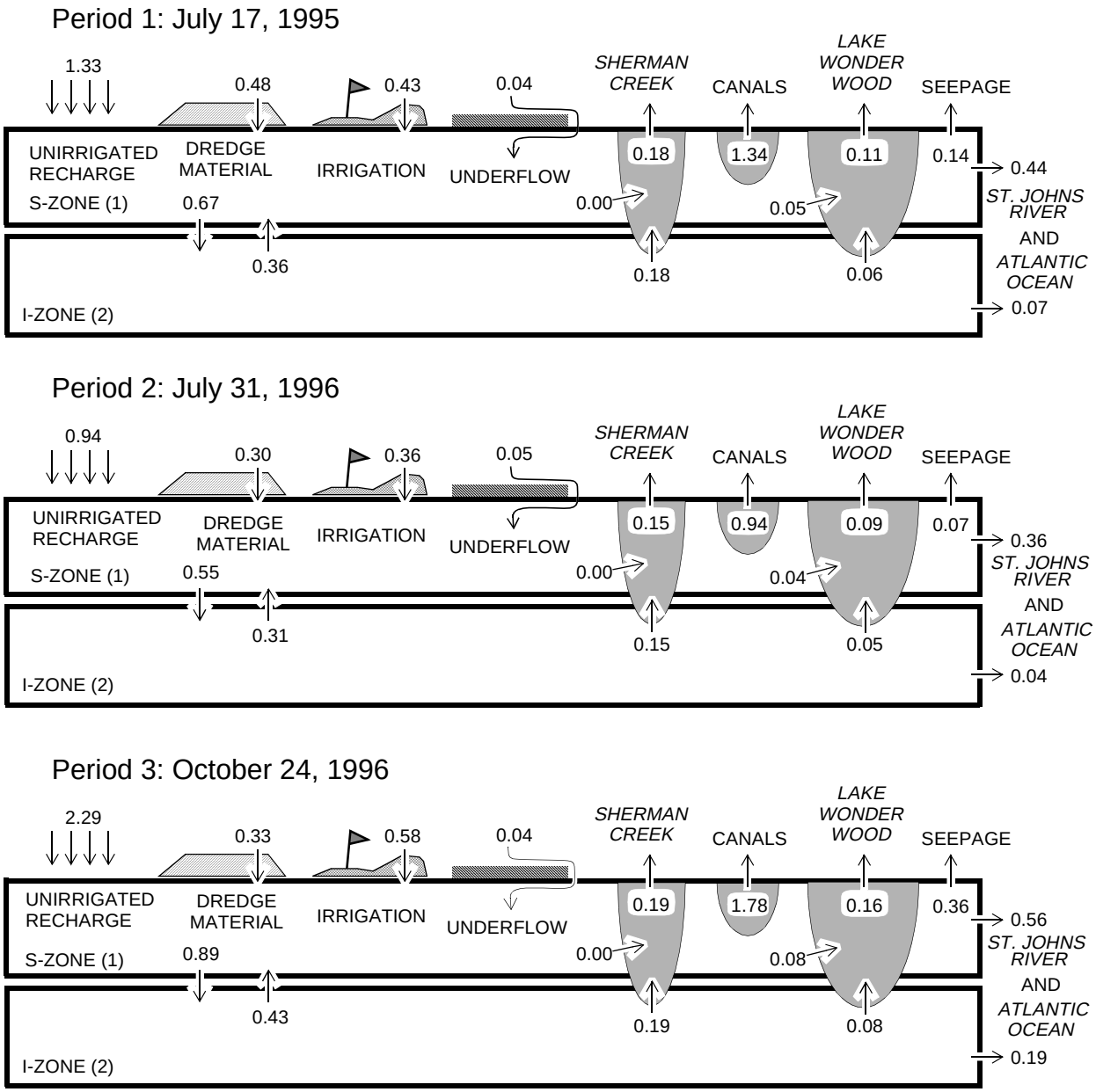

Figure 24. Simulated volumetric flow budget for the three calibaration periods on July 17, 1995; July 31, 1996; and October 24, 1996.

ground-water flow rates because the effective recharge rate to the unirrigated areas is about equal to the average amount of recharge received during a year. The total flow through the surficial aquifer system averaged 2.3 ft^3/s (period 1) and ranged from 1.7 ft^3/s (period 2) to 3.2 ft^3/s (period 3, fig. 24). For the extreme effective recharge rates estimated from the hydrograph for well 8-5I (fig. 10), the range in total simulated flow through the surficial aquifer system is about 1 to 4 ft^3/s.

Irrigation accounts for about 20 percent of the water that circulates through the surficial aquifer system during all three periods (fig. 24). Most of the irrigation water is applied to the golf greens and fairways and the sports facilities north of the golf course. Much of the golf-course irrigation water passes through the I-zone and is discharged to Sherman Creek and Lake Wonder Wood (fig. 25). The sharp bends and sudden changes in particle direction are the effects of movement between the S-zone and the I-zone. Golf-course irrigation supplies about 0.06 ft^3/s (33 percent) of the ground-water discharge to Sherman Creek and about 0.04 ft^3/s (35 percent) of the ground-water discharge to Lake Wonder Wood.

As the recharge rate increases, the water table rises and diffuse discharge seeps from areas that formerly were recharge areas. These areas mostly are between the southwest runway and Patrol Rd., northeast of the dredge material holding areas, and over the baseball fields (fig. 26). Simulation of advective transport of contaminants based on an average recharge rate is problematic in these areas. A contaminant being transported near the water table in one of these areas could be discharged from the surficial aquifer system earlier and in a different location than expected based on the average recharge rate. For example, an intense recharge event could cause contaminants to be discharged along the southwest runway 200 to 400 ft upgradient of the perennial drains and 5 to 20 years sooner than predicted by a steady-state simulation.

As recharge rates increase, the absolute quantity of water circulating through the I-zone increases, but the fraction of ground-water flow circulating through the I-zone decreases compared to the total ground-water flow through the surficial aquifer system (fig. 24). The I-zone transmitted between 0.55 and 0.89 ft^3/s (33 and 27 percent of the ground-water flow) during periods 2 and 3, respectively.

Most of the I-zone is recharged in areas where the marsh-muck confining unit is less than 1 ft thick (fig. 6). Recharge from the dredge material holding areas (where the marsh-muck confining unit is more than 1 ft thick) to the I-zone is an exception because of head differences of about 15 ft between the water table and the I-zone. Localized areas of higher recharge rates to the I-zone from irrigation-augmented recharge appear as denser patches of particles in figure 27. Contaminants migrating from areas that recharge the I-zone generally will have longer flow paths and residence times than those that migrate exclusively through the S-zone.

EVOLUTION OF MAYPORT PENINSULA AND SURFICIAL AQUIFER SYSTEM

The surficial aquifer system at NAVSTA Mayport is a dynamic system that has been modified by natural and anthropogenic forces over the last 200 years. The freshwater flow system is expanding and entrained saltwater continues to be flushed from the system. The chloride concentration in many of the wells screened about 20 ft below sea level range from about 20 to 25,000 mg/L. Concentrations in excess of typical sea water values (19,400 mg/L) indicate that the original water from the salt marshes has not yet been displaced. Water levels of about 3 to 6 ft above the average level of the St. Johns River also indicate that the freshwater lens is still developing. If the Ghyben-Herzberg approximation is applied, the water levels in these same wells would suggest that the interface should be more than 100 ft below the well screens.

Anthropogenic activities associated with the construction and modification of NAVSTA Mayport since 1942 have caused the majority of change to the surficial aquifer system. More than 1 mi^2 of salt marsh and tidally-affected areas have been reclaimed by the construction of runways, building of support facilities, and maintenance of the turning basin. In addition to expanding the domain of the surficial-aquifer system, recharge rates have been dramatically increased by intensive irrigation.

The extent and morphology of the Mayport peninsula has been documented sporadically since the early 1800's (U.S. Department of the Navy, 1995). The earliest maps of the Mayport peninsula were developed during British occupation in 1822 (U.S. Department of the Navy, 1995). A U.S. Coast Survey

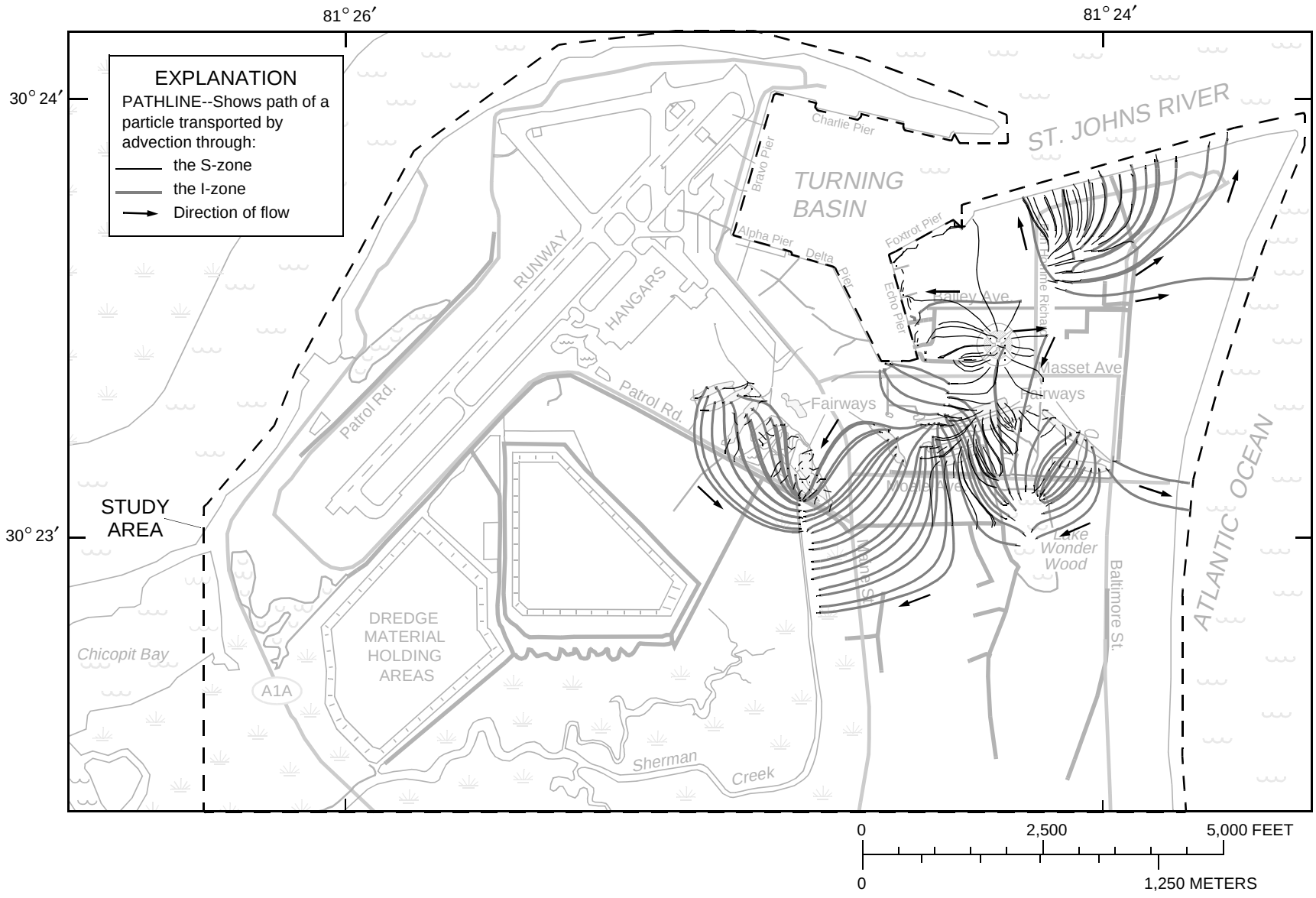

Figure 25. Simulated flow paths from areas where recharge occurs at rates greater than 45 in/yr to their respective discharge points during period 1.

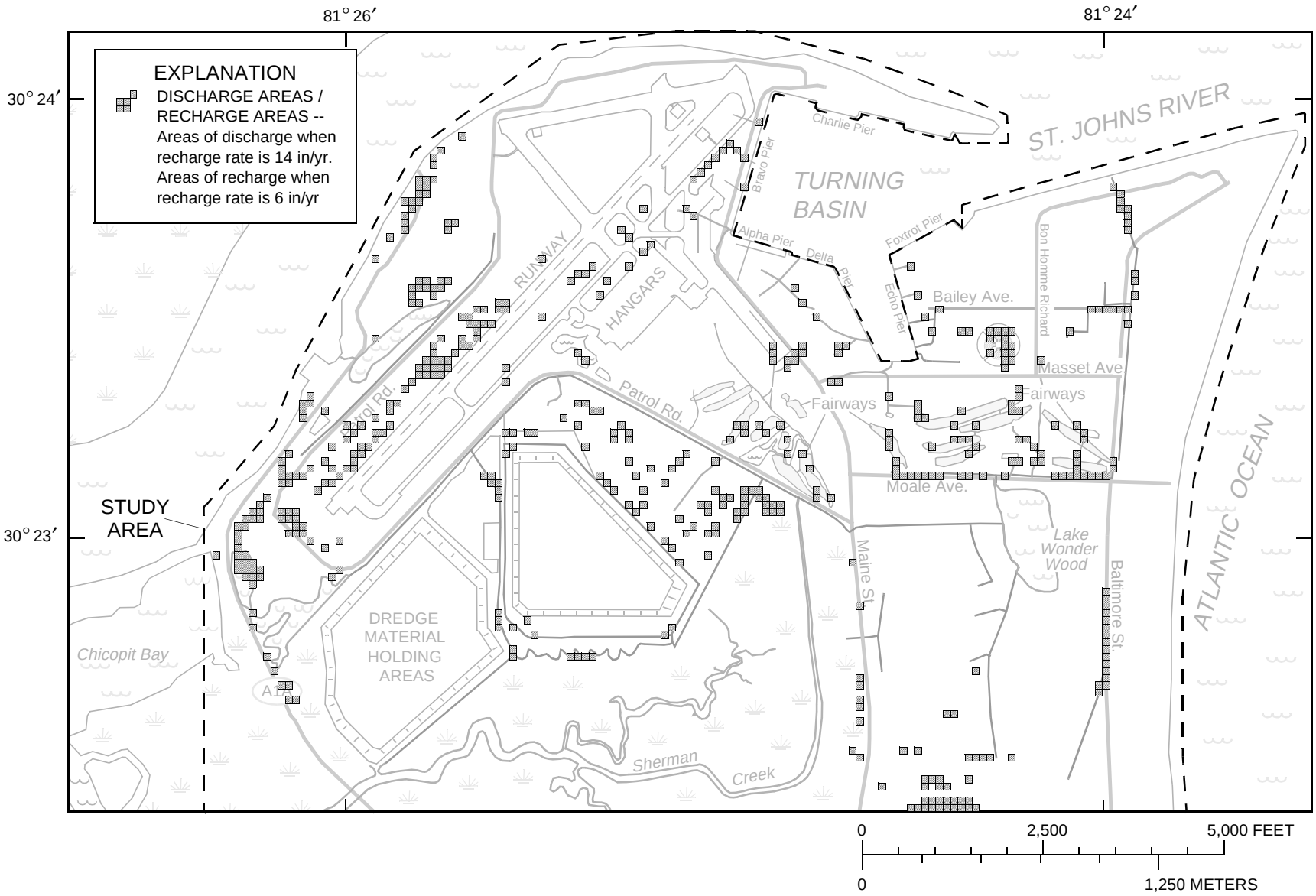

Figure 26. Simulated areas of discharge when the surficial aquifer system is recharged at 14 in/yr that are not discharge areas when the system is recharged at 6 in/yr.

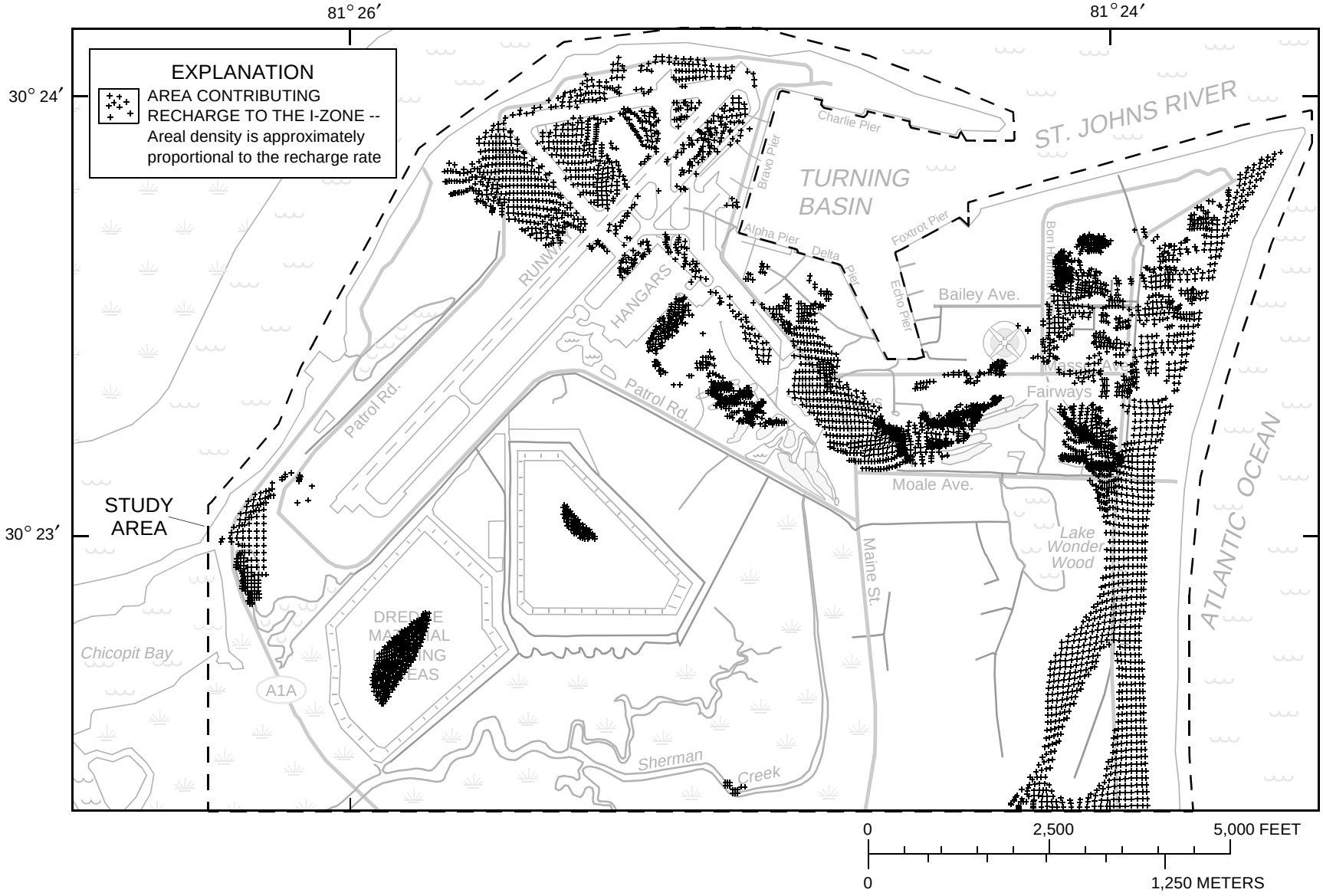

Figure 27. Areas that contribute recharge to the I-zone when the surficial aquifer system is recharged with the distribution from period 1 (N′ = 8 in/yr).

map from 1853 was the first to document the large salt marsh west of the coastal sand dunes. The shoreline, extent of marsh, and drainage features that existed in 1918 and 1940 were depicted by maps from the U.S. Geological Survey and NAVSTA Mayport historians, respectively (U.S. Department of the Navy, 1995). Further changes in the extent and morphology of the peninsula were documented by aerial photographs of NAVSTA Mayport taken since 1952.

The surficial aquifer system has been strongly affected by the rapidly changing morphology of the peninsula. Expansion of land mass by either natural accretion or anthropogenic activities has increased the lateral and vertical extent of the fresh ground-water flow system. Natural accretion gradually moves the freshwater/saltwater interface seaward, whereas the reclamation projects are more analogous to a sudden uplift causing commensurate changes in the rates and distribution of recharge to and discharge from the surficial aquifer system. The typical reclamation project at NAVSTA Mayport raised about a 0.25-mi^2 area from 1 to 12 ft above sea level over a 5-year period.

Prior to land being accreted or reclaimed, ground-water flow in the offshore and salt marsh areas was negligible. As the land mass expanded and the altitude of the land surface increased, additional surfaces became available for freshwater recharge. The additional freshwater recharge increased the ground-water flow rate and began displacing the entrained saline pore water.

Simulated Displacement of Saline Water

The advective displacement of saline pore water was simulated using a particle-tracking routine, MODPATH (Pollock, 1994). The density contrast between saline and freshwater zones was assumed to have a negligible effect on the flow system and was not simulated. A comparison between density-dependent and uniform-density simulations of generalized cross-sections through NAVSTA Mayport showed that the displacement of saline pore water by freshwater recharge can be adequately simulated as a uniform-density flow field (app. B) because the topographically driven gradients are several times greater than the density-driven gradients.

Particle traveltimes and advective displacement rates are proportional to the effective porosity estimates. If effective porosity estimates are doubled, ground-water velocities will be halved and traveltimes will double. Porosity measurements from cores collected in the unsaturated zone near Lake Wonder Wood and north of the southwest runways ranged from 45 to 51 percent. The porosity of these samples is suspected of being biased upward by the measurement method (the volume of the cores was determined by drying and weighing the samples). The measured porosities also are not entirely representative of the aquifer matrix because the matrix contains oyster shells and debris that were too large to be collected in the cores. A lower effective porosity of 40 percent was used for all particle-tracking simulations because the core porosities, as measured, represent the total porosity. Effective porosity differs from total porosity in that only the interconnected pore spaces are included.

The connate pore water was approximated by a uniform array of particles placed in the middle of the I-zone. Particles were not placed in the S-zone because water quickly moves through the S-zone to discharge at the surface or enters the I-zone. The average residence time in the S-zone was about 12 years under average 1996 conditions and an effective porosity of 40 percent.

The dilution of connate saltwater by freshwater recharge was depicted by particle spreading within the I-zone and removal at simulated surface-water features. Graphically approximating the relative concentration of saltwater in the I-zone with a single layer of particles can be locally deceptive because the areal particle concentration is decreased or increased by factors other than freshwater recharge. Vertical movement near discharge areas causes the areal concentration of particles to increase. This effect is more pronounced when the recharge is diffuse and the discharge is focused. Increases in aquifer thickness or effective porosity will cause the areal concentration of particles to increase whereas decreases in either aquifer property will have the opposite effect.

Steady-State Displacement with 1996 Recharge Rates

Saltwater displacement initially was simulated with the steady-state model driven by the recharge rates that were estimated for 1996 (period 1). The saltwater displacement patterns in the I-zone are shown in figure 28 at the end of 50-year intervals for the 200-year simulation period. Initial pore-water distributions were assumed to be 100 percent fresh in the S-zone and 100 percent saline in the I-zone.

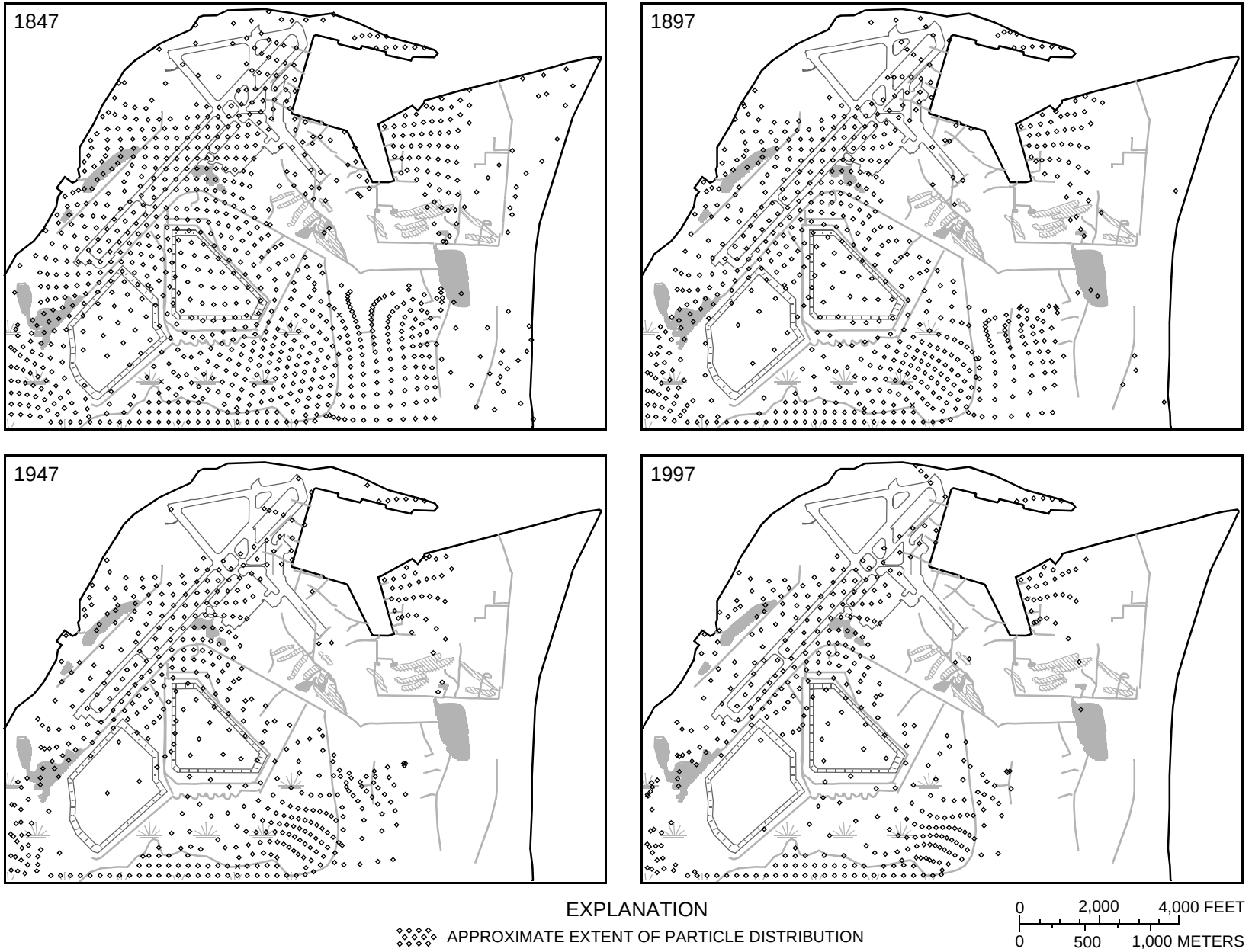

Figure 28. Particle distributions in the I-zone after 50, 100, 150, and 200 years of travel simulated by the steady-state model using the average 1996 flow field.

Saltwater displacement was complete and rapid in the vicinity of recharge areas to the I-zone (fig. 27). Saltwater was completely displaced between well 8-5S and the St. Johns River, beneath the golf course, and along the Atlantic Ocean in 50 years or less (fig. 28). More moderate rates of saltwater displacement occurred beneath and south of the dredge material holding areas. Dilution and spreading of the connate water is apparent after 50 years of freshwater recharge and is nearly complete beneath the western dredge material holding area after 200 years.

Very little saltwater was displaced near the hangars, north of the dredge material holding areas, and along the southwestern runway during the 200-year simulation period (fig. 28). Ground-water flow and saltwater displacement in the I-zone were restricted by the marsh-muck confining unit (fig. 6) and an area of low transmissivity northwest of the hangars in the I-zone (fig. 16). Another pocket of reduced saltwater displacement existed between Echo pier and Bon Homme Richard St. (figs. 1 and 28). In addition to the presence of the marsh-muck confining unit and an area of low transmissivity along the St. Johns River, ground-water movement in the I-zone was further restricted by Echo and Foxtrot piers.

The veracity of the steady-state, saltwater displacement simulation was assessed by comparing the final particle distribution (200 year) to chloride concentrations measured in 1993 (U.S. Department of the Navy, 1995) and 1996 from the I-zone (fig. 29). Areas of little saltwater displacement should have chloride concentrations of about 19,400 mg/L, which is the typical chloride concentration of seawater. Areas that have passed many pore volumes of freshwater should have chloride concentrations of less than 100 mg/L. The simulated saltwater distribution after 200 years of displacement did not consistently describe the measured chloride distribution in the I-zone (fig. 29). Measured chloride values and the simulated saltwater distribution agreed in the areas between well 8-5S and the St. Johns River, north of the dredge material holding areas, and along the Atlantic Ocean. The simulated saltwater distribution did not reflect the measured chloride concentrations beneath and to the south of the dredge material holding areas, between the eastern dredge material holding area and the golf course, or along the southwestern runway (fig. 29).

The changes in stresses, boundary conditions, and hydraulic properties of the Mayport peninsula have been great enough that no one, steady-state, flow field can adequately simulate the saltwater displacement from the surficial aquifer system. Even if the 50-year displacement pattern were compared instead of the 200-year pattern, many discrepancies would exist between the simulated pattern and the measured chloride values. Greater saltwater displacement was simulated south of the western golf course than the chloride measurements indicate (figs. 28-29). Insufficient displacement was simulated north of Moale Ave. and to the east of Echo pier and does not adequately account for the measured chloride concentrations of less than 200 mg/L.

Transient Displacement

A transient model of the Mayport peninsula was developed that accounted for the known changes in hydraulic properties, boundary conditions, and stresses over the last 200 years. The transient flow field of the surficial aquifer system was simulated with 10 stress periods that approximated the shifting morphology and changing boundaries that occurred between 1798 and 1997.

Stress periods were based primarily on changes in surface-water features and data availability. The surface-water features were allowed to expand, contract, or move as needed between stress periods. The distribution and extents of surface-water features were determined from maps of the Mayport peninsula for the years 1822, 1853, 1918, 1940, and 1964 (U.S. Department of the Navy, 1995) and aerial photographs taken during 1952, 1962, 1972, 1977, 1982, 1989, and 1995 (Cheryl Mitchell, Staff Civil Engineer Mayport, U.S. Navy, written commun., 1996). The division of the simulation period into stress periods and the significant hydrologic changes between periods are listed in table 9.

Hydraulic properties of the surficial aquifer system were modified over time by anthropogenic activities at NAVSTA Mayport. For example, the addition of dredge material locally increased the thickness of the marsh-muck confining unit and elevated the base of the S-zone; the dredging of Sherman Creek and Lake Wonder Wood breached the marsh-muck confining unit; and the construction of quay walls has introduced impermeable barriers between the surficial aquifer system and the turning basin. MODFLOW does not simulate time-variant hydraulic properties (McDonald and Harbaugh, 1988), so a new MODFLOW package (VAR1, app. C) was

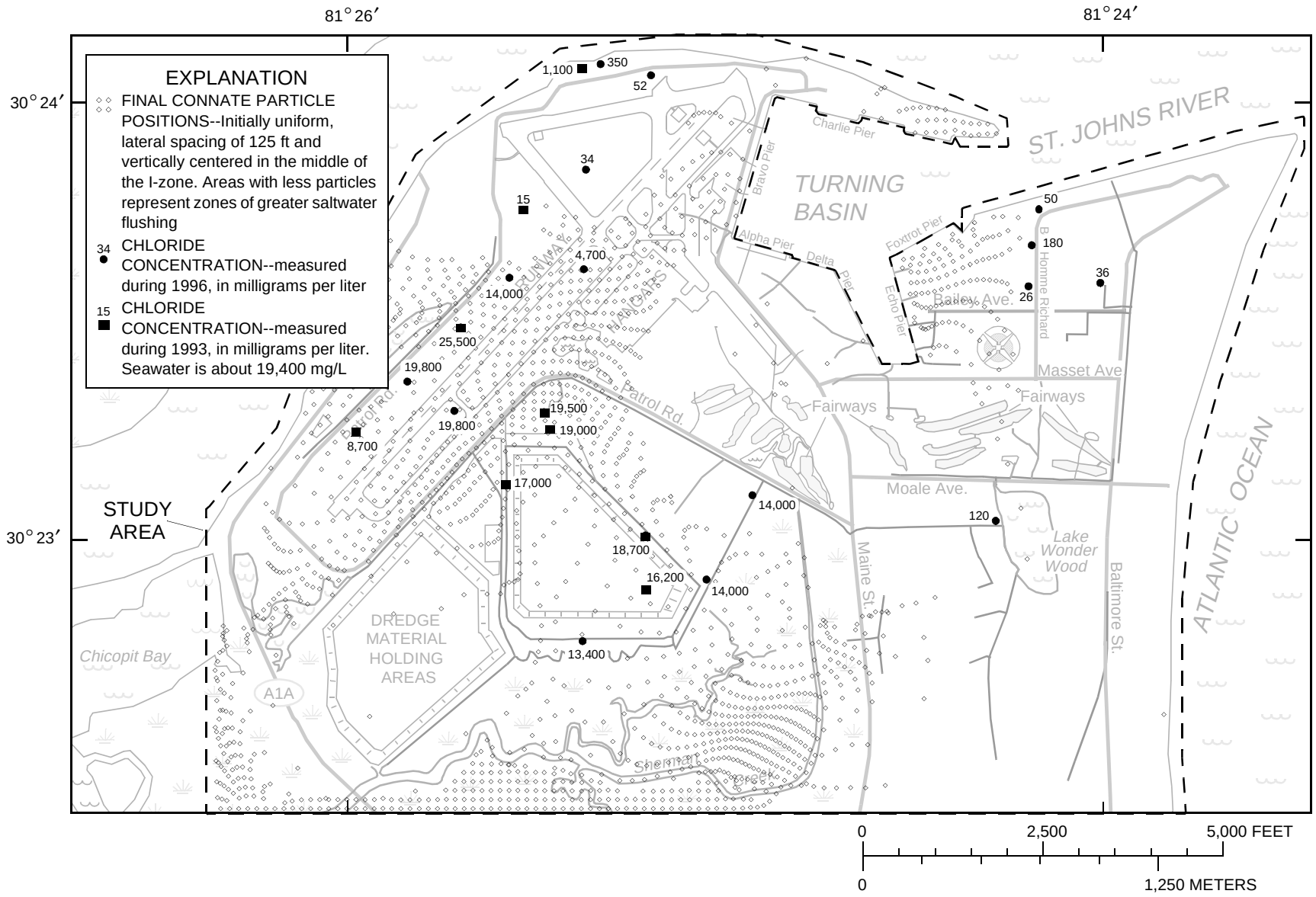

Figure 29. Flushing of connate saltwater from the I-zone over a 200-year period simulated by the steady-state model using the average 1996 flow field.

Table 9. Simulated recharge, irrigation, and discharge rates applied to the transient model of NAVSTA Mayport, 1798 to 1997

[mi^2, square miles; in/yr, inches per year; recharge, irrigation, and discharge in cubic feet per second; --, not applicable]

Stress period	Last year of stress period	Upland area, mi^2	Natural recharge rate, in/yr	Recharge and irrigation	Discharge		Percent of 1996 rate	Significant change from previous stress period
					Canals, lakes, and seepage	St. Johns River and Atlantic Ocean		
1	1880	0.91	5	0.34	0.18	0.16	15	--
2	1920	1.54	5	.57	.27	.30	25	Mayport peninsula expanded by natural accretion.
3	1945	2.01	5	.74	.24	.50	33	Ribault Bay formed; NAVSTA Mayport commissioned in 1942.
4	1952	2.75	5	.89	.49	.40	39	Alpha, Beta, and Charlie piers were built.
5	1962	2.99	5	.98	.56	.42	43	Delta pier added and southwest runways extended.
6	1972	2.99	6	1.11	.73	.39	49	Lake Wonder Wood dredged.
7	1977	3.41	6	1.67	1.21	.47	73	Golf course irrigation started; Sherman Creek dredged.
8	1982	3.41	8	1.71	1.23	.48	75	Sports facility irrigation started.
9	1994	3.42	8	2.28	1.77	.51	100	Echo pier and hangars added; ornamental plant irrigation started; dredge material holding area exceeded 30 feet above sea level.
10	1997	3.42	8	2.28	1.77	.51	100	Foxtrot pier added.

written to accommodate the time-variant hydraulic properties. This package is not a major modification of MODFLOW and is documented in appendix C. Away from Sherman Creek, Lake Wonder Wood, and the areas where the base of the S-zone was elevated above sea level, it was assumed that the hydraulic property estimates from the calibrated model were adequate and did not change. A uniform specific yield of 0.1 and storage coefficient of 5×10^{-5} were assumed for the S-zone and I-zone, respectively.

Historical recharge rate estimates were speculative but were extrapolated from 1996 estimates. A spatially uniform recharge rate of 5 in/yr was applied during stress periods 1, 2, and 3 (1800 to 1945) and was extrapolated from the smaller estimates during 1996. The estimates were constrained by assuming the elevation of the land surface was lower prior to 1945 than in 1996 and assuming that the surficial aquifer system lacked the storage capacity to retain water after intense precipitation events. Spatial recharge variation due to impervious surfaces was simulated in stress periods 4 through 10 (1946 to 1997) and was based on aerial photographs. The recharge rate to unirrigated areas was increased to 6 and 8 in/yr in stress periods 6 and 8 (table 9), respectively, to reflect the increasing storage capacity of the surficial aquifer system. The effect of irrigation projects was simulated in stress periods 7 through 10 (1973 to 1997).

The effects of the shifting morphology, changing boundaries, and increasing recharge rates are shown by changes in the water table extent, elevation, and configuration (fig. 30). Prior to 1880, the freshwater flow system was confined to a thin finger of land that covered less than 1 mi^2. By 1945, the upland area had increased to about 2 mi^2, mostly due to natural accretion. The ground-water flow system was immediately modified after the establishment of NAVSTA Mayport as evidenced by the filling of Ribault Bay, the extending of the runways to the southwest, and the redirecting of the creek that flows through present day Lake Wonder Wood. Between 1952 and 1972, about 1 mi^2 of marsh was converted to an upland area south of the runways and the inlet for Delta pier, Sherman Creek, and Lake Wonder Wood was dredged. Between 1972 and 1977, the effects of irrigation associated with the addition of the golf course are shown by the expanded 5-ft contour (fig. 30). The addition of irrigated sports facilities and ornamental plants between 1978 and 1994 caused the water table to rise to more than 10 ft above sea level east of Maine St. During this same period, the altitude of the dredge material holding areas exceeded 30 ft, thus these areas could sustain higher recharge rates (fig. 30).

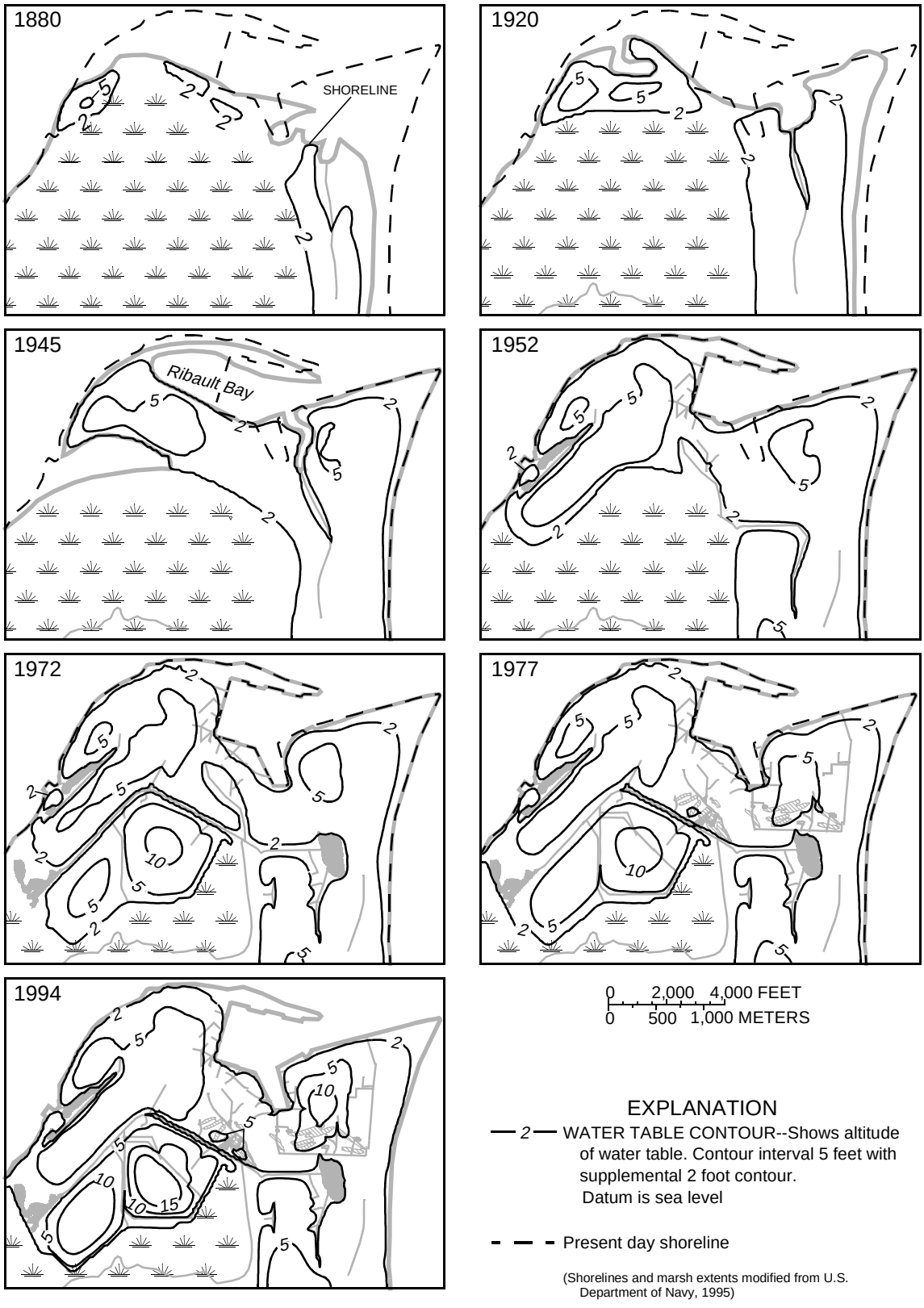

Figure 30. Water table in the S-zone (layer 1) at selected times as simulated by the transient model.

Natural accretion and land reclamation projects have expanded the upland area of the Mayport peninsula and increased the amount of flow through the surficial aquifer system (table 9). The simulated flow through the system increased more than sixfold from 0.34 to 2.28 ft^3/s between 1880 and 1996 (table 9). Irrigation has also increased the flow through the system as evidenced by the increase in simulated flow from 1.11 to 1.67 ft^3/s following the commencement of golf course irrigation between 1972 and 1977.

Water levels rose as the upland area expanded and recharge to the surficial aquifer system increased (fig. 31). Part of the water-level rise was due to the increased length of the flow paths between recharge and discharge points. Shortening the flow paths will lower water levels as was done by dredging the inlet for Delta pier near well 20-2S between 1953 and 1962. The second water-level decline between 1963 and 1972 near well 20-2S was caused by the dredging of Lake Wonder Wood. Most of the water-level rise simulated between 1973 and 1997 was due to recharge induced by golf course irrigation.

Saltwater displacement from the I-zone was confined to a relatively narrow strip that paralleled Maine St. and extended to the town of Mayport during the first 100 years (fig. 32). An area of unflushed connate water existed for the first 150 years beneath the creek that was rerouted from the St. Johns River to the western marsh. This unflushed connate water began to dissipate in the ensuing 50 years after intense irrigation altered the previous flow paths (fig. 32).

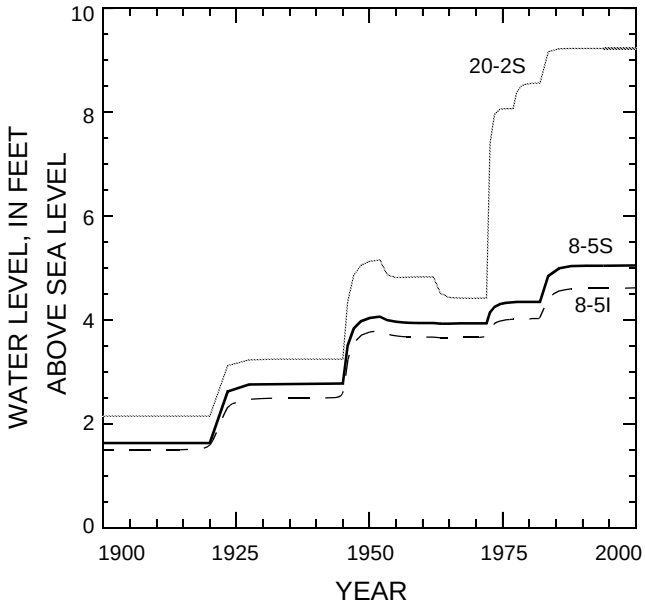

Figure 31. Water levels in selected wells simulated by the transient model (Well locations are shown in fig. 1).

The transient simulation showed less saltwater displacement than the steady-state simulation around the dredge material holding areas, west of the golf course, and along the southwestern runways (fig. 32). The simulations differed because the principal stresses that displaced the saltwater more thoroughly in the steady-state simulation have existed only for the last 25 to 50 years. The transient simulation indicated that more saltwater displacement occurred between Echo pier and Bon Homme Richard St. when compared to simulation results from the steady-state model. The transient simulation indicates that additional displacement also occurred because Echo and Foxtrot piers did not exist until 1983 and 1995, respectively.

The simulated saltwater distribution after 200 years of transient displacement described the measured chloride distribution in the I-zone better than the steady-state simulation (fig. 33). The greatest discrepancy between the simulated saltwater distribution and the measured chloride concentrations occurred between the hangars and the runway; the particle distribution suggests very little displacement, but the measured chloride concentration in this area is 4,700 mg/L. The difference probably was due to over-extrapolation of the extent of the marsh-muck confining unit to the north of well 2-34I (location shown in fig. 3a). The discrepancy also may have resulted from neglecting variable-density and dispersive effects, given the proximity to the internal freshwater/saltwater interface (app. B).

SIMULATION OF MOVEMENT OF CONTAMINANTS

The advective movement of conservative contaminants from selected sites within the SWMUs to discharge points was simulated with MODPATH (Pollock, 1994). Contaminant movement was simulated by the steady-state model driven by the recharge rates that were estimated for 1996 (period 1). Particles were released at the water table to approximate the initial position of contaminants at selected sites. Most of the particles were discharged to the nearest surface-water feature and traveled less than 1,000 ft before being discharged from the ground-water system (fig. 34). Particles that traversed longer flow paths migrated through the I-zone (sites 4b, 5d, 13a, 13b, 13c, and 15 in fig. 34).

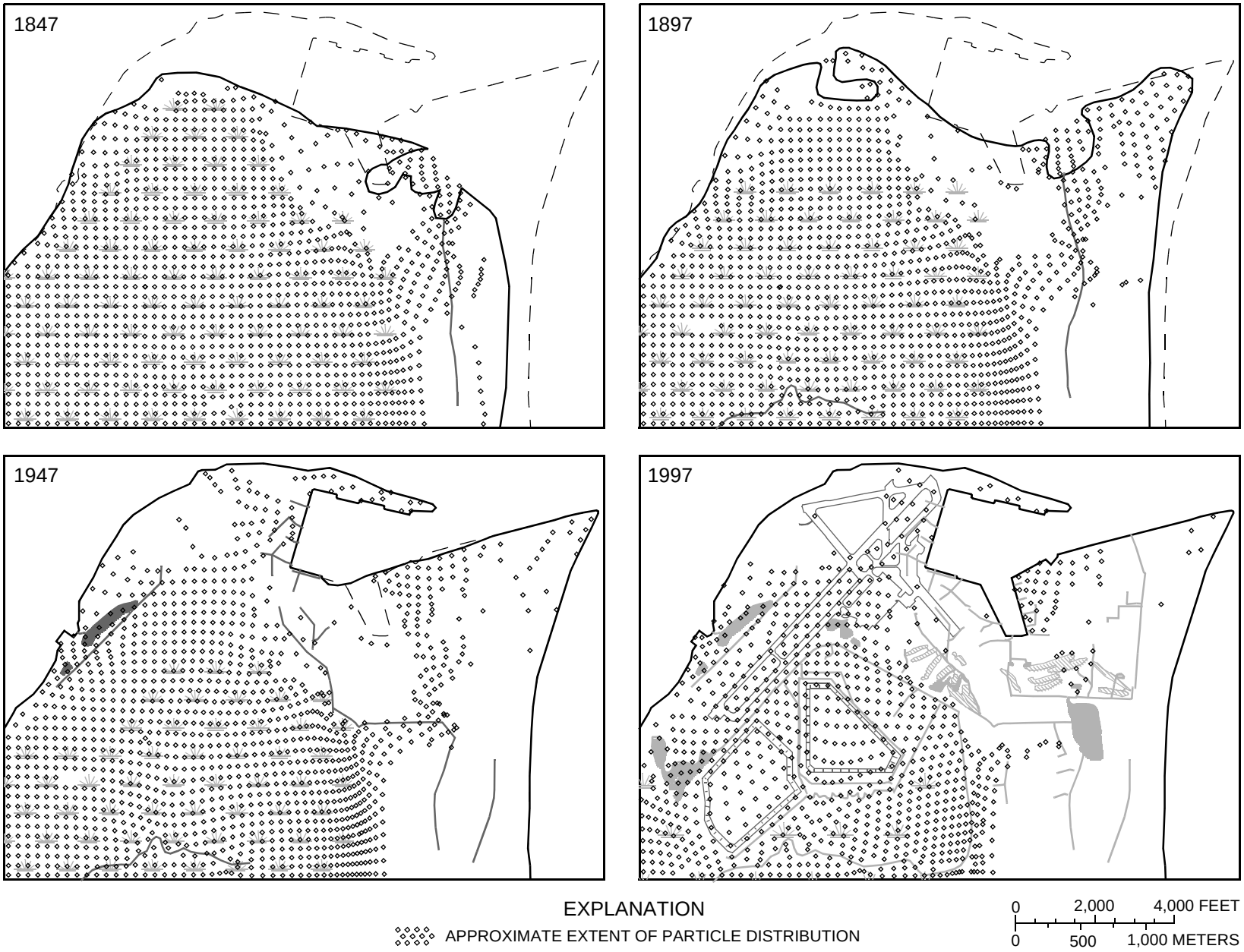

Figure 32. Particle distributions in the I-zone after 50, 100, 150, and 200 years of travel simulated by the transient model from 1798 to 1997.

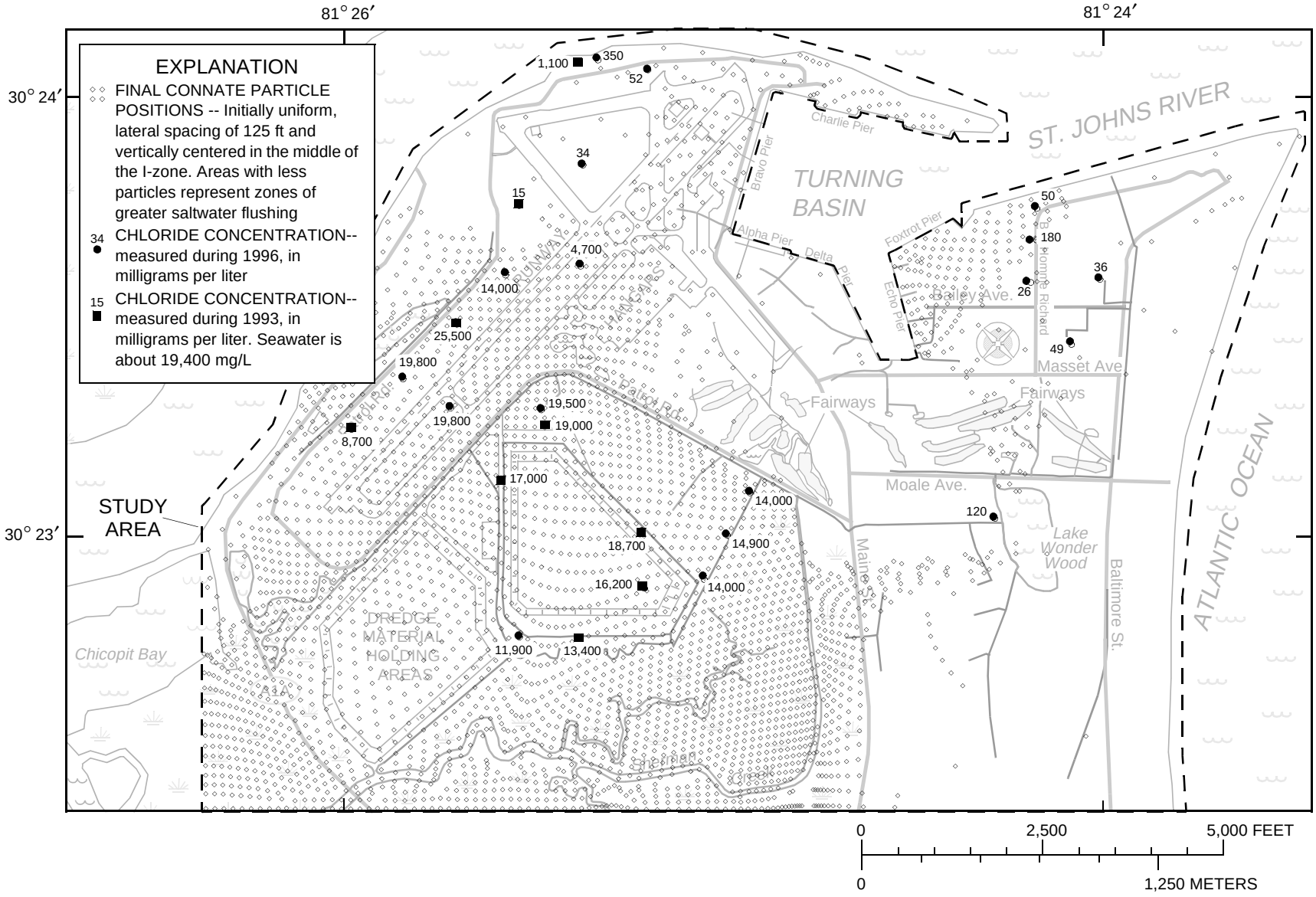

Figure 33. Flushing of connate saltwater from the I-zone over a 200-year period simulated by the transient model from 1798 to 1997.

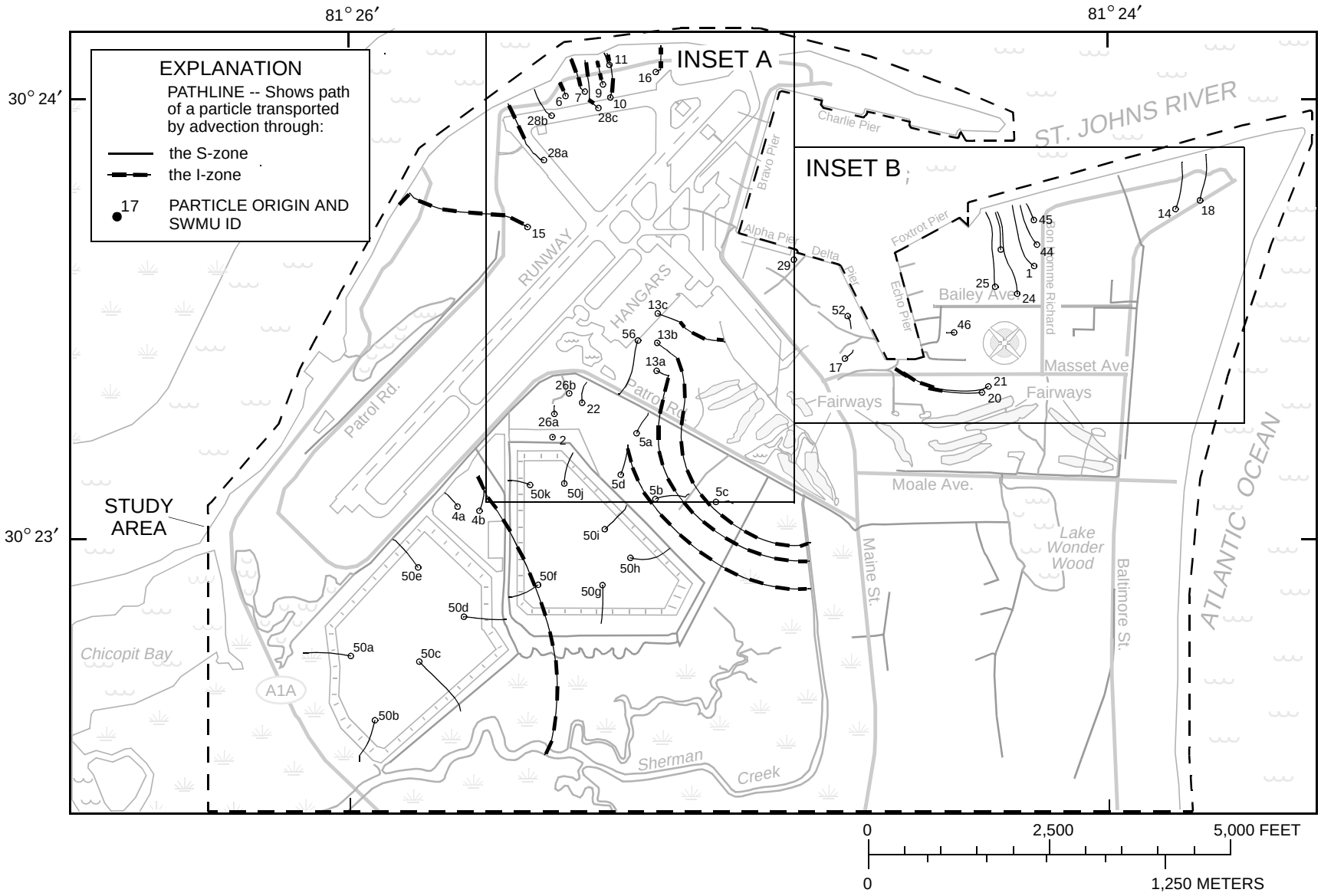

Figure 34. Pathlines from selected sites at the water table to their discharge points simulated by the steady-state model using the average 1996 flow field.

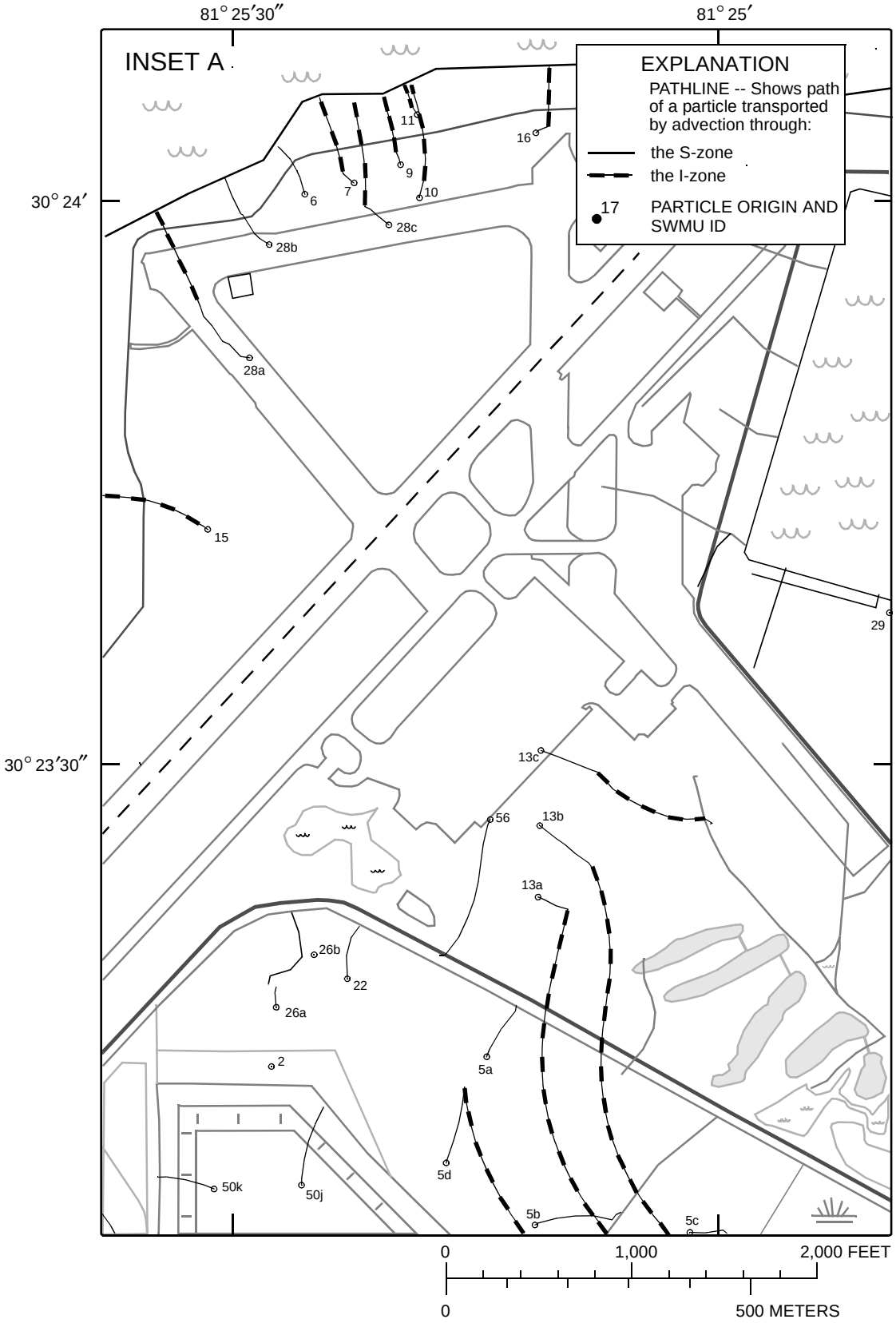

Figure 34. Inset A.

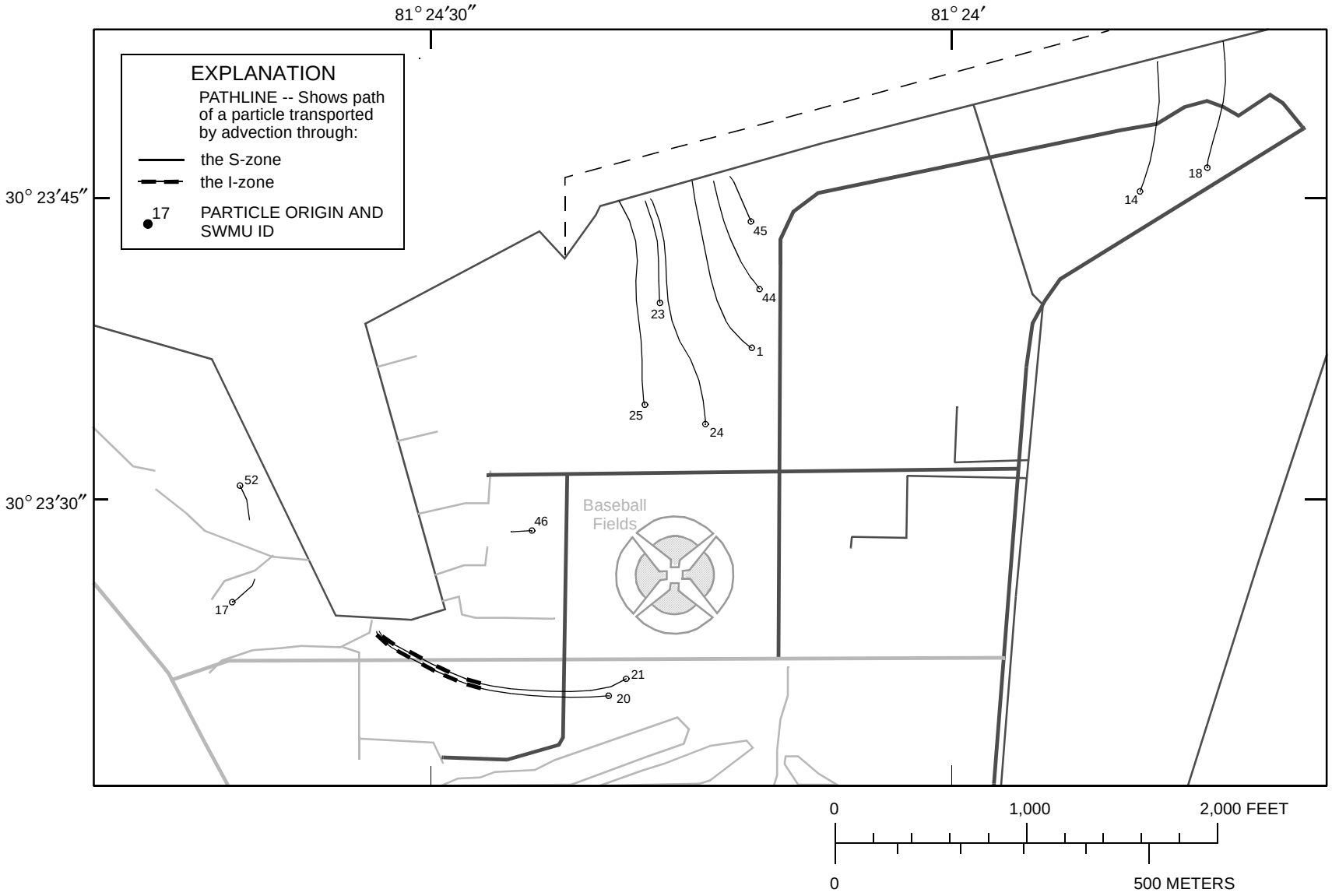

Figure 34. Insert B.

Differences in the direction of the lateral hydraulic gradient exist between the S-zone and the I-zone over much of the study area where the marsh-muck confining unit is present (fig. 6). In areas where the difference is great, sharp bends and sudden changes in particle direction are exhibited by the flow paths, as particles move between the S-zone and the I-zone (sites 4b, 5d, and 13a in fig. 34). Particle movement from the S-zone to the I-zone along paths 4b and 5d are the most extreme examples, where the direction of the lateral hydraulic gradients differ by about 180 degrees. For both particles, initial movement in the S-zone is north towards the Patrol Road canal and downward (fig. 34). After crossing the marsh-muck confining unit and entering the I-zone, the particles reverse direction and head south towards Sherman Creek.

Most of the water that crosses the marsh-muck confining unit to enter the I-zone originates at or near a ground-water divide or mound. The flow field around a ground-water divide or mound is divergent and the dominant hydraulic gradient is downwards. Small displacements at the locations of particle release can greatly alter the particle paths and points of discharge.

The effects of the divergent flow field are best illustrated by tracing a north-south transect of particles across the water table beneath the western dredge material holding area and examining their paths in plan and section (fig. 35). Of the 15 particles released,

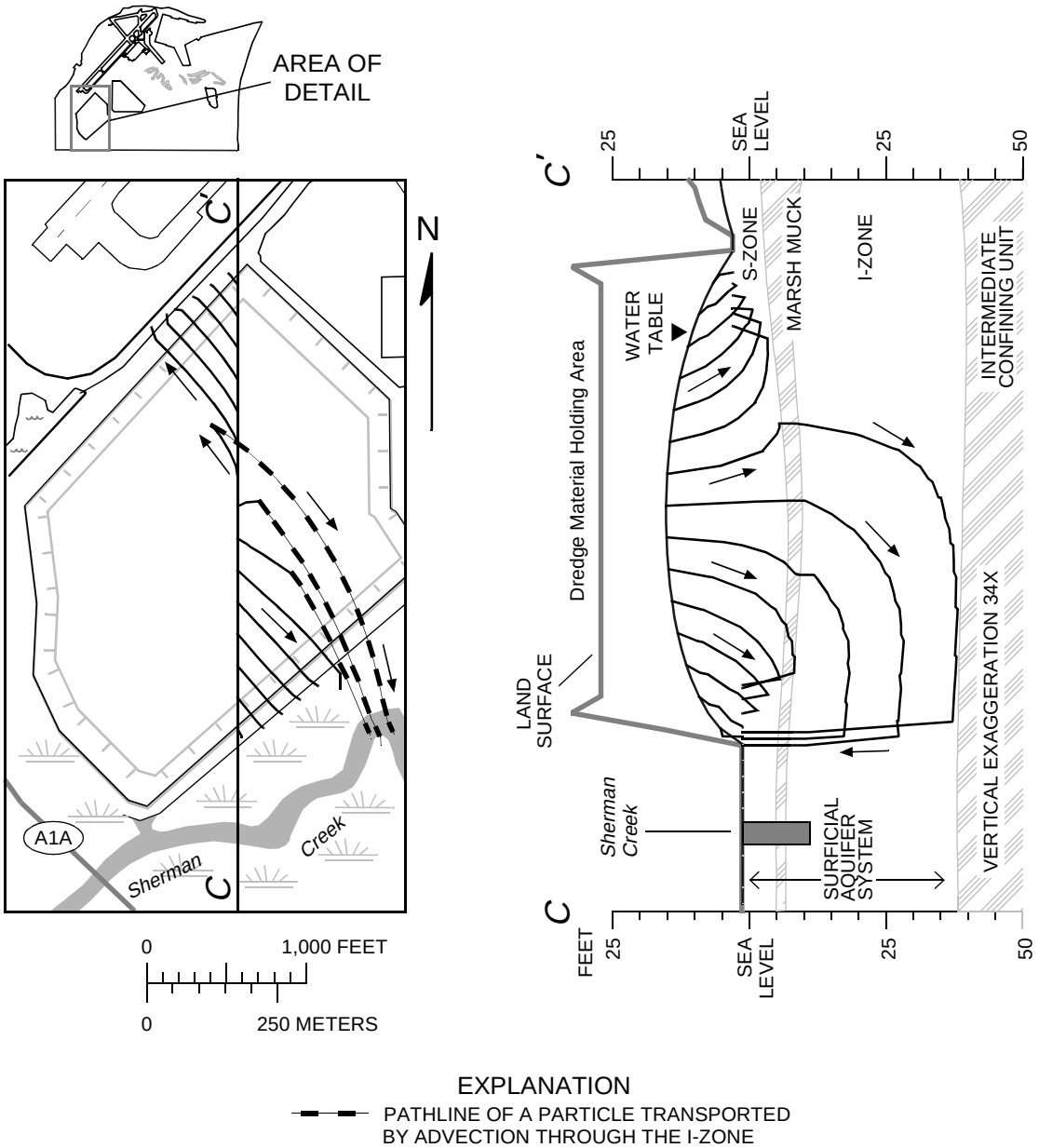

Figure 35. Effects of variable recharge on the location of contributing points to an observation point.

12 particles traveled exclusively through the S-zone and were discharged along the flanks of the dredge material holding area (fig. 35). The three remaining particles were released within 300 ft of the ground-water divide and moved downward into the I-zone (fig. 35). The effect of opposing lateral hydraulic gradients in the S-zone and the I-zone on particle paths are clearly seen in section C-C′ (fig. 35).

The traveltimes from the selected sites shown in figure 34 to their respective discharge points were estimated using an effective porosity of 40 percent (table 10). About 45, 80, and 90 percent of the traveltimes were less than 10, 50, and 100 years, respectively. Short traveltimes of less than a year for sites 2, 26b, and 29 are the result of these sites being located in discharge areas. Traveltimes of more than 100 years were associated with the longer flow paths from sites 4b, 5d, 13a, 13b, and 15 (table 10). Traveltimes reported for the selected sites in figure 34 are not representative of the traveltimes over the entire study area.

A generalized map of traveltimes was constructed for the study area by releasing a particle at each of the nodes in layer 1 and calculating the traveltime from the water table to the particle's discharge point (fig. 36). Most areas within 1,000 ft of a surface-water feature or a storm sewer had traveltimes of less than 50 years. Flow paths with traveltimes of more than 500 years mostly originated from ground-water divides near the hangars and runways, in the dredge material holding areas, and near the intersection of Bailey Ave. and Bon Homme Richard St.

CONTRIBUTING AREAS AND GROUND-WATER AGE

To assess the extent of ground-water contamination and the potential migration of contaminants, the origins of ground-water samples need to be identified. The contributing point for an observation point can be identified by back-tracking a particle from the observation point to the water table (fig. 37). If the recharge to the surficial-aquifer system always equalled the average rate, a steady-state flow field would exist and each observation point would correspond to only one contributing point at the water table. This one contributing point would supply water to the same observation point continuously.

Table 10. Approximate traveltimes of particle movement from selected sites to their respective discharge points as simulated by the steady-state model using the average 1996 flow field

[Associated particle paths are displayed in figure 34; <, less than]

Site identifier	Approximate traveltime, in years, for particles released at the water table[a]
1	44
2	< 1
4a	2
4b	560
5a	3
5b	17
5c	10
5d	270
6	13
7	22
9	16
10	25
11	10
13a	230
13b	200
13c	88
14	33
15	130
16	53
17	4
18	32
20	24
21	25
22	6
23	21
24	59
25	38
26a	2
26b	< 1
28a	96
28b	76
28c	26
29	< 1
44	19
45	5
46	1
50a	4
50b	5
50c	10
50d	6
50e	3
50f	4
50g	5
50h	11
50i	8
50j	6
50k	2
52	6
56	11

[a] Traveltimes are based on an effective porosity of 40 percent throughout the study area.

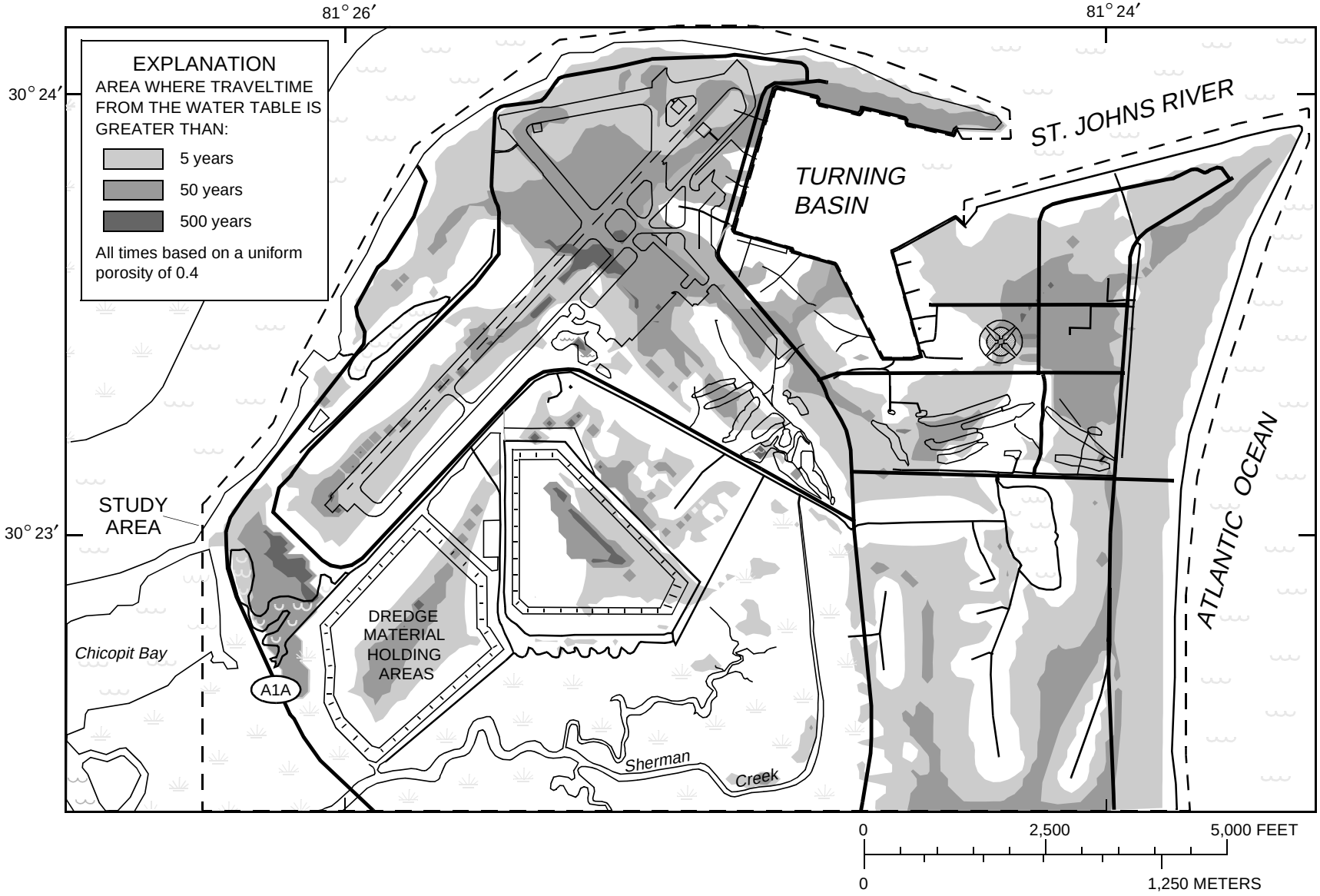

Figure 36. Particle traveltimes from the water table to the surface-water discharge point simulated by the steady-state model using the average 1996 flow field.

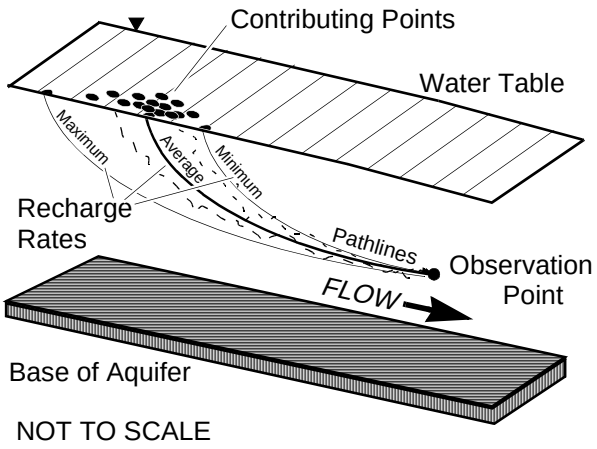

Figure 37. Effects of variable recharge on the location of contributing points to an observation point.

The flow field of the surficial-aquifer system beneath NAVSTA Mayport is not under steady-state conditions because recharge rates are variable. The effective recharge rate in the unirrigated areas typically ranges from 5 to 7 in/yr but can exceed 20 in/yr after intense precipitation events. Irrigation induced recharge can also vary on a seasonal basis over a range of more than 50 in/yr.

In a variable flow field, many points exist at the water table for each observation point, because these points on the water table each contribute water to the observation point a fraction of the time. Contributing points under the average recharge rate will supply water to the observation point much more frequently than points under the minimum or maximum recharge rates (fig. 37). The maximum frequency of contribution for observation points at NAVSTA Mayport occurs between the average and minimum recharge rates because the median recharge rate is less than the average recharge rate.

Ground-water samples are collected from observation wells, not points. Unlike an observation point, the screen of an observation well has a finite, cross-sectional area through which many pathlines pass. The finite area of a well screen translates to a finite contributing area at the water table even in a steady-state flow field. For a steady-state flow field, the ratio of cross-sectional screen area to contributing area can be approximated by the ratio of the average, lateral ground-water velocity at the screen to the recharge rate in the contributing area. In actuality, the contributing area is larger and more diffuse because of the effects of variable recharge rates (fig. 38).

Ground-water samples represent the average water quality of the aquifer over a period of time. The time period sampled represents the range of travel-times along flowpaths from contributing areas to the open interval of the sampled well and is proportional to the wetted length of the well screen. For example, the time period sampled from a well screened across the water table can be approximated by equation 3, which assumes the age of the sampled water ranges from 0 to Δt_{Sample} years. The time period sampled by a typical well screened across the water table at NAVSTA Mayport would be about 5 years based on a wetted screen length of 8 ft, a recharge rate of 8 in/yr, and an effective porosity of 40 percent.

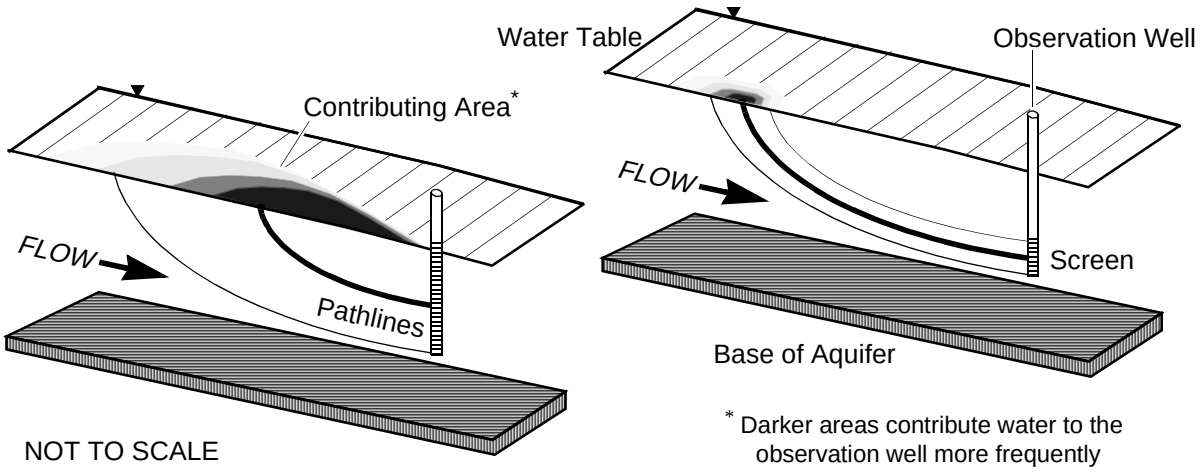

Figure 38. Effects of screen length, depth of screen below the water table, and variable recharge rates on the contributing area to an observation well.

The time period sampled by wells screened across the water table is variable because the wetted screen length fluctuates with time. This causes the contributing area to be skewed towards the observation well (fig. 38). Spatial variations in the recharge rate, such as the difference between the golf greens and the unirrigated areas or between the pervious and impervious areas, will also skew the time period sampled. The contributing area and associated time period sampled will be large but most of the water will come from the area with the higher recharge rate, which weights the time period sampled to a much smaller subperiod.

Commonly, the youngest water enters the top of the screen and the oldest water enters the bottom of the screen. However, this pattern can be reversed if the flow paths reverse direction as they did at sites 4b and 5d (fig. 34). Under similar flow conditions, if a well samples water from multiple contributing areas, the oldest water could enter the well anywhere along the screen length.

The contributing areas for 224 wells at NAVSTA Mayport were identified by back-tracking a particle from the midpoint of the wetted screen using the steady-state model and the average 1996 flow field. For most wells, the centroid of the contributing area is located at the end of the pathline back-tracked from the well (fig. 39); however, this is not the case if the well intercepts multiple contributing areas. The traveltimes from the midpoint of the wetted screens to the centroid of the contributing areas are listed in table 11.

The length of the contributing area for each well was approximated by the lateral distance between contributing points to the top and bottom of the wetted well screen (table 11). The estimate assumed the length of the contributing area was relatively short and only one contributing area existed for each well; this is the case for many of the wells. These estimates were appropriate when the traveltime to the midpoint was about the same as the average traveltime to the top and bottom of the wetted screen (table 11).

Contributing area estimates for some wells were inappropriate because the well screens intercepted multiple contributing areas. If the traveltime to the midpoint of the screen does not fall between the traveltimes to the top and bottom of the screen, the well has multiple contributing areas. For example, the pathline for well 2-17I (figs. 3 and 39) indicates the contributing area is in the eastern dredge material holding area. However, the traveltime from the midpoint of 2-17I (61 years) does not fall between the traveltimes to the top and bottom of the well screen (86 and 73 years, respectively). Therefore, well 2-17I has multiple contributing areas and receives water from both the eastern and western dredge material holding areas.

Other contributing area estimates were misleading because the well screens were supplied by areas with different recharge rates. If the traveltime to the midpoint of the open interval is close to either the top or bottom traveltimes, the sample does not represent an average of the sample period because it has been skewed towards the higher recharge rate in the contributing area. Contributing areas to wells 14-1S and 14-2S (northeast corner of fig. 3b) are supplied by recharge from unirrigated areas and underflow from beneath the impervious area. Most of the water received by well 14-2S originates from the far end of its contributing area whereas well 14-1S is supplied mostly by the contributing area close to the well (table 11).

The contributing areas of the wells also were affected by the historical landscape changes at NAVSTA Mayport. The effects of the landscape changes were investigated by back-tracking particles from the midpoint of the wetted screens using the transient model for the period from 1798 to 1997. The pathlines and traveltimes from the transient model were compared to corresponding pathlines and traveltimes based on steady-state results. Contributing areas for about 65 percent of the wells were the same because traveltimes were less than 15 years for both models (table 11). The stresses and boundary conditions of both models were very similar during the period from 1982 to 1997 so substantial differences in contributing areas would not be expected.

Both transient and steady-state models produced the same results for the origin of ground-water from wells located in areas of reclaimed marsh and screened in the I-zone. Although the contributing areas and traveltimes varied, all of the contributing areas were in the former salt marsh area and the traveltimes were about 100 years or greater. The water sampled from these wells represents connate water which agrees with the chloride measurements. These wells account for about 10 percent of the observation wells in NAVSTA Mayport.

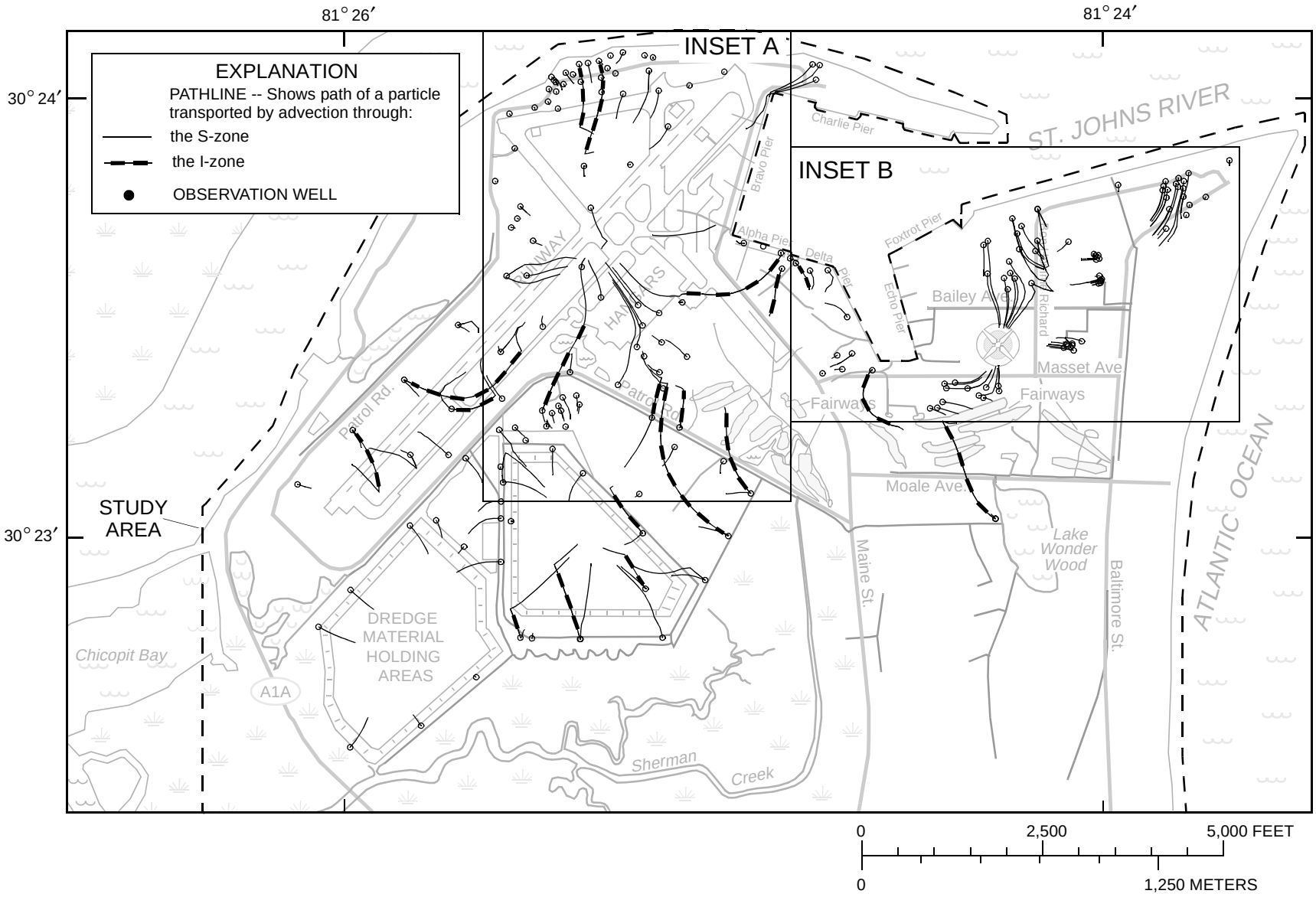

Figure 39. Back-tracked particle paths from selected observation wells to contributing areas simulated by the steady-state model using the average 1996 flow field.

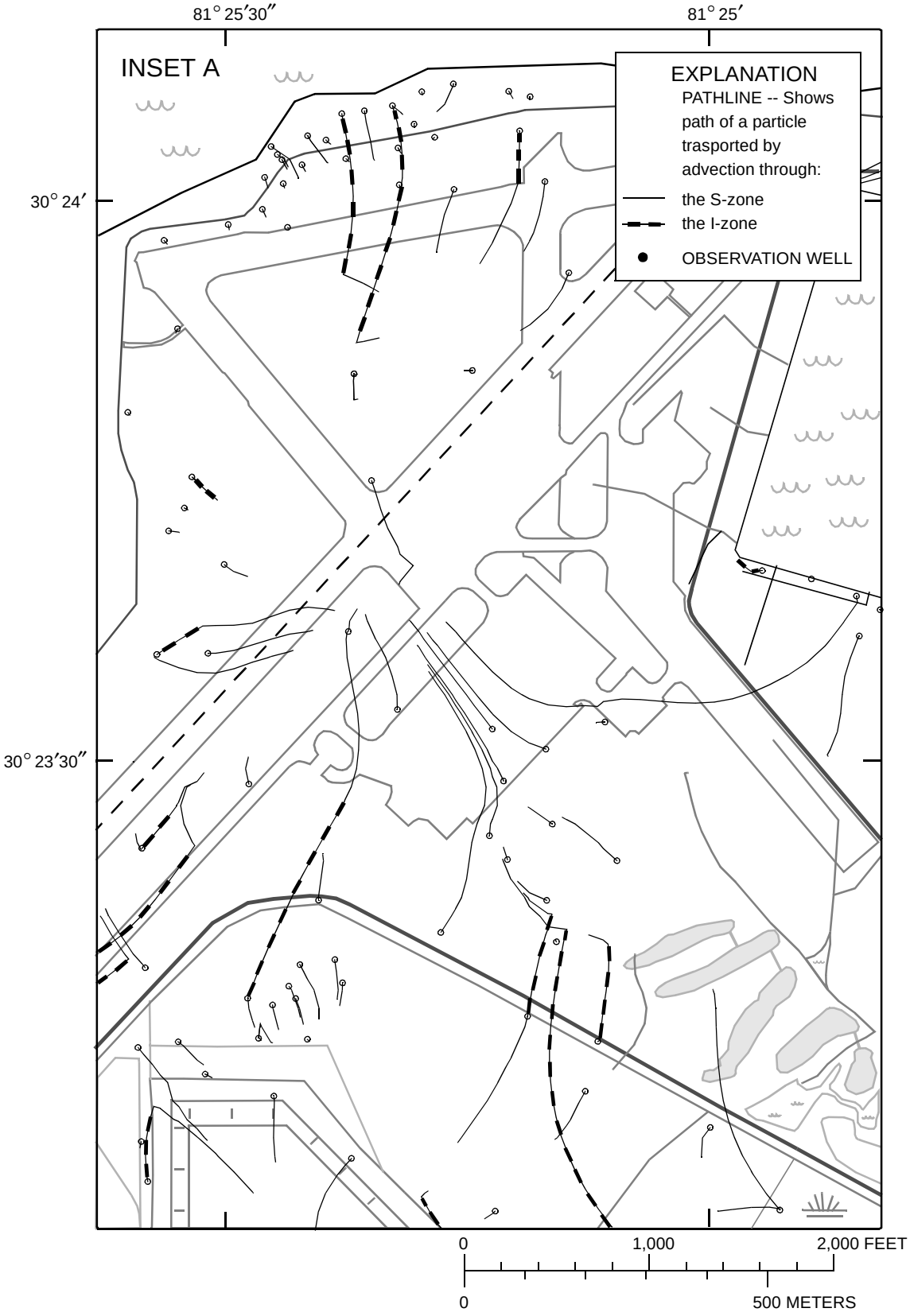

Figure 39. Inset A.

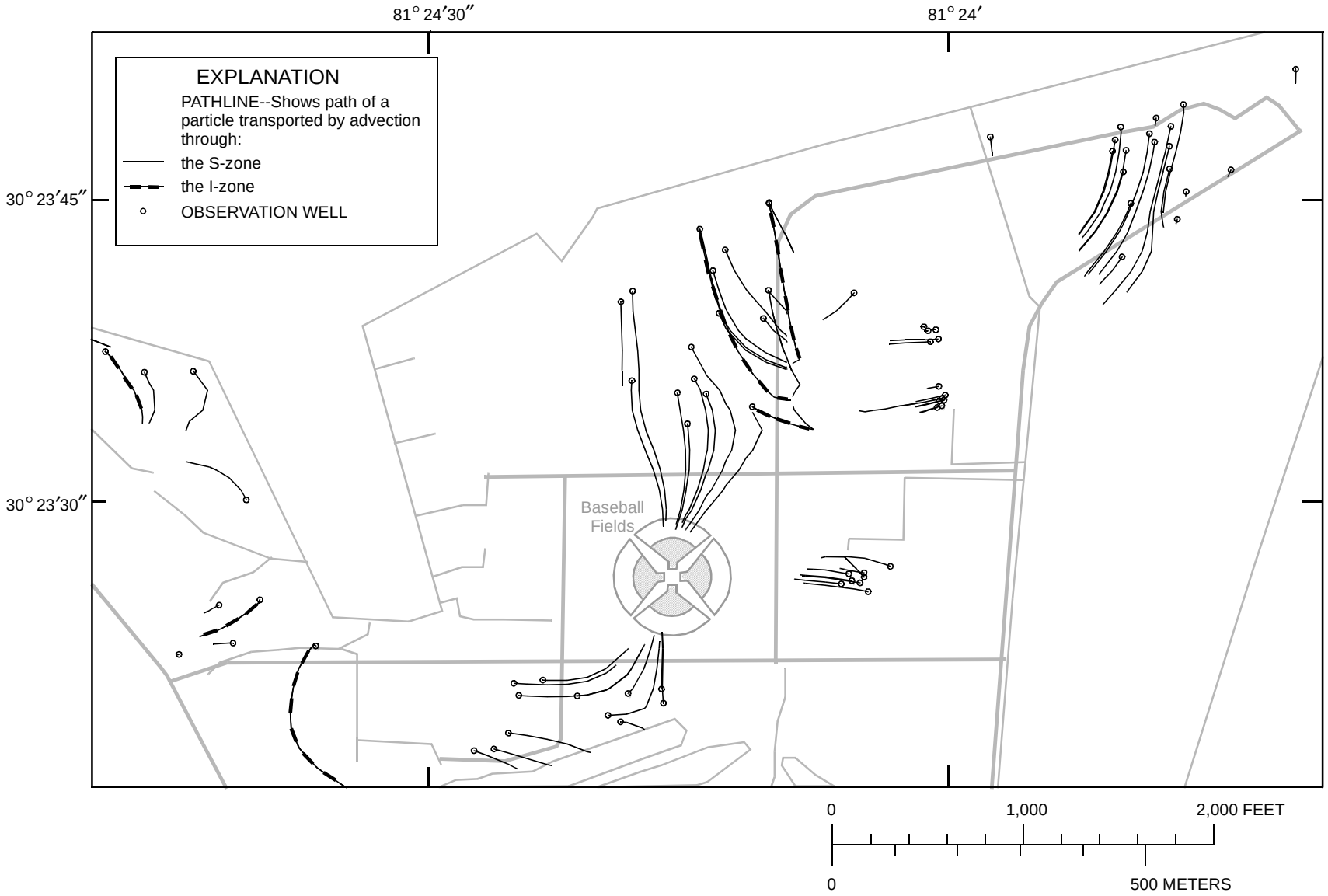

Figure 39. Inset B.

Steady-state estimates of traveltimes to contributing areas that ranged between 15 and 50 years differed most from the transient estimates. Estimates of traveltimes and pathlines from the transient model typically were 10 to 20 years less and about half as long as estimates based on steady-state model results for this subset of wells. About 90 percent of the 45 affected wells are screened in the S-zone east of Maine St. The results from the steady-state and transient models differ because many buildings, streets, and parking lots were built east of Maine St. between 1972 and 1994. The expanded impervious area increased the average distance between contributing areas and observation wells.

Generalized maps of ground-water age were constructed for the S-zone and I-zone by back-tracking particles from all of the nodes in layers 1 and 2 and calculating the traveltimes to their respective contributing points at the water table. The maps are generalized because average traveltimes for volumes that range from 30,000 to 700,000 ft^3 are being approximated with one pathline. The traveltimes were estimated with the steady-state model, using average 1996 flow field conditions, and a uniform effective porosity of 40 percent. Residence time in the unsaturated zone was neglected.

Results of the simulations indicate that most of the water in the S-zone is less than 5 years old (fig. 40). Water in the S-zone that is between 5 and 50 years old is present beneath impervious areas, canals and lakes, and south of Lake Wonder Wood, where the S-zone is thicker. The oldest water in the S-zone is in the salt marsh south and east of the dredge material holding areas (fig. 40). Water from the I-zone diffusely discharges to the S-zone in these areas.

Table 11. Approximate length of contributing area, time period sampled, traveltimes from the top, midpoint, and bottom of the wetted screen estimated with the steady-state model using the average 1996 flow field, and the traveltime from the midpoint of the wetted screen estimated with the transient model

[Well locations are shown in figure 3; parentheses indicate that the traveltime to the top of the screen was greater than to the bottom of the screen; ft, feet; <, less than; >, greater than]

Well identifier	Approximate length of contributing area, in ft[a]	Period sampled, in years	Steady-state traveltime, in years from the screen			Transient travel-time from midpoint
			Top	Midpoint	Bottom	
1-1I	18	20	89	101	108	55
1-1S	31	< 1	54	55	55	12
1-2S	9	< 1	62	62	62	10
1-P1	297	3	< 1	3	4	3
1-P2	131	2	2	3	3	3
1-P3	167	5	9	11	14	11
2-1S	224	6	7	9	12	9
2-2S	502	13	< 1	2	13	2
2-3S	365	4	< 1	2	4	2
2-4S	593	13	< 1	6	13	6
2-6S	112	9	< 1	3	9	3
2-7S	149	3	< 1	1	3	1
2-8S	100	6	< 1	2	6	2
2-9I	28	48	27	49	74	37
2-9S	53	6	< 1	2	6	2
2-10S	25	6	< 1	3	7	3
2-11I	1,462	41	131	173	173	> 200
2-11S	651	18	< 1	9	18	9
2-12I	230	(49)	120	66	71	> 200
2-12S	960	13	< 1	5	13	5
2-13S	302	10	< 1	4	10	4
2-15I	325	(18)	76	58	59	> 200
2-15S	1,454	150	10	18	160	18
2-16S	888	11	< 1	7	11	7
2-17I	1,826	(12)	86	61	73	> 200
2-17S	613	8	< 1	3	9	3
2-18I	9	64	745	768	810	> 200
2-18S	199	9	< 1	6	10	6
2-19S	444	8	2	4	10	4
2-20S	317	8	3	8	11	8
2-21S	261	11	1	11	12	11
2-22I	37	84	186	219	270	> 200
2-22S	230	5	5	8	9	8
2-23I	41	< 1	42	43	43	> 200
2-23S	304	10	< 1	10	10	10
2-24S	< 1	< 1	< 1	< 1	< 1	< 1
2-25I	258	7	135	115	142	> 200
2-25S	288	9	3	6	12	6
2-26I	99	15	49	56	63	> 200
2-26S	358	9	4	8	13	8
2-27I	118	11	69	74	80	> 200
2-28S	195	3	< 1	2	3	2
2-29S	844	31	< 1	8	31	8
2-30S	601	15	< 1	5	15	5
2-31I	75	139	306	362	445	> 200
2-31S	581	27	< 1	4	27	4
2-32I	272	103	355	407	458	> 200

[a] The length of the contributing area for each well was approximated by the lateral distance between contributing points to the top and bottom of the wetted well screen. This estimate is inappropriate if the traveltime to the midpoint is not close to halfway between the top and bottom estimates.

Table 11. Approximate length of contributing area, time period sampled, traveltimes from the top, midpoint, and bottom of the wetted screen estimated with the steady-state model using the average 1996 flow field, and the traveltime from the midpoint of the wetted screen estimated with the transient model--(Continued)

[Well locations are shown in figure 3; parentheses indicate that the traveltime to the top of the screen was greater than to the bottom of the screen; ft, feet; <, less than; >, greater than]

Well identifier	Approximate length of contributing area, in ft[a]	Period sampled, in years	Steady-state traveltime, in years from the screen			Transient travel-time from midpoint
			Top	Midpoint	Bottom	
2-32S	549	80	< 1	80	80	16
2-33I	224	72	175	207	247	> 200
2-33S	230	30	< 1	4	30	4
2-34I	3	156	533	608	689	> 200
2-34S	106	11	1	12	12	12
2-35I	150	302	304	429	606	> 200
2-35S	102	7	5	12	12	12
2-36I	1,511	718	452	656	1,170	> 200
2-36S	648	71	< 1	5	71	5
2-37I	77	40	319	312	359	> 200
2-37S	93	11	19	23	30	6
2-38I	22	48	237	260	285	> 200
2-38S	866	21	< 1	16	21	16
2-P1	398	7	7	10	14	10
2-P10	612	6	< 1	4	6	4
2-P11	383	3	< 1	1	3	1
2-P12	39	< 1	< 1	< 1	< 1	< 1
2-P13	58	5	3	5	8	5
2-P2	106	2	7	8	9	8
2-P3	299	3	1	3	4	3
2-P4	407	5	2	3	7	3
2-P5	149	11	2	5	13	5
2-P6	424	65	4	69	69	> 200
2-P7	60	2	14	16	16	16
2-P8	1,118	20	2	21	22	9
2-P9	532	6	2	4	8	4
8-1S	17	7	< 1	3	7	3
8-2S	47	3	< 1	1	3	1
8-3S	76	3	< 1	1	3	1
8-4S	124	5	< 1	2	5	2
8-5I	72	4	10	11	13	11
8-5S	43	4	< 1	2	4	2
8-6S	29	4	4	6	8	6
8-7S	50	5	< 1	2	5	2
8-8S	22	3	3	4	5	4
8-9S	387	28	< 1	3	28	3
8-11S	62	4	< 1	2	4	2
8-12S	32	5	< 1	3	5	3
8-13I	131	2	47	47	49	67
8-13S	41	4	5	7	9	7
8-14S	15	5	28	28	32	26
8-15I	151	5	34	39	39	52
8-15S	202	10	< 1	9	10	9
8-16S	202	10	< 1	9	10	9
8-17S	176	6	< 1	3	6	3
8-18S	119	8	< 1	3	8	3
8-19S	257	12	< 1	7	13	7
8-P1	98	4	10	12	14	12

[a] The length of the contributing area for each well was approximated by the lateral distance between contributing points to the top and bottom of the wetted well screen. This estimate is inappropriate if the traveltime to the midpoint is not close to halfway between the top and bottom estimates.

Table 11. Approximate length of contributing area, time period sampled, traveltimes from the top, midpoint, and bottom of the wetted screen estimated with the steady-state model using the average 1996 flow field, and the traveltime from the midpoint of the wetted screen estimated with the transient model--(Continued)

[Well locations are shown in figure 3; parentheses indicate that the traveltime to the top of the screen was greater than to the bottom of the screen; ft, feet; <, less than; >, greater than]

Well identifier	Approximate length of contributing area, in ft[a]	Period sampled, in years	Steady-state traveltime, in years from the screen			Transient travel-time from midpoint
			Top	Midpoint	Bottom	
8-P2	27	3	< 1	2	3	2
8-P3	38	2	1	2	3	2
8-P4	500	14	< 1	10	14	10
8-P5	72	11	< 1	5	11	5
8-P6	585	46	< 1	45	46	3
9-1S	32	5	< 1	2	5	2
9-2S	36	3	< 1	1	3	1
9-3S	180	23	< 1	22	23	2
10-P1	18	5	2	7	7	7
11-1S	571	(69)	145	145	76	27
11-2S	537	(112)	152	170	40	49
11-3S	539	(97)	135	78	38	30
13-1S	79	< 1	< 1	< 1	< 1	< 1
13-2S	191	3	< 1	< 1	3	< 1
13-3S	25	2	< 1	< 1	2	< 1
13-4S	452	6	< 1	2	6	2
13-5S	268	7	< 1	2	7	2
13-6S	297	7	14	17	21	17
13-8S	368	11	7	13	18	13
13-10S	404	9	14	17	23	17
13-P1	260	6	< 1	3	7	3
13-P4	45	< 1	6	6	7	6
13-P5	1,379	28	< 1	28	28	8
13-P6	84	5	9	12	14	12
14-1S	826	45	< 1	2	45	2
14-2S	614	35	< 1	34	35	9
14-3S	83	4	27	29	31	18
14-4S	35	2	41	41	42	17
14-5S	10	< 1	56	57	57	17
14-6S	563	33	< 1	32	33	5
14-7S	89	4	23	25	27	18
14-8S	11	< 1	47	48	48	17
14-9S	69	3	22	24	26	17
14-10S	23	1	15	16	17	16
14-11S	56	3	20	21	23	17
14-12S	60	3	8	9	11	9
14-13S	69	3	29	31	33	18
14-14S	38	2	38	38	39	17
14-P1	143	4	< 1	2	4	2
14-P2	83	4	1	3	5	3
1406-2	< 1	< 1	122	122	122	121
1406-7	7	1	209	210	210	78
1406-8	5	2	4	6	6	6
1406-11	< 1	< 1	< 1	< 1	< 1	< 1
1406-13	7	< 1	17	17	17	17
1406-15	153	(11)	45	34	34	69
1406-17	674	66	< 1	66	66	55
1406-23I	< 1	< 1	8	8	8	8

[a] The length of the contributing area for each well was approximated by the lateral distance between contributing points to the top and bottom of the wetted well screen. This estimate is inappropriate if the traveltime to the midpoint is not close to halfway between the top and bottom estimates.

Table 11. Approximate length of contributing area, time period sampled, traveltimes from the top, midpoint, and bottom of the wetted screen estimated with the steady-state model using the average 1996 flow field, and the traveltime from the midpoint of the wetted screen estimated with the transient model--(Continued)

[Well locations are shown in figure 3; parentheses indicate that the traveltime to the top of the screen was greater than to the bottom of the screen; ft, feet; <, less than; >, greater than]

Well identifier	Approximate length of contributing area, in ft[a]	Period sampled, in years	Steady-state traveltime, in years from the screen			Transient travel-time from midpoint
			Top	Midpoint	Bottom	
15-1S	43	5	< 1	3	5	3
15-2S	311	10	< 1	3	10	3
15-3S	73	4	< 1	3	5	3
15-5I	68	3	11	13	14	13
15-5S	29	5	1	4	6	4
15-P1	19	3	2	3	4	3
15-P2	28	3	< 1	2	4	2
15-P3	553	21	2	20	23	10
15-P4	254	9	< 1	6	10	6
16-1I	116	3	12	14	15	14
16-1S	177	4	9	14	14	14
16-2S	35	4	2	4	6	4
16-3S	32	5	< 1	2	5	2
16-4S	124	2	3	4	5	4
17-1S	107	10	< 1	3	11	3
17-2S	103	4	< 1	3	4	3
17-3S	169	14	6	19	20	19
17-P1	14	1	< 1	< 1	1	< 1
17-P2	1,207	(5)	65	60	60	81
18-1S	46	3	< 1	1	3	1
18-2S	48	3	< 1	1	3	1
18-3S	55	2	< 1	2	3	2
20-1S	178	2	6	7	8	7
20-2S	32	2	2	2	4	2
20-3S	529	5	< 1	4	6	4
21-1S	200	3	2	3	5	3
21-2S	184	3	2	3	4	3
21-3S	158	2	3	4	5	4
22-1S	277	13	< 1	5	13	5
22-2S	317	13	< 1	7	14	7
23-1S	75	2	41	42	43	19
23-2S	121	4	37	39	40	23
23-3S	120	3	27	29	30	19
23-4S	106	2	45	46	48	22
23-5I	36	47	242	262	289	> 200
23-5S	822	47	< 1	47	48	18
23-6S	14	1	26	27	27	22
23-7S	91	3	43	44	46	20
24-1S	111	3	26	28	29	20
26-1S	176	10	5	9	15	9
26-2S	253	12	< 1	5	13	5
26-3S	178	11	< 1	5	11	5
26-4S	201	12	< 1	5	12	5
28-1S	41	6	< 1	3	6	3
44-1I	164	36	90	109	126	> 200
44-1S	43	1	4	4	5	4
44-2S	24	1	8	9	10	9
44-3S	10	< 1	35	36	36	20

[a] The length of the contributing area for each well was approximated by the lateral distance between contributing points to the top and bottom of the wetted well screen. This estimate is inappropriate if the traveltime to the midpoint is not close to halfway between the top and bottom estimates.

Table 11. Approximate length of contributing area, time period sampled, traveltimes from the top, midpoint, and bottom of the wetted screen estimated with the steady-state model using the average 1996 flow field, and the traveltime from the midpoint of the wetted screen estimated with the transient model--(Continued)

[Well locations are shown in figure 3; parentheses indicate that the traveltime to the top of the screen was greater than to the bottom of the screen; ft, feet; <, less than; >, greater than]

Well identifier	Approximate length of contributing area, in ft[a]	Period sampled, in years	Steady-state traveltime, in years from the screen			Transient travel-time from midpoint
			Top	Midpoint	Bottom	
45-1I	197	38	110	127	148	> 200
45-1S	297	3	< 1	3	3	3
45-2S	19	< 1	23	24	24	17
52-1S	39	24	23	23	47	23
56-1S	999	27	< 1	27	27	6
B-1I	329	(2)	35	33	33	36
B-1S	255	7	< 1	3	7	3
BE-1S	85	2	2	3	4	3
BE-2S	119	2	< 1	1	2	1
BE-3S	75	2	1	2	3	2
BE-4S	98	2	2	3	4	3
BE-7S	85	2	2	3	4	3
BE-8I	148	2	10	12	12	12
BE-9S	68	2	2	3	4	3
BQ-2S	148	3	3	4	5	4
BQ-3S	142	3	3	5	6	5
BQ-4S	37	< 1	< 1	< 1	< 1	< 1
BQ-5S	51	< 1	< 1	< 1	< 1	< 1
BQ-6S	34	< 1	< 1	< 1	< 1	< 1
CU-1S	60	1	5	6	6	6
CU-2S	96	2	4	5	6	5
CU-3S	38	1	7	8	8	8
CU-4S	34	< 1	10	10	10	10
CU-5S	16	< 1	13	14	14	14
CU-6S	2	< 1	40	40	40	14
CU-7S	52	1	7	7	8	7
CU-8I	34	3	19	20	22	17
TC-1I	5	< 1	4	5	5	5
TC-2S	191	< 1	1	2	2	2
TC-3S	22	< 1	2	2	2	2
TC-4S	491	4	1	5	6	5
TC-5S	445	3	< 1	3	4	3
TC-6S	582	5	< 1	3	5	3

[a] The length of the contributing area for each well was approximated by the lateral distance between contributing points to the top and bottom of the wetted well screen. This estimate is inappropriate if the traveltime to the midpoint is not close to halfway between the top and bottom estimates.

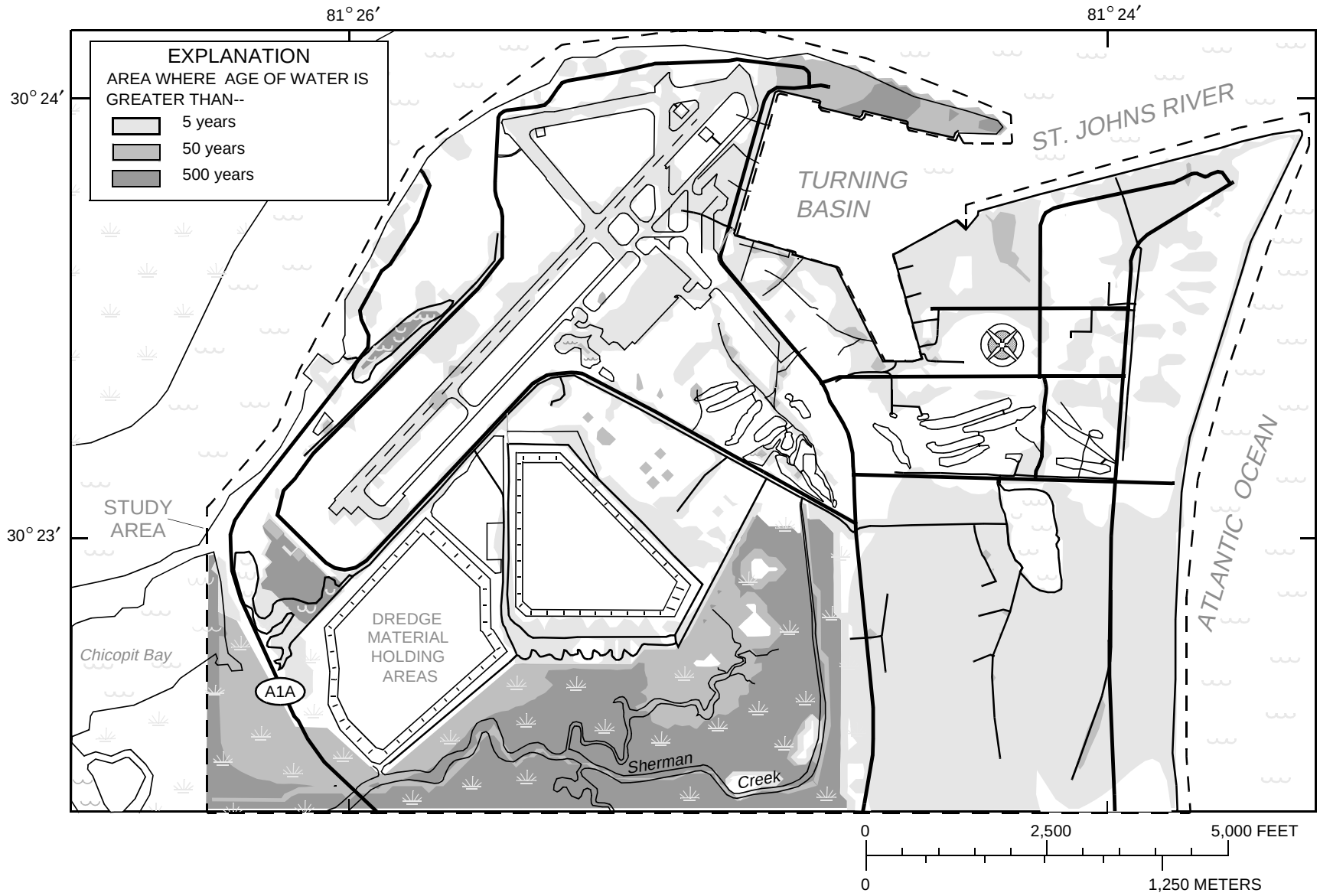

Figure 40. Age of water in the S-zone simulated by the steady-state model using the average 1996 flow field and with a uniform effective porosity of 40 percent.

All of the water in the I-zone, except for a small area beneath golf greens near well 20-2S, is more than 5 years old (fig. 41). Most of the water in the I-zone between 5 and 50 years old is in an area where the marsh-muck confining unit is absent and beneath part of the western dredge material holding area. The oldest water in the I-zone is in stagnant zones beneath the hangars and runways and east of Echo and Foxtrot piers (fig. 41).

MODEL LIMITATIONS

The flow model addresses questions about the advective movement of contaminants through the surficial aquifer system beneath NAVSTA Mayport fairly well, but it cannot mimic the true system exactly. This model, or any other model, is limited by simplification of the conceptual model, discretization effects, difficulty in obtaining sufficient measurements to account for all of the spatial variation in hydraulic properties throughout the model area, and limitations in the accuracy of land surface altitude measurements.

The conceptual model has been simplified by assuming most of the current questions raised by site assessments and remediation plans can be addressed with either a steady-state ground-water flow model or a transient model that considers gross changes over periods of 5 years or more. However, available data indicate that during 1996, water-levels fluctuated seasonally as much as 8 ft, and the surficial aquifer system infrequently approaches, at best, a quasi-steady state condition. Both the steady-state and transient models were adequate to estimate the advective movement of dissolved constituents over a few years or more, but are not adequate to estimate the advective movement of contaminants over a couple of years or less.

Estimates of future contaminant migration are limited by future land uses at NAVSTA Mayport and the reactive nature of the contaminants. Historical land use changes at NAVSTA Mayport indicate that the stresses identified for 1996 are unlikely to remain the same and future ground-water movement beneath NAVSTA Mayport will be affected by changes in land use. Many of the contaminants that were identified at NAVSTA Mayport are sorbtive which retards their movement and the contaminants move at velocities less than the surrounding ground water.

Lateral discretization of the study area into a rectangular grid of cells and vertical discretization into layers forced an averaging of hydraulic properties. Each cell represents a homogeneous block or some volumetric average of the aquifer medium. Discretization errors occurred in even the smallest model cells, which were 100 ft on a side and about 3 ft thick, because the S-zone contains clay lenses that are less than 1 ft thick interbedded in the more permeable sands. Due to the averaging of the hydraulic properties, the model cannot simulate the dispersive effects on flow caused by aquifer heterogeneity.

The model of a heterogeneous aquifer system was simplified further by the methods used to describe the spatial variability of the hydraulic conductivity distributions. The lateral hydraulic conductivity distributions of the S-zone and I-zone of the surficial aquifer system were assumed to be log-normally distributed. The vertical hydraulic conductivity of the marsh-muck confining unit and the vertical anisotropy of the S-zone were uniform multipliers that changed by fixed amounts throughout each area. The lack of sufficient measurements to account for all of the spatial variation in hydraulic properties throughout the model area necessitated these simplifications. Simplifying the model to this degree does not invalidate the model results, but does mean that model results should be interpreted at scales larger than the representative elemental volume of hydraulic conductivity.

SUMMARY

As part of the Installation Restoration Program, NAVSTA Mayport is considering remedial-action alternatives to control the movement of contaminants from sites that may otherwise discharge to the surface. The evaluation of remedial-action alternatives requires a quantifiable understanding of how the ground-water flow system responds to current conditions and how the system will respond to future stresses imposed on the system. Numerical simulation provides the most tractable way of achieving this level of understanding.

The geologic units of interest in the study area consist of sediments of Holocene to Miocene age that extend from land surface to the top of the Hawthorn Group. Previous investigators have defined this sequence as the surficial aquifer system. Because this study is concerned with ground-water movement near the surface, this sequence has been further subdivided into three local geohydrologic units: the S-zone, the marsh-muck confining unit, and the I-zone. The geohydrologic structure within the study area was defined by depth and thickness data from geologists' logs.

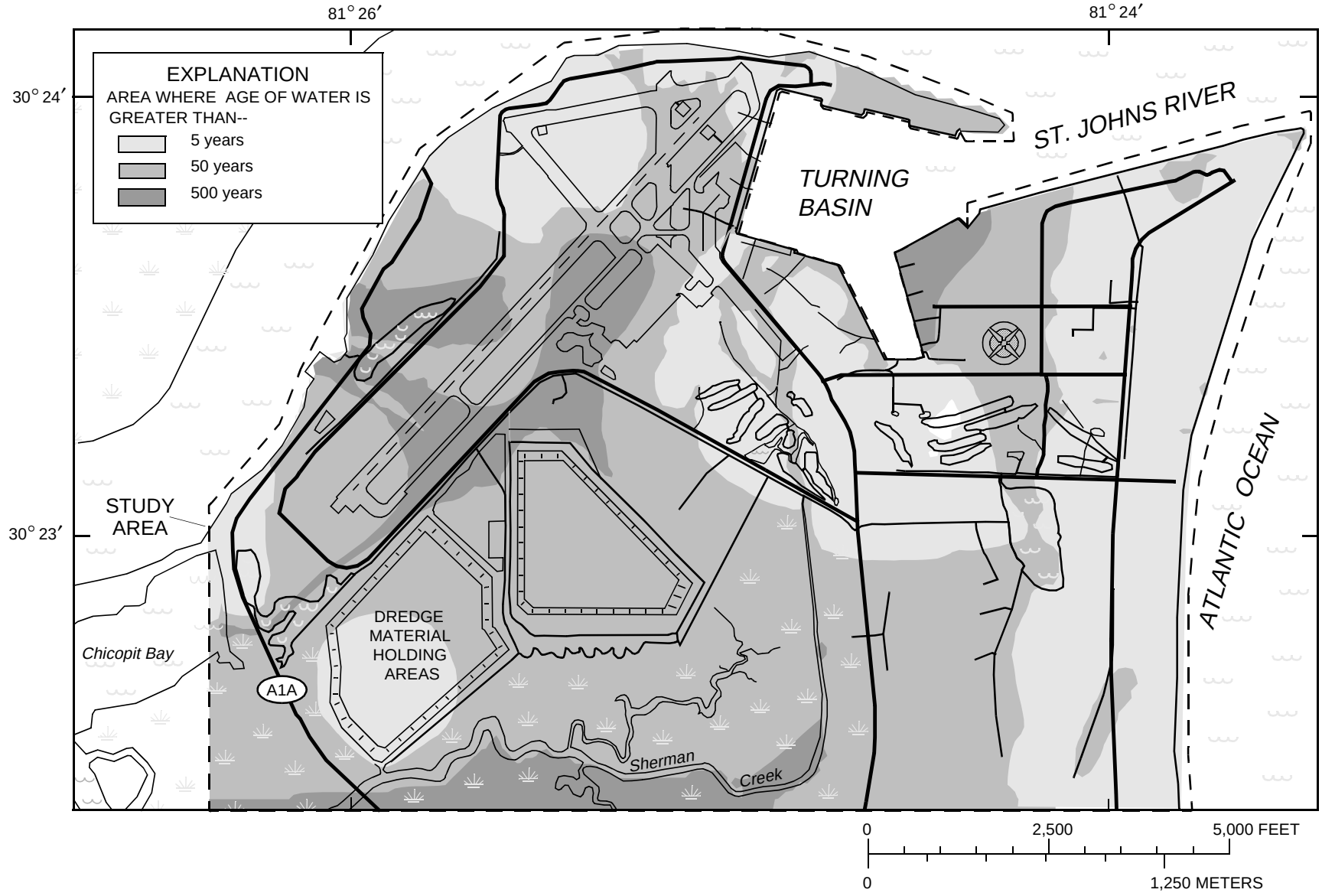

Figure 41. Age of water in the I-zone simulated by the steady-state model using the average 1996 flow field with a uniform effective porosity of 40 percent.

The chloride-ratio method was used to estimate the recharge rate in the study area. The recharge rate and associated uncertainty were estimated with annual atmospheric chloride deposition rates between 1985 and 1994 and 22 ground-water chloride measurements from the surficial-aquifer system beneath NAVSTA Mayport. The recharge rate was estimated to be 7 in/yr. The range in recharge rate for a 95 percent confidence interval is 4 to 15 in/yr.

Ground-water flow through the surficial aquifer system was simulated with a two-layer, finite-difference model that extended vertically from the water table to the top of the intermediate confining unit. Multi-well aquifer tests, single-well aquifer tests, and slug tests were conducted at NAVSTA Mayport to estimate the hydraulic properties of the surficial aquifer system. The lateral hydraulic conductivities estimated by these tests were the final values used in the ground-water flow model because ground-water discharge could not be quantified. The lateral hydraulic conductivity distributions of the S-zone (layer 1) and the I-zone (layer 2) were estimated by kriging the log-hydraulic conductivities from the aquifer tests.

The dominant surface-water features adjacent to NAVSTA Mayport are the St. Johns River and the Atlantic Ocean; these features communicate directly with both the S-zone and I-zone of the surficial aquifer system. The distribution of surface-water features was determined from aerial photographs and plans of NAVSTA Mayport. All lateral model boundaries in each layer were assumed to be no-flow boundaries that coincided with either surface-water features or were parallel to ground-water flow paths.

The effective-recharge approach was used to calibrate a series of independent steady-state models to the available data which consisted of "snapshot" images of a transient system. The model was calibrated to 229 water-level measurements from 181 wells during three synoptic surveys (July 17, 1995; July 31, 1996; and October 24, 1996). Model calibration was facilitated by a parameter estimation program that estimated the effective recharge rates and the vertical hydraulic conductivities.

The unweighted minimum, maximum, average, and RMS errors in water levels from the calibrated model were -2.78, 1.92, 0.00, and 0.82 ft, respectively, and did not exhibit any apparent trend across the study area. Most of the estimated parameters are not highly correlated. Model error was determined to be most sensitive to changes in recharge rates to the unirrigated areas and golf course irrigation.

The analysis of ground-water flow and potential movement of contaminants within the surficial aquifer system primarily was addressed using the calibrated model driven by the effective recharge rate distribution estimated for period 1. This recharge rate distribution was assumed to be representative of the average rate of water application to the surficial aquifer system because the effective recharge rate to the unirrigated areas was about 8 in/yr. The total flow through the surficial aquifer system averaged 2.3 ft^3/s and ranged from 1 to 4 ft^3/s during 1996. Irrigation accounts for about 20 percent of the water that circulates through the surficial aquifer system. Most of the I-zone is recharged by areas where the marsh-muck confining unit is less than 1 ft thick. Contaminants migrating from areas that recharge the I-zone will have longer flow paths and residence times than those that exclusively migrate through the S-zone.

The surficial aquifer system at NAVSTA Mayport is a dynamic system and has been modified greatly by natural and anthropogenic forces over the last 100 years. The freshwater flow system is expanding and entrained saltwater is still being flushed from the system. The advective displacement of the saline pore water initially was simulated as discrete particles being flushed by a steady-state flow field. The simulated saltwater distribution after 200 years of displacement did not consistently describe the chloride distribution in the I-zone measured during 1993 and 1996.

A transient model of the Mayport peninsula was developed to better approximate the saltwater displacement and accounted for the known changes in hydraulic properties, boundary conditions, and stresses over the last 200 years. The transient flow field of the surficial aquifer system was simulated with 10 stress periods that approximated the shifting morphology and changing boundaries between 1798 and 1997. A new MODFLOW package (VAR1) was written to simulate the temporal variation of hydraulic properties caused by construction activities at NAVSTA Mayport. The simulated saltwater distribution after 200 years of transient displacement described the measured chloride distribution in the I-zone better than the steady-state simulation.

The advective movement of conservative contaminants from selected sites within the solid waste management units to discharge points was

simulated with MODPATH. Particles were released at the water table to approximate the initial position of contaminants at selected sites. Most of the particles were discharged to the nearest surface-water feature and traveled less than 1,000 ft before being discharged from the ground-water system. The traveltimes were estimated using an effective porosity of 40 percent. A generalized map of traveltimes showed most areas within 1,000 ft of a surface-water feature or a storm sewer had traveltimes of less than 50 years.

The contributing areas for 224 wells at NAVSTA Mayport were identified by back-tracking a particle from the midpoint of the wetted screen with the steady-state model. Some of the contributing area estimates were inappropriate or misleading because the well screens intercepted multiple contributing areas or were supplied by areas of different recharge rates.

The effect of the historical changes at NAVSTA Mayport on contributing areas to wells was investigated. Particles were back-tracked from the midpoint of the wetted screens with the transient model and compared to the steady-state results. Traveltimes to contributing areas that ranged between 15 and 50 years as estimated by the steady-state model differed most from the transient estimates. Estimates of traveltimes and pathlines from the transient model typically were 10 to 20 years less and about half as long as estimates from the steady-state model. The difference is attributed to the increase in the average distance between contributing areas and observation wells resulting from the expansion of the impervious surfaces near the affected wells.

REFERENCES

Baker, L.A., 1991, Appendix B, Regional estimates of atmospheric dry deposition, *in* Acidic Deposition and Aquatic Ecosystems—Regional Case Studies: New York, Springer-Verlag, p. 645-652.

Bidlake, W.R., Woodham, W.M., and Lopez, M.A., 1993, Evapotranspiration from areas of native vegetation in west-central Florida: U.S. Geological Survey Open-File Report 84-143, 35 p.

Bouwer, Herman, and Rice, R.C., 1976, A slug test for determining hydraulic conductivity of unconfined aquifers with completely or partially penetrating wells: Water Resources Research, 12 (3), p. 423-428.

Brown, D.P., Johnson, R.A., Baker, J.S., 1984, Hydrogeologic data from a test well at Kathryn Abbey Hanna Park, City of Jacksonville, Florida: U.S. Geological Survey Open-File Report 84-143, 27 p.

Causey, L.V., and Phelps, G.G., 1978, Availability and quality of water from shallow aquifers in Duval County, Florida: U.S. Geological Survey Water-Resources Investigations Report 78-92, 36 p.

Cooper, H.H., Jr., and Jacob, C.E., 1946, A generalized graphical method for evaluating formation constants and summarizing well field history: Transactions of the American Geophysical Union, v. 27, p. 526-534.

Cooper, H.H., Jr., Kohout, F.A., Glover, R.E., and Henry, H.R., 1964, Sea water in coastal aquifers: U.S. Geological Survey Water Supply Paper 1613-C, p. 6-11.

Davis, J.H., Planert, M., and Andrews, W.J., 1996, Simulation of ground-water flow at the U.S. Naval Air Station Jacksonville, Florida, with an evaluation of changes to ground-water movement caused by proposed remedial designs at operable unit 1: U.S. Geological Survey Open-File Report 96-597, 47 p.

Domenico, P.A., and Schwartz, F.W., 1990, Physical and chemical hydrogeology: New York, John Wiley and Sons, Inc., 824 p.

Farnsworth, R.K., Thompson, E.S., and Peck, E.L., 1982, Evaporation atlas for the contiguous 48 United States: National Oceanographic and Atmospheric Administration Technical Report, NWS-33, 26 p.

Franks, B.J., 1980, The surficial aquifer at the U.S. Naval Station near Mayport, Florida: U.S. Geological Survey Open-File Report 80-765, 13 p.

Gill, T.E., Murray, W., and Wright, M.H., 1981, Practical optimization: Orlando, Fla., Academic Press Inc., 401 p.

Halford, K.J., 1992, Incorporating reservoir characteristics for automatic history matching: Baton Rouge, La., Louisiana State University, Ph.D. dissertation, 150 p.

———1997, Effects of unsaturated zone on aquifer test analysis in a shallow-aquifer system: Ground Water, v. 35, no. 3, p. 512-522.

———1998, Ground-water flow in the surficial aquifer system and potential movement of contaminants from selected waste-disposal sites at Cecil Field Naval Air Station, Jacksonville, Florida: U.S. Geological Survey Water-Resources Investigations Report 97-4278.

Halford, K.J., Murray, L.C., Jr., Spechler, R.M., Phelps, G.G., and Bradner, L.A., 1993, Potentiometric surface of the Upper Floridan aquifer in the St. Johns River Water Management District and vicinity, May 1993: U.S. Geological Survey Open-File Report 93-451, 1 sheet.

Healy, R.W., 1990, Simulation of solute transport in variably saturated porous media with supplemental information on modifications to the U.S. Geological Survey's

computer program VS2D: U.S. Geological Survey Water-Resources Investigations Report 90-4025, 125 p.

Isaaks, E.H., and Srivastava, R.H., 1989, Applied geostatistics: New York, Oxford University Press, 561 p.

Krause, R.E., and Randolph, R.B., 1989, Hydrology of the Floridan aquifer system in southeast Georgia and adjacent parts of Florida and South Carolina: U.S. Geological Survey Professional Paper 1403-D, 65 p.

Krulikas, R.K., and Giese, G.L., 1995, Recharge to the surficial aquifer system in Lee and Hendry Counties, Florida: U.S. Geological Survey Water-Resources Investigations Report 95-4003, 21 p.

Lappala, E.G., Healy, R.W., and Weeks, E.P., 1987, Documentation of computer program VS2D to solve the equations of fluid flow in variably saturated porous media: U.S. Geological Survey Water-Resources Investigations Report 83-4009, 184 p.

McDonald, M.G., and Harbaugh, A.W., 1988, A modular three-dimensional finite-difference ground-water flow model: U.S. Geological Survey Techniques of Water-Resources Investigations, book 6, chap. A1, 576 p.

National Atmospheric Deposition Program, NADP/NTN annual data summary-precipitation chemistry in the United States: 1985-1994.

Owenby, J.R., and Ezell, D.S., 1992, Monthly station normals of temperature, precipitation, and heating and cooling degree days 1961-90—Florida: National Oceanographic and Atmospheric Administration Climatography of the United States, no. 81, 26 p.

Pollock, D.W., 1994, User's guide for MODPATH/MODPATH-PLOT, version 3: A particle tracking post-processing package for MODFLOW, the U.S. Geological Survey finite-difference ground-water flow model: U.S. Geological Survey Open-File Report 94-464 [variously paged].

Spechler, R.M., 1994, Saltwater intrusion and quality of water in the Floridan aquifer system, northeastern Florida: U.S. Geological Survey Water-Resources Investigations Report 92-4174, 76 p.

Stem, L.T., Dollar, H.D., Howell, D.A., Lewis, D.L., Wettstein, C.A., and Yamataki, H., 1978, Soil survey of city of Jacksonville, Duval County, Florida: U.S. Department of Agriculture, Soil Conservation Service, 113 p.

Sumner, D.M., 1996, Evapotranspiration from successional vegetation in a deforested area of the Lake Wales Ridge, Florida: U.S. Geological Survey Water-Resources Investigations Report 96-4244, 38 p.

Theis, C.V., 1935, The relation between the lowering of the piezometric surface and the rate and duration of discharge of a well using ground-water storage: Transactions of the American Geophysical Union, v. 16, p. 519-524.

U.S. Department of the Navy, Southern Division Naval Facilities Engineering Command, 1995, Resource Conservation and Recovery Act (RCRA) corrective action program general information report, Naval Station, Mayport, Florida: UIC No. N60201, SouthDiv Contract N62467-89-D-0317/028, July 1995, 286 p.

U.S. Environmental Protection Agency, 1988, Ambient water quality criteria: Office of Water, Regulations, and Standards Division, EPA-440/5-86-008, 256 p.

U.S. Geological Survey, 1996, Water resources data for Florida, water year 1995: v. 1A, Northeast Florida surface water, 357 p.

Yeh, W.W.-G., 1986, Review of parameter identification procedures in groundwater hydrology: Water Resources Research, v. 22, no. 2, p. 95-108.

APPENDIXES

Appendix A. Well information at NAVSTA Mayport

[All measurements are in feet, except as noted]

Well ID	Easting[a]	Northing[a]	Top of casing	Casing length	Screen length	Depth to water	Base of S-zone	Base of I-zone	Thickness		Lateral hydraulic conductivity, in ft/d	
									Marsh-muck confining unit	I-zone	S-zone	I-zone
1-1I	372,827	2,202,318	14.09	30	5	7	12	55	2	41	2	10
1-1S	372,829	2,202,287	16.96	5	10	9	15	58	2	41	3	10
1-2S	372,520	2,202,618	16.89	5	10	11	22	59	5	32	5	4
1-P1	372,912	2,203,345	7.11	5	5	5	23	49	3	23	16	3
1-P2	373,339	2,202,891	11.77	10	5	8	23	54	1	30	16	12
1-P3	372,166	2,202,846	11.04	5	10	7	20	56	7	28	14	3
2-1S	365,499	2,199,298	10.33	3	7	5	10	63	2	50	8	35
2-2S	368,574	2,199,856	7.56	3	7	4	10	63	3	50	7	42
2-3S	364,605	2,199,039	17.20	5	10	9	20	60	4	36	12	20
2-4S	365,011	2,199,897	8.29	3	10	4	10	59	4	45	15	18
2-6S	365,493	2,199,780	9.43	3	7	3	10	65	3	51	8	24
2-7S	365,927	2,197,406	10.49	4	7	7	22	55	5	28	8	69
2-8S	365,839	2,200,145	10.55	3	7	4	11	72	2	59	6	20
2-9I	366,128	2,200,339	10.49	15	10	4	11	72	2	59	4	16
2-9S	366,127	2,200,346	10.50	3	7	4	11	72	2	59	4	16
2-10S	366,392	2,200,334	10.02	5	5	4	12	72	3	57	4	15
2-11I	368,640	2,198,821	5.77	25	5	3	9	59	6	44	7	53
2-11S	368,644	2,198,830	5.73	2	10	3	9	59	6	44	7	53
2-12I	368,320	2,198,212	5.42	14	5	3	10	57	5	42	7	45
2-12S	368,318	2,198,210	5.51	2	10	3	10	57	5	42	7	45
2-13S	365,693	2,200,320	7.57	2	10	3	10	70	3	57	9	16
2-15I	367,585	2,200,458	6.89	15	10	3	11	66	5	50	4	14
2-15S	367,585	2,200,461	6.65	5	10	3	10	65	5	50	4	14
2-16S	365,475	2,200,289	6.73	2	10	2	9	67	5	54	12	17
2-17I	365,768	2,197,417	7.83	25	5	4	22	52	4	25	8	70
2-17S	365,775	2,197,410	7.73	3	10	4	22	52	4	25	8	70
2-18I	366,069	2,200,556	6.51	25	5	1	9	68	1	58	5	14
2-18S	366,070	2,200,556	6.37	2	10	1	9	68	1	58	5	14
2-19S	366,211	2,200,026	32.50	25	10	23	34	93	3	56	4	22
2-20S	366,631	2,199,689	32.09	25	10	19	31	91	6	53	4	35
2-21S	367,897	2,200,052	7.56	3	10	1	8	65	3	54	5	28
2-22I	365,528	2,199,563	7.19	25	5	2	8	62	3	52	7	30
2-22S	365,528	2,199,568	8.09	2	10	2	9	63	3	52	7	30
2-23I	368,951	2,199,409	5.36	25	5	2	5	59	6	48	8	50
2-23S	368,954	2,199,414	5.22	3	10	2	5	59	6	48	8	50
2-24S	365,637	2,199,026	32.29	4	10	23	33	84	2	50	7	44
2-25I	367,458	2,198,859	31.78	50	5	18	35	86	5	46	3	51
2-25S	367,453	2,198,864	32.07	25	10	18	36	87	5	46	3	51
2-26I	367,495	2,198,092	32.35	50	5	20	37	84	5	41	9	48
2-26S	367,500	2,198,100	32.41	30	10	20	38	84	5	41	9	48
2-27I	366,592	2,197,396	7.99	25	5	4	10	55	6	39	7	57
2-28S	364,987	2,198,675	17.36	4	10	6	22	62	3	37	10	28
2-29S	364,775	2,199,943	9.43	2	10	5	9	54	4	41	22	14
2-30S	365,514	2,200,721	8.91	3	10	5	11	68	4	52	15	12
2-31I	364,247	2,199,945	9.08	25	5	2	12	45	11	23	26	10
2-31S	364,241	2,199,940	9.14	2	10	2	12	45	11	23	26	10
2-32I	364,817	2,200,580	9.10	25	5	3	7	54	7	40	46	14
2-32S	364,813	2,200,576	9.10	2	10	3	7	54	7	40	46	14
2-33I	365,496	2,201,368	9.33	25	5	2	10	64	5	49	27	8
2-33S	365,491	2,201,362	9.47	2	10	2	11	63	5	47	27	8
2-34I	366,614	2,202,542	10.81	25	5	1	7	66	14	45	27	0.1
2-34S	366,609	2,202,537	10.46	2	10	0	6	65	14	45	27	0.1
2-35I	363,450	2,200,286	7.40	24	5	0	7	32	5	21	10	10
2-35S	363,445	2,200,281	7.36	2	10	0	7	32	5	21	10	10

Appendix A. Well information at NAVSTA Mayport--(Continued)

[All measurements are in feet, except as noted]

Well ID	Easting[a]	Northing[a]	Top of casing	Casing length	Screen length	Depth to water	Base of S-zone	Base of I-zone	Thickness		Lateral hydraulic conductivity, in ft/d	
									Marsh-muck confining unit	I-zone	S-zone	I-zone
2-36I	364,162	2,200,982	7.57	25	5	2	9	32	10	13	17	51
2-36S	364,158	2,200,977	7.58	2	10	2	9	32	10	13	17	51
2-37I	364,907	2,201,740	6.84	25	5	1	14	51	10	28	1	4
2-37S	364,902	2,201,736	6.93	2	10	1	14	51	10	28	1	4
2-38I	365,577	2,202,418	8.16	25	5	2	9	64	10	46	58	1
2-38S	365,563	2,202,403	8.14	2	10	2	9	64	10	46	58	1
2-P1	365,497	2,199,064	7.75	3	5	2	8	59	2	49	8	39
2-P10	363,416	2,195,900	32.02	30	5	31	33	68	1	33	10	21
2-P11	364,396	2,196,199	31.85	30	5	31	37	70	2	31	8	30
2-P12	365,157	2,196,870	32.75	25	5	29	43	74	3	28	8	47
2-P13	367,409	2,199,403	11.87	5	5	1	14	69	5	50	3	46
2-P2	365,498	2,198,464	7.97	4	5	3	14	56	3	39	8	42
2-P3	363,421	2,198,075	31.93	27	5	23	36	66	2	28	14	11
2-P4	364,241	2,198,967	32.74	30	5	26	36	71	4	31	13	15
2-P5	366,453	2,201,087	7.15	6	5	4	10	68	2	55	5	5
2-P6	367,965	2,200,322	5.10	5	5	4	7	62	3	53	6	19
2-P7	366,597	2,197,397	7.95	5	5	4	9	55	7	40	7	57
2-P8	367,732	2,197,417	6.35	5	5	3	8	55	5	42	5	39
2-P9	362,978	2,197,566	32.18	30	5	26	35	65	1	29	17	13
8-1S	366,285	2,204,731	10.19	6	10	6	15	51	1	35	2	17
8-2S	366,262	2,204,968	13.93	5	10	10	19	54	0	34	3	16
8-3S	366,363	2,205,070	13.72	5	10	11	19	54	0	34	6	16
8-4S	366,255	2,205,098	11.90	5	10	9	18	52	0	34	5	16
8-5I	366,645	2,203,938	13.34	25	5	7	15	56	1	40	2	11
8-5S	366,640	2,203,929	13.00	5	10	6	14	56	1	40	2	11
8-6S	366,149	2,204,829	11.57	5	10	8	17	52	0	35	2	17
8-7S	366,601	2,205,103	11.73	5	10	8	17	52	0	35	3	19
8-8S	366,883	2,205,161	13.12	5	10	9	17	53	1	35	1	26
8-9S	366,890	2,204,961	12.55	5	10	6	16	53	1	35	2	24
8-11S	366,493	2,205,204	11.46	5	10	9	18	51	0	33	6	17
8-12S	366,970	2,205,290	12.93	8	10	9	17	53	1	36	1	30
8-13I	366,853	2,205,390	11.33	35	5	8	15	51	0	36	1	29
8-13S	366,853	2,205,390	11.33	5	10	8	15	51	0	36	1	29
8-14S	366,701	2,205,362	10.72	5	10	8	15	51	0	35	2	23
8-15I	366,579	2,205,347	9.96	34	5	7	16	50	0	34	3	21
8-15S	366,394	2,205,227	10.03	5	10	8	17	50	0	33	9	16
8-16S	366,394	2,205,227	10.03	5	10	8	17	50	0	33	9	16
8-17S	366,230	2,205,126	10.89	5	10	8	17	51	0	34	7	16
8-18S	366,161	2,205,002	8.80	5	10	6	15	49	0	34	3	16
8-19S	366,196	2,205,169	5.24	4	10	3	11	45	0	34	5	17
8-P1	367,186	2,204,937	12.89	10	5	7	16	54	1	36	4	31
8-P2	368,584	2,205,241	12.70	5	10	10	18	54	0	36	5	38
8-P3	368,104	2,205,052	13.17	5	10	10	18	55	0	37	2	41
8-P4	367,808	2,204,485	14.67	5	10	8	18	58	3	37	9	21
8-P5	367,286	2,203,956	14.00	5	10	4	16	58	2	41	6	8
8-P6	366,740	2,203,360	14.87	5	10	6	14	63	2	48	7	2
9-1S	367,081	2,205,219	14.42	8	10	11	18	55	1	36	2	34
9-2S	367,012	2,205,466	13.39	5	10	10	17	53	0	36	2	36
9-3S	367,183	2,205,508	11.53	5	10	9	15	51	0	37	3	40
10-P1	365,964	2,204,746	10.68	10	10	7	15	51	0	36	2	18
11-1S	369,851	2,205,131	12.16	10	10	11	21	55	0	33	9	20
11-2S	369,902	2,205,332	10.42	10	10	9	20	52	0	32	9	21
11-3S	369,803	2,205,343	9.97	7	10	9	19	52	0	33	9	23
13-1S	368,004	2,202,052	13.06	3	7	7	12	67	0	55	21	2

Appendix A. Well information at NAVSTA Mayport--(Continued)

[All measurements are in feet, except as noted]

Well ID	Easting[a]	Northing[a]	Top of casing	Casing length	Screen length	Depth to water	Base of S-zone	Base of I-zone	Thickness		Lateral hydraulic conductivity, in ft/d	
									Marsh-muck confining unit	I-zone	S-zone	I-zone
13-2S	367,476	2,201,307	12.79	3	7	6	11	71	2	58	13	3
13-3S	367,741	2,200,862	10.41	3	7	6	12	68	2	54	6	8
13-4S	367,688	2,201,086	9.88	2	10	5	10	68	1	56	7	5
13-5S	367,719	2,201,499	10.04	3	10	4	11	67	1	55	13	3
13-6S	367,684	2,201,905	9.66	2	10	2	10	65	2	53	28	1
13-8S	367,394	2,202,014	10.47	2	10	2	10	66	5	52	42	1
13-10S	367,455	2,201,732	9.65	2	10	2	10	66	3	54	31	1
13-P1	366,076	2,201,716	11.04	5	5	3	12	69	5	52	18	1
13-P4	368,069	2,201,301	9.31	5	5	5	11	65	0	54	15	4
13-P5	367,115	2,200,912	6.45	5	5	4	8	66	3	55	2	5
13-P6	366,880	2,202,120	10.16	5	5	1	8	67	9	50	28	0
14-1S	374,860	2,203,771	7.56	3	9	6	20	53	0	32	13	23
14-2S	374,681	2,203,726	8.64	3	10	7	22	54	0	32	12	21
14-3S	374,653	2,203,661	6.17	3	10	4	19	51	0	32	8	22
14-4S	374,826	2,203,692	6.37	3	10	4	19	51	0	33	14	24
14-5S	374,934	2,203,729	7.42	3	10	5	20	52	0	32	11	24
14-6S	374,997	2,203,839	5.97	3	10	4	18	51	0	32	11	23
14-7S	374,640	2,203,604	5.96	3	10	4	19	51	0	32	8	22
14-8S	374,926	2,203,629	6.58	3	10	5	19	52	0	33	15	25
14-9S	374,694	2,203,500	6.38	3	10	4	19	52	0	32	10	23
14-10S	374,927	2,203,515	5.77	3	10	4	18	51	0	33	13	26
14-11S	374,732	2,203,341	6.88	3	10	4	19	52	0	33	18	26
14-12S	374,688	2,203,072	9.92	3	10	7	21	55	0	34	15	29
14-13S	374,708	2,203,608	5.68	3	10	4	18	51	0	32	10	23
14-14S	374,852	2,203,650	6.55	3	10	4	19	52	0	33	14	24
14-P1	374,025	2,203,676	6.50	5	5	4	21	51	0	30	13	14
14-P2	375,562	2,204,016	5.71	6	5	4	18	50	0	33	21	24
1406-2	370,014	2,202,496	6.80	3	10	4	10	55	0	45	14	9
1406-7	369,366	2,202,734	7.69	3	10	6	10	56	0	46	13	8
1406-8	368,855	2,202,872	7.50	3	10	5	8	56	0	48	13	6
1406-11	369,122	2,202,827	7.67	3	10	6	9	56	0	46	13	7
1406-13	369,768	2,202,491	6.82	3	10	4	9	55	0	46	14	9
1406-15	369,572	2,202,595	5.93	3	10	3	8	54	0	46	13	8
1406-17	369,381	2,202,518	7.24	4	10	5	9	56	0	47	14	7
1406-23I	369,494	2,202,660	7.40	50	5	6	10	56	0	46	13	8
15-1S	365,726	2,203,211	12.14	5	10	6	14	62	1	47	4	5
15-2S	365,942	2,202,905	11.77	3	10	3	13	65	1	51	7	1
15-3S	365,641	2,203,087	11.26	6	10	5	14	63	1	47	7	3
15-5I	365,767	2,203,379	12.45	25	5	6	16	61	0	45	3	8
15-5S	365,772	2,203,377	12.37	8	10	6	15	61	0	45	3	8
15-P1	365,689	2,204,182	13.28	10	5	6	16	56	0	40	3	17
15-P2	365,420	2,203,729	10.83	5	10	5	13	56	0	43	5	16
15-P3	365,854	2,202,424	10.07	5	10	2	11	67	3	52	9	0
15-P4	362,689	2,199,535	10.51	5	10	3	12	37	2	23	11	9
16-1I	367,542	2,205,254	12.64	25	5	10	16	53	0	37	11	51
16-1S	368,463	2,203,118	12.45	10	10	8	13	61	1	47	13	5
16-2S	367,483	2,205,468	10.65	5	10	8	14	51	0	37	5	52
16-3S	367,599	2,205,439	11.19	5	10	8	15	52	0	37	6	55
16-4S	367,679	2,204,979	14.65	5	10	11	18	56	1	37	20	38
17-1S	370,214	2,201,128	8.60	3	10	6	10	59	0	48	19	21
17-2S	370,144	2,201,319	8.34	3	10	5	10	58	0	48	18	18
17-3S	370,349	2,201,346	8.17	4	10	5	10	58	0	48	19	17
17-P1	369,942	2,201,071	7.97	5	5	4	9	59	0	50	16	23
17-P2	370,630	2,201,114	7.72	7	5	6	10	57	0	47	22	18

Appendix A. Well information at NAVSTA Mayport--(Continued)

[All measurements are in feet, except as noted]

Well ID	Easting[a]	Northing[a]	Top of casing	Casing length	Screen length	Depth to water	Base of S-zone	Base of I-zone	Thickness		Lateral hydraulic conductivity, in ft/d	
									Marsh-muck confining unit	I-zone	S-zone	I-zone
18-1S	374,966	2,203,261	7.42	3	10	5	19	53	0	34	15	29
18-2S	375,011	2,203,400	6.82	3	10	5	19	52	0	33	11	27
18-3S	375,236	2,203,510	7.49	3	10	5	19	52	0	33	16	27
20-1S	372,101	2,200,764	13.49	5	10	4	14	57	4	39	26	23
20-2S	372,164	2,200,732	13.68	4	10	4	14	57	4	39	27	23
20-3S	371,946	2,200,862	12.01	3	10	4	13	57	3	41	24	21
21-1S	372,202	2,200,875	13.21	5	10	3	12	57	5	40	27	21
21-2S	372,370	2,200,897	12.79	5	10	3	12	56	4	40	21	21
21-3S	372,380	2,200,826	12.36	5	10	2	12	56	4	40	21	21
22-1S	366,583	2,200,639	7.15	2	10	1	10	68	2	56	3	9
22-2S	366,541	2,200,765	6.70	3	10	1	10	68	2	56	3	8
23-1S	372,595	2,202,382	13.59	5	10	6	14	55	3	38	2	7
23-2S	372,450	2,202,388	12.86	5	10	5	14	55	4	38	1	6
23-3S	372,221	2,202,449	12.72	4	10	6	16	56	5	35	4	5
23-4S	372,225	2,202,900	9.72	5	10	6	21	54	8	26	7	2
23-5I	372,563	2,203,212	7.45	39	5	5	26	54	11	17	6	1
23-5S	372,558	2,203,212	7.42	3	10	5	26	54	11	17	6	1
23-6S	372,660	2,202,788	12.78	5	10	8	20	54	5	30	3	4
23-7S	372,535	2,202,458	13.65	5	10	7	15	55	4	37	2	6
24-1S	372,501	2,202,232	12.51	5	10	4	12	54	3	39	2	7
26-1S	366,352	2,200,738	5.85	2	10	1	10	67	2	56	4	9
26-2S	366,292	2,200,621	6.88	2	10	2	11	69	2	56	4	11
26-3S	366,204	2,200,520	7.05	2	10	1	10	69	2	57	4	14
26-4S	366,329	2,200,554	7.21	2	10	1	10	69	2	57	4	12
28-1S	365,616	2,204,661	11.85	8	10	8	16	53	0	36	3	18
44-1I	372,909	2,202,904	11.69	32	5	8	22	50	3	25	3	5
44-1S	372,906	2,202,902	11.78	5	10	8	22	50	3	25	3	5
44-2S	372,883	2,202,762	13.79	5	10	9	20	54	3	30	2	5
44-3S	372,629	2,203,003	10.87	5	10	8	25	54	7	22	4	2
45-1I	372,912	2,203,340	7.24	30	5	5	23	49	3	23	16	3
45-1S	372,912	2,203,345	7.14	5	5	5	23	49	3	23	16	3
45-2S	372,691	2,203,107	9.12	4	10	6	25	53	9	19	6	2
52-1S	370,281	2,201,849	7.48	3	10	5	10	57	0	47	16	12
56-1S	367,378	2,201,436	8.97	2	10	2	7	67	3	57	21	2
B-1I	372,332	2,199,058	7.19	33	5	6	30	49	2	18	27	66
B-1S	372,331	2,199,065	7.19	5	10	6	30	49	2	18	27	66
BE-1S	373,798	2,202,376	9.38	4	10	5	19	55	0	36	24	29
BE-2S	373,766	2,202,420	10.35	4	10	6	20	56	0	35	29	31
BE-3S	373,757	2,202,314	9.98	4	10	6	19	55	0	36	24	29
BE-4S	373,768	2,202,347	9.27	4	10	5	18	54	0	36	24	29
BE-7S	373,792	2,202,351	9.73	4	10	6	19	55	0	36	24	29
BE-8I	373,783	2,202,360	9.93	30	5	6	19	55	0	36	24	29
BE-9S	373,781	2,202,323	9.80	4	10	6	19	55	0	36	24	29
BQ-2S	373,723	2,202,645	10.18	4	10	6	22	56	1	34	27	31
BQ-3S	373,764	2,202,658	8.63	3	10	5	20	54	1	34	27	31
BQ-4S	373,712	2,202,700	11.95	4	10	8	24	57	1	33	26	27
BQ-5S	373,751	2,202,705	10.58	4	10	7	22	56	1	33	26	27
BQ-6S	373,691	2,202,720	12.27	4	10	8	24	57	1	32	24	23
CU-1S	373,313	2,201,477	11.28	3	10	7	13	54	0	41	6	16
CU-2S	373,275	2,201,426	11.28	3	10	6	12	54	1	41	5	15
CU-3S	373,390	2,201,482	11.29	3	10	7	13	54	0	41	6	16
CU-4S	373,369	2,201,431	11.54	3	10	7	13	54	0	41	6	16
CU-5S	373,410	2,201,387	11.71	3	10	7	14	55	0	40	7	18
CU-6S	373,522	2,201,514	11.05	3	10	7	14	54	0	41	7	18

Appendix A. Well information at NAVSTA Mayport--(Continued)

[All measurements are in feet, except as noted]

Well ID	Easting[a]	Northing[a]	Top of casing	Casing length	Screen length	Depth to water	Base of S-zone	Base of I-zone	Thickness		Lateral hydraulic conductivity, in ft/d	
									Marsh-muck confining unit	I-zone	S-zone	I-zone
CU-7S	373,328	2,201,442	11.33	3	10	7	13	54	0	41	6	16
CU-8I	373,390	2,201,460	11.37	25	5	7	13	54	0	41	6	16
TC-1I	371,600	2,200,675	9.60	35	5	4	13	55	1	41	22	24
TC-2S	371,527	2,200,595	10.89	4	10	6	15	57	1	41	22	26
TC-3S	371,427	2,200,587	8.68	3	10	4	13	55	0	41	22	26
TC-4S	371,652	2,200,865	8.78	3	10	4	11	54	0	43	22	20
TC-5S	371,627	2,200,926	8.73	3	10	4	11	54	0	43	21	19
TC-6S	371,773	2,200,942	9.84	3	10	4	11	55	1	42	21	19

[a] Florida State Plane Coordinate System.

APPENDIX B. A SIMPLIFIED APPROACH TO SIMULATING THE DISPLACEMENT OF SALINE PORE WATER BY FRESHWATER RECHARGE IN A RECLAIMED SALT MARSH

The density difference between the freshwater recharge and the saline pore water can complicate analysis of the ground-water flow system in a setting with land being accreted. The frequently used assumption (Anderson and Woessner, 1992) that the saline zones are not part of the active flow system is inadequate. Exclusion of the saline zones assumes that the freshwater/saltwater interfaces are in equilibrium which is not so when land is being accreted.

The displacement of saline pore water and associated dissolved solids by freshwater recharge can be simulated explicitly, accounting for variable-density effects. This approach is deterministic but, nonetheless, many "reasonable" assumptions must be invoked. The data requirements for this approach also are large. A history of the natural accretion and marsh reclamation is needed, in addition to knowledge of its current state. In addition to knowing the hydraulic stresses and boundaries of the system, the distribution of solute sources and sinks and the initial solute distribution must be known in order to adequately simulate solute transport.

The density contrast between the saline and freshwater zones can be assumed to have a negligible effect on the flow system and negated from the simulation. The effectiveness of this approach assumes that ground-water flow gradients caused by topographic effects are substantially larger than density gradients within the flow field. This assumption improves as the recharge rates increase, the hydraulic conductivity decreases, and the thickness of the flow system decreases.

Purpose and Scope

The purpose of this appendix is to demonstrate that the displacement of saline pore water by freshwater recharge in a shallow, coastal aquifer, such as the surficial aquifer system at NAVSTA Mayport, can be adequately simulated as a uniform-density flow field. This is achieved by comparing density-dependent and uniform-density simulations of generalized cross-sections through NAVSTA Mayport, which are typical of reclaimed land in a salt-marsh environment.

Cross-Sectional Models

The significance of simulating density-dependent flow in a ground-water flow system with land being accreted and freshwater recharge flushing a saltwater aquifer was investigated by comparing two cross-sectional models. The density-dependent section was simulated with SUTRA (Voss, 1984) and the uniform-density section was simulated with MODFLOW (McDonald and Harbaugh, 1988). While the uniform-density section could have been simulated with SUTRA, MODFLOW typically is used to solve for the uniform-density flow field.

The geohydrologic framework for investigating density-dependent effects was a 500 m long by 20 m thick generalized section through NAVSTA Mayport (fig. B1). The upper 10 m represented the gross thickness of the surficial aquifer system and the lower 10 m approximated the top of the intermediate confining unit. The left boundary represented a no-flow boundary through a ground-water divide. The right boundary approximated the edge of a deep saltwater body that was in communication with the surficial aquifer system.

Ground-water flow and saltwater displacement at NAVSTA Mayport are strongly affected by the occurrence and extent of the marsh-muck confining unit which is characterized by a relatively low hydraulic conductivity (1×10^{-3} m/d) compared to the S-zone and I-zone aquifers (5 m/d). The effect of the marsh-muck confining unit was investigated with three geohydrologic sections (cases one, two, and three); (1) the marsh-muck confining unit is absent; (2) the 2.5 m thick marsh-muck confining unit extends 250 m from the left boundary; and (3) the marsh-muck confining unit exists across the entire section.

The uniform-density and variable-density models of each section were discretized into 101 nodes laterally and 26 nodes vertically. Slight differences existed between the discretization of the two models because the uniform-density section was simulated with a block-centered, finite-difference model (MODFLOW; McDonald and Harbaugh, 1988) and the density-dependent section was simulated with a finite-element model (SUTRA; Voss, 1984). The

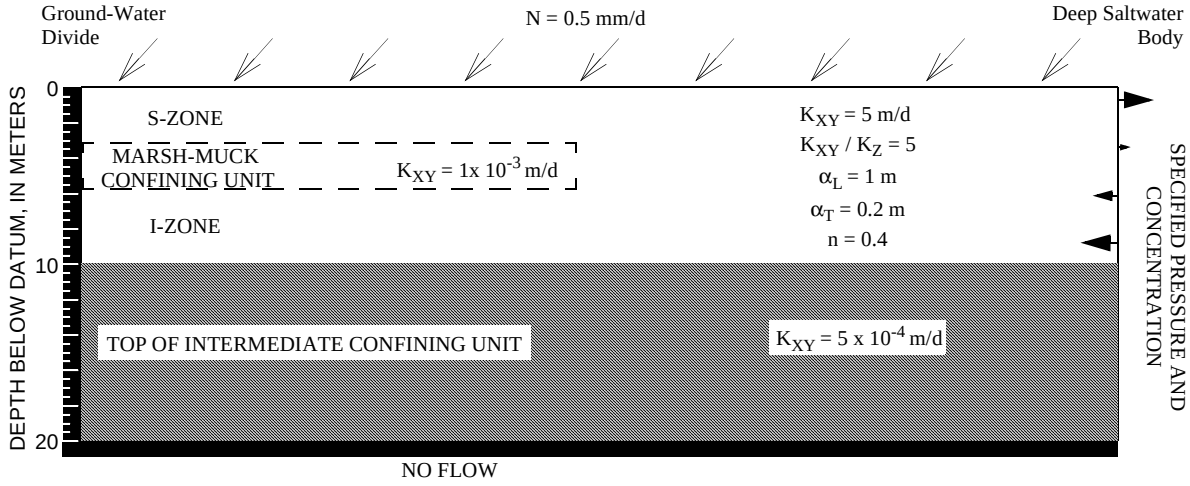

Figure B1. Cross-section showing geohydrologic framework, hydraulic properties, and boundary conditions of a generalized section through the surficial aquifer system at NAVSTA Mayport.

MODFLOW model laterally was discretized into 101 columns that are 5 m wide except for the first and last columns which were 2.5 m wide. Vertically, the MODFLOW model was discretized into 20 rows (0.5 m high) in the upper 10 m and 6 rows that expanded with a uniform multiplier to cover the lower 10 m. The SUTRA model was discretized into 2500 rectangular elements that were 5 m wide by 0.5 m high in the upper 10 m and were of variable height in the lower 10 m, similar to the heights used in the MODFLOW model.

The deep saltwater body (the right edge of the model) was simulated as a specified pressure and concentration boundary that was set to the hydrostatic pressure of a column of seawater (ρ = 1.025 g/cc). Seawater hydrostatic pressures were assigned in both the density-dependent and uniform-density simulations. A uniform concentration of 0.0357 kg_{solute}/kg_{fluid} was assigned to the deep saltwater body nodes in the density-dependent simulations. The ground-water divide (the left edge of the model) was simulated as a no-flow boundary.

The initial conditions of the density-dependent problems (SUTRA) were steady-state solutions of uniform saltwater flow. These solutions were driven by a uniform recharge rate of 0.5 mm/d of saltwater (ρ = 1.025 g/cc and C = 0.0357 kg_{solute}/kg_{fluid}) applied to the upper boundary. The 0.5 mm/d recharge was maintained throughout the saltwater displacement simulation but the saltwater was replaced with freshwater (ρ = 1.000 g/cc and C = 0.000 kg_{solute}/kg_{fluid}).

In addition to specifying initial and boundary solute concentrations, the longitudinal and transverse dispersivities of the surficial aquifer system must be defined to solve the associated solute transport problem. Longitudinal and transverse dispersivities of 1 and 0.2 m, respectively, were used for all of the transport problems investigated. Sanford and Konikow (1989) found these values adequately described the mixing along a freshwater/saltwater interface.

The water table was not simulated as a free surface and the transmissivity of the S-zone was based on a 3 m thickness for all simulations. The free surface upper boundary was ignored because SUTRA does not actively solve for this boundary. The simulation of the water table was not the most accurate for any of the problems but all of the solutions were adequate for comparing density-dependent to uniform-density flushing. The third case simulated, accounting for the effects of a continuous marsh-muck confining unit, produced the highest water table which had a maximum elevation of about 3.2 m (fig. B2) and would have been closer to 2.8 m with the correct solution.

Saltwater Displacement

The advective displacement of saline pore water was simulated using a particle-tracking routine, MODPATH (Pollock, 1994) and an effective porosity of 40 percent. The connate pore water was approximated by a uniform array of particles placed within the volume of the surficial aquifer system (fig. B3). The displacement and dilution of connate saltwater by freshwater recharge was depicted by particle spreading and discharging to the deep saltwater body.

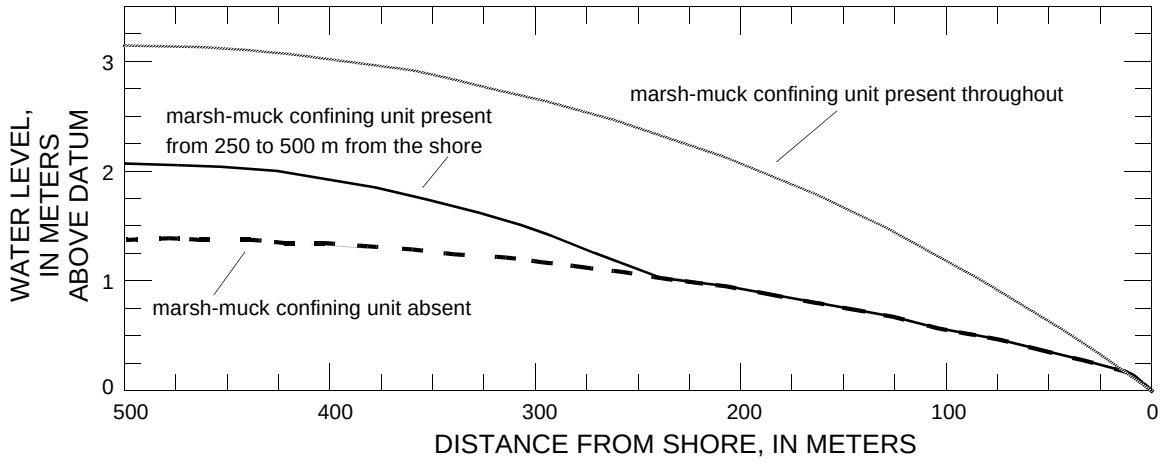

Figure B2. Steady-state, uniform-density, water table profiles along 3 hypothetical cross-sections through NAVSTA Mayport that are driven by a recharge rate of 0.5 mm/d.

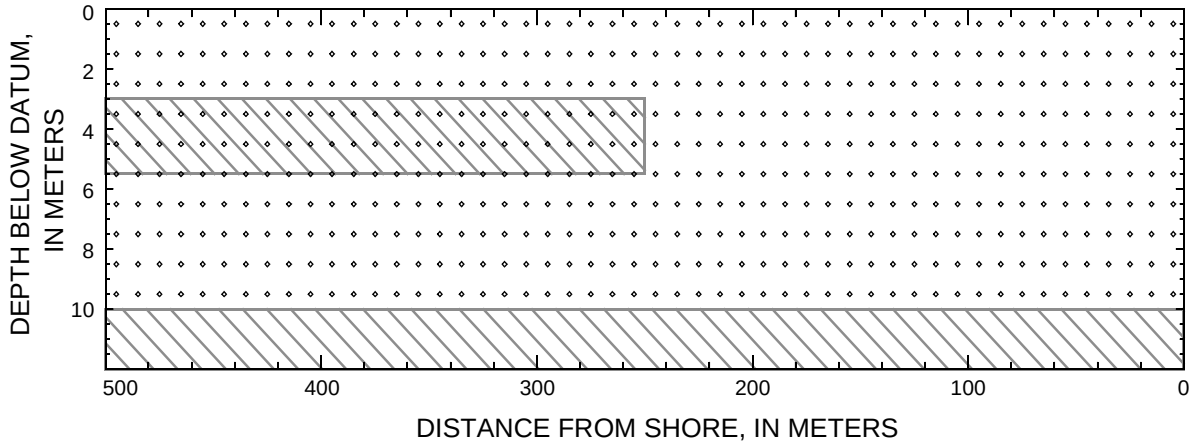

Figure B3. Initial particle distributions in generalized section experiments for NAVSTA Mayport.

Saltwater displacement was fastest from the section without the marsh-muck confining unit because the entire thickness was available for conveying the recharge to the seaward outlet (fig. B4). Density-dependent effects were minimal throughout most of this section because strong density contrasts never formed, except at the seaward outlet. This can be seen by examining any 20 m wide column within the section and noting the similarity between adjacent vertical concentration profiles.

Density-dependent effects were the most pronounced for the second case, with the marsh-muck confining unit extended partially across the section. Density gradients were greatest in the middle of the geohydrologic section at the end of the marsh-muck confining unit (fig. B5). The density effects are shown by the relative concentration decrease just below the tip of the marsh-muck confining unit and the relative concentration bulge between 8 and 10 m below the datum. Density-dependent effects appear because the strong downward flow from the marsh-muck confining unit maintains a 4 m long vertical interface with a strong solute concentration contrast.

The third case, with the marsh-muck confining unit present throughout the entire section, flushed the lower zone faster than noted in case 2. Simulations of the density-dependent and uniform-density conditions were quite similar (fig. B6). The continuous confining unit reduced the effective thickness of the flow system and the resulting higher water table caused more water to flow across the marsh-muck confining unit (fig. B2). Density-dependent effects were largely absent because the system was horizontally stratified and sharp vertical concentration profiles could not develop.

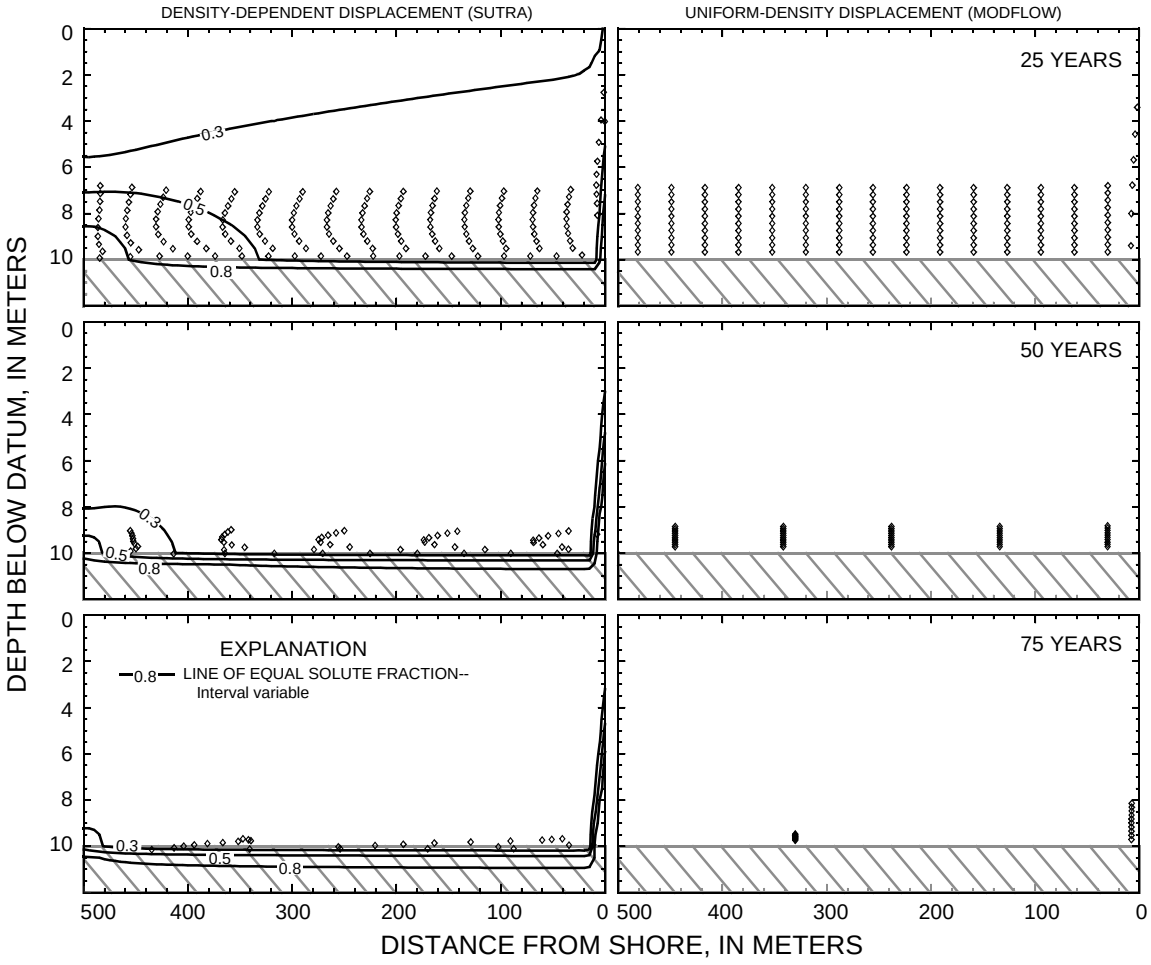

Figure B4. Comparison between density-dependent (SUTRA) and uniform-density (MODFLOW) simulations of saltwater displacement from a generalized section of NAVSTA Mayport with the marsh-muck confining unit absent.

Conclusions

A comparison between density-dependent (SUTRA) and uniform-density (MODFLOW) simulations in generalized sections through NAVSTA Mayport showed that the effects of density differences on the flow system are minor. The uncertainty of the hydraulic conductivity distribution and the lateral extent of the marsh-muck confining unit introduce greater errors than those associated with neglecting density differences. These results indicate that density-dependent effects can be neglected and that flushing of the aquifer system can be simulated adequately with MODFLOW.

Density-dependent effects were most pronounced where the marsh-muck confining unit extended through half of the section. Ignoring density effects caused a relatively sharp interface in the center of the section but displaced the interface by less than 30 m. Topographic gradients were much greater than any density gradients and dominated the flow field.

While density-dependent effects control the seaward freshwater/saltwater interface, the effects can be approximated well with a uniform-density simulation by specifying the hydrostatic head due to the density difference between the freshwater and saltwater bodies. This approximation works because the concentration of dissolved solids in the saltwater body does not change and is not diluted over time.

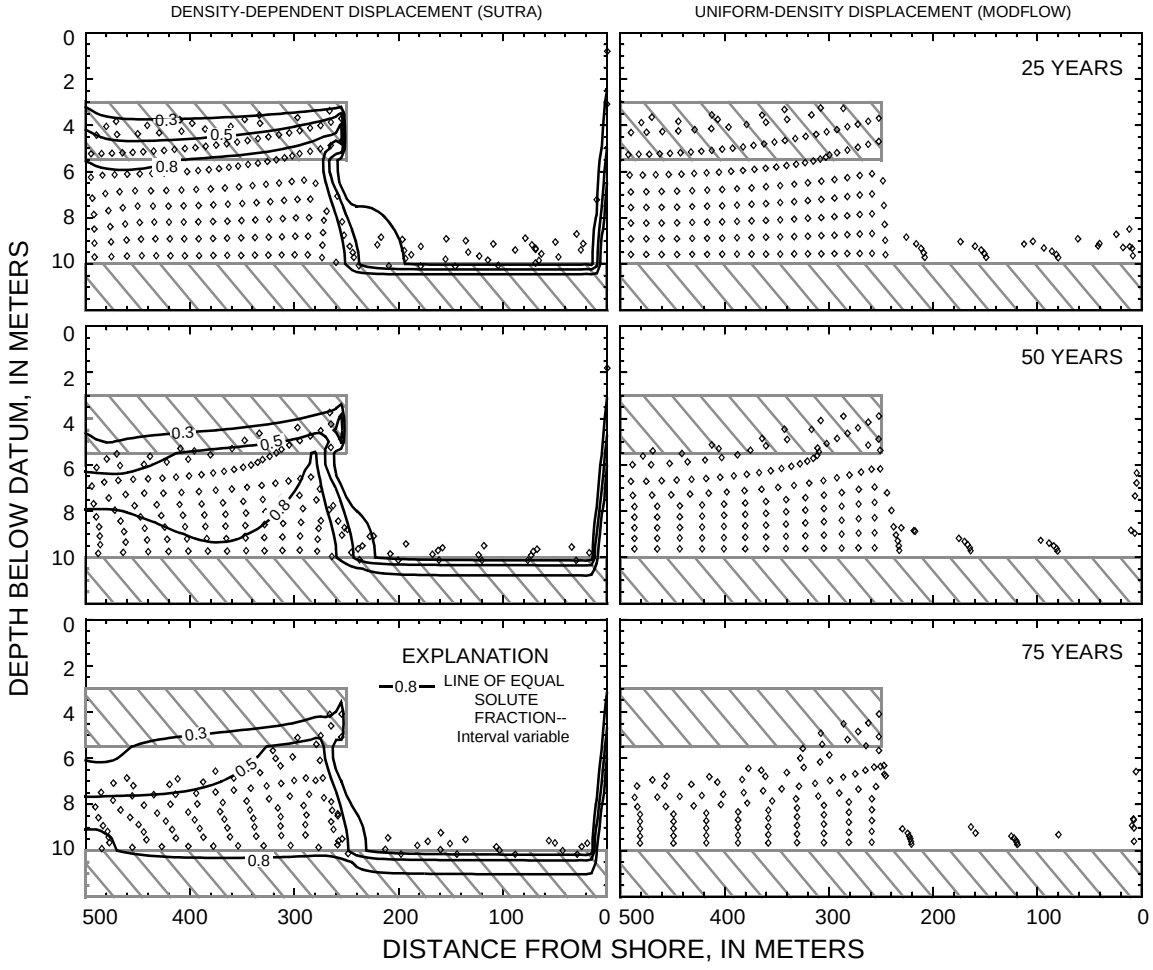

Figure B5. Comparison between density-dependent (SUTRA) and uniform-density (MODFLOW) simulations of saltwater displacement from a generalized section of NAVSTA Mayport with the marsh-muck confining unit present through 250 m of the 500 m long section.

The contribution of dissolved solids from the top of the intermediate confining unit was negligible. These results indicate that both the ground-water flow and geochemical-reaction paths within the surficial-aquifer system can be explained by treating the lower confining unit as an inert, impervious boundary. It also suggests that the water quality at or near the top of the intermediate confining unit is more indicative of that unit's depositional history and development than the development of the surficial aquifer system.

REFERENCES

Anderson, M. P., and Woessner, W. W., 1992, Applied groundwater modeling: Simulation of flow and advective transport: San Diego, Academic Press, Inc., 381 p.

McDonald, M.G., and Harbaugh, A.W., 1988, A modular three-dimensional finite-difference ground-water flow model: U.S. Geological Survey Techniques of Water-Resources Investigations, book 6, chap. A1, 576 p.

Pollock, D.W., 1994, User's guide for MODPATH/MODPATH-PLOT, version 3: A particle tracking post-processing package for MODFLOW, the U.S. Geological Survey finite-difference ground-water flow model: U.S. Geological Survey Open-File Report 94-464 [variously paged].

Sanford, W.E., and Konikow, L.F., 1989, Simulation of calcite dissolution and porosity changes in saltwater mixing zones in coastal aquifers: Water Resources Research, v. 25 (4), p. 655-667.

Voss, C.I., 1984, SUTRA A finite-element simulation model for saturated-unsaturated, fluid-density-dependent ground-water flow with energy transport or chemically-reactive single-species solute transport: Water-Resources Investigations Report 84-4369, 409 p.

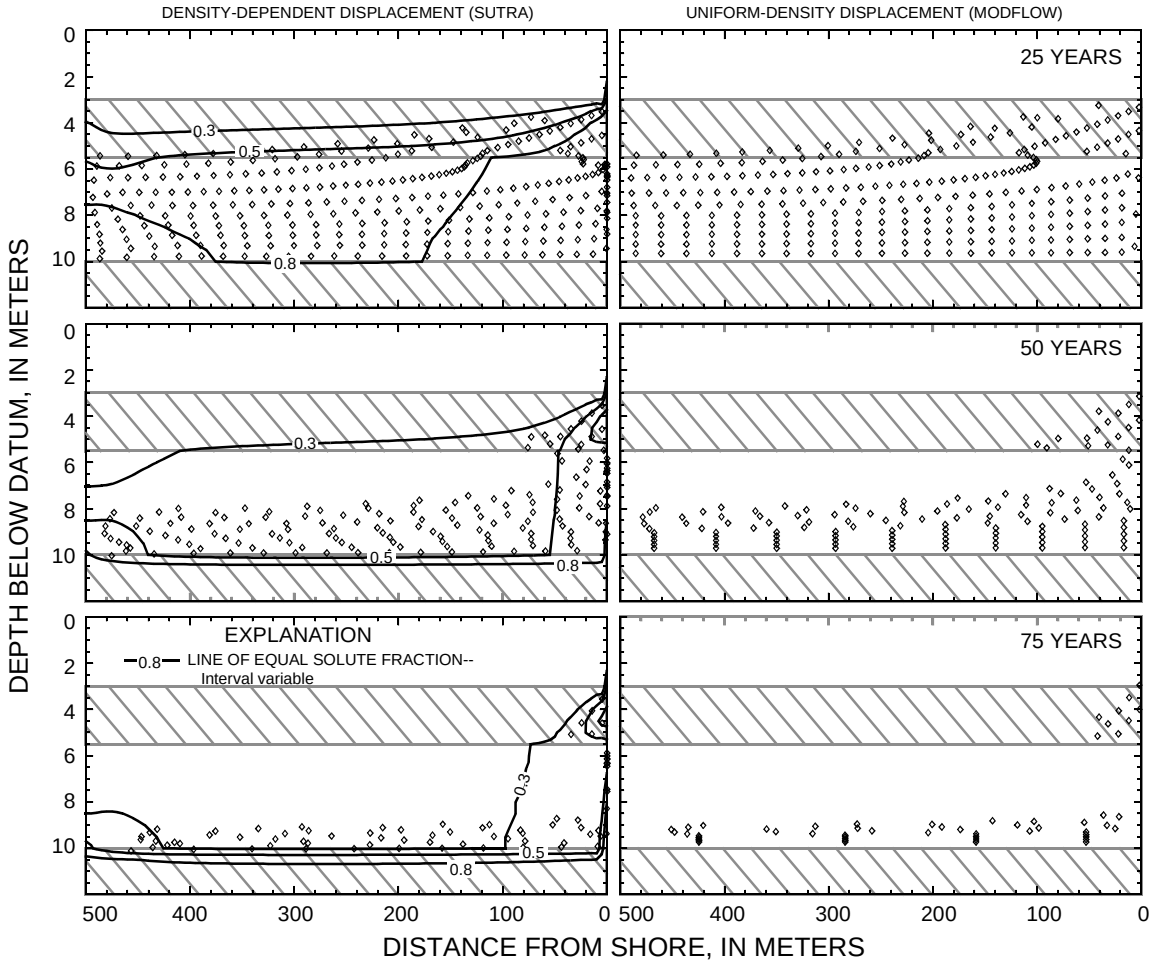

Figure B6. Comparison between density-dependent (SUTRA) and uniform-density (MODFLOW) simulations of saltwater displacement from a generalized section of NAVSTA Mayport with the marsh-muck confining unit present throughout the entire section.

Appendix C. Time-Variant Hydraulic-Property Package

The Time-Variant Hydraulic-Property Package was developed to accommodate temporal changes in inter-node conductance, hydraulic conductivity, the top and bottom elevations of model layers, and the primary and secondary storage coefficients. The package allows hydraulic properties to be modified step-wise from one stress period to the next. The hydraulic properties of a cell are modified by either being multiplied or replaced. The Time-Variant Hydraulic-Property Package does not alter the formulation of the finite-difference equations in MODFLOW (McDonald and Harbaugh, 1988). Because the package is not a complex modification of MODFLOW, documentation in this appendix is the minimum amount required to implement the package. Modifications to the main program to implement the Time-Variant Hydraulic-Property package are given in Appendix D.

Input Instructions

Input for the Time-Variant Hydraulic-Property Package is read from the unit in IUNIT(21) specified in the basic package input (see McDonald and Harbaugh, 1988, chap. 4, p. 9-11).

FOR EACH SIMULATION

VAR1AL

1. Data: MXVAR
   Format: I10

FOR EACH STRESS PERIOD

VAR1RP

2. Data: ITMP
   Format: I10

3.

Data:	Layer	Row	Column	Modifier	Property	Action (optional)
Format:	I10	I10	I10	F10.0	A10	A78

(Input item 3 normally consists of one record for each time-variant hydraulic-property cell modified. If ITMP is zero or less, item 3 is not read.)

Explanation of Fields Used in Input Instructions

MXCHD is the maximum number of time-variant hydraulic-property cells to be modified.

ITMP is a flag.

If $ITMP \leq 0$, hydraulic-property data from a previous stress period will be reused and input from item 3 will not be read.

If $ITMP > 0$, it is the number of records of hydraulic-property data that will be read for the current stress period.

Layer is the layer number of the cell affected by the modification of the hydraulic property.

Row is the row number of the cell affected by the modification of the hydraulic property.

Column is the column number of the cell affected by the modification of the hydraulic property.

Modifier is the multiplier or replacement value of the hydraulic property to be modified.

Property identifies which hydraulic property is to be modified. The properties are identified by the keys listed in table C1.

Action specifies if the hydraulic property is to be multiplied or replaced by the modifier. If the string “REPLACE” (case insensitive) is detected, the modifier will replace the old value. Otherwise, the old value will be multiplied by the modifier.

Table C1. Hydraulic properties modified by VAR1 and the property keys that identify the properties to be modified.

Hydraulic property	Key[a]	MODFLOW array[b]
Inter-node conductance along rows[c]	X-conductance	CR
Inter-node conductance along columns[c]	Y-conductance	CC
Inter-node conductance between layers[c]	Z-conductance	CV
Inter-node conductances along rows and columns[c]	XY-conductance	CR, CC
Inter-node conductances along columns and between layers[c]	YZ-conductance	CC, CV
Inter-node conductances along rows and between layers[c]	XZ-conductance	CR, CV
Inter-node conductances along rows and columns and between layers[c]	XYZ-conductance	CR, CC, CV
Hydraulic conductivity of layer 1	HYd. conductivity	HY
Elevation of the layer top	TOP of layer	TOP
Elevation of the layer bottom	BOTtom of layer	BOT
Primary storage coefficient	SC1	SC1
Secondary storage coefficient	SC2	SC2

[a] Only the underlined fragment of the key is needed.
[b] See McDonald and Harbaugh (1988) for further description of the arrays.
[c] Inter-node conductances modified by the X-conductance, Y-conductance, and Z-conductance keys when applied to the <i,j,k> node are shown below:

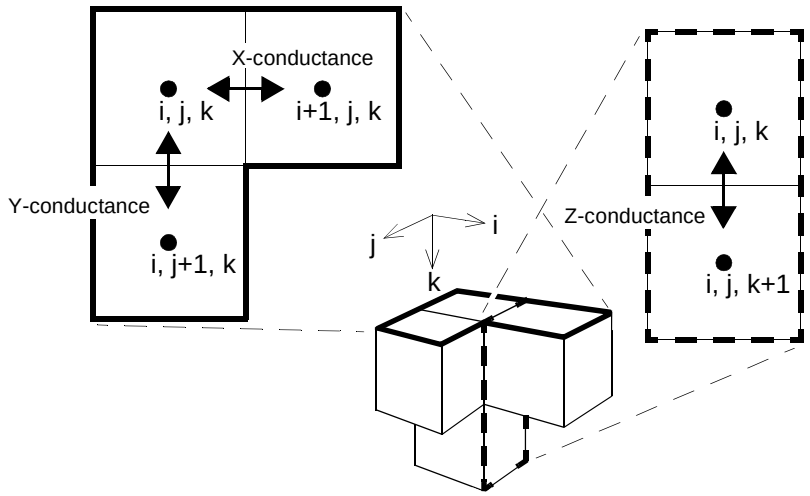

Program Listing for Module VAR1AL

```
      SUBROUTINE var1AL(ISUM,LENX,MXvar,IN,IOUT)
C
C-----VERSION 1.000 12-14-96
C
C     ******************************************************************
C     ALLOCATE ARRAY STORAGE FOR time dependent changes in conductance
c     and storage ...........
C     ******************************************************************
C
C     SPECIFICATIONS:
C     ------------------------------------------------------------------
C     ------------------------------------------------------------------
C
C1------IDENTIFY PACKAGE AND INITIALIZE # OF BCF Cells........
      WRITE(IOUT,1)
    1 FORMAT(1H0,'var1 -- var PACKAGE, VERSION 1, 12/14/96')
      Nvars=0
C
C2------READ AND PRINT MXBND AND IvarCB (MAX # OF BOUNDS AND UNIT
C2------FOR CELL-BY-CELL FLOW TERMS FOR var)
      READ(IN,'(i10)') MXvar
      WRITE(IOUT,3) MXvar
    3 FORMAT(1H ,'MAXIMUM OF',I6,' BCF properties can be updated.')
c
      ISP = 0
      ISUM = ISUM+ISP
C
C5------PRINT AMOUNT OF SPACE USED BY THE var PACKAGE
      WRITE(IOUT,4) ISP
    4 FORMAT(1X,I5,' ELEMENTS IN X ARRAY ARE USED FOR time-dependent',
     1      ' BCF updates.')
      ISUM1 = ISUM-1
      WRITE(IOUT,5) ISUM1,LENX
    5 FORMAT(1X,I6,' ELEMENTS OF X ARRAY USED OUT OF',I7)
      IF(ISUM1.GT.LENX) WRITE(IOUT,6)
    6 FORMAT(1X,'   ***X ARRAY MUST BE DIMENSIONED LARGER***')
C
C6------RETURN
      RETURN
      END
c.....................................................................
c
```

Program Listing for Module VAR1RP

```
c
      SUBROUTINE var1RP(mxvar,IBOUND,SC1,HY,CR,CC,CV,DELR,DELC,
     +           BOT,TOP,SC2,ISS,NCOL,NROW,NLAY,in,iout)
C
C-----VERSION 1.000 12-14-96
C
C     ******************************************************************
C     READ AND MODIFY BLOCK-CENTERED FLOW PACKAGE  DATA BY STRESS PERIOD
C     ******************************************************************
C
c    The following arrays can be modified:
c                CR( i, j, k)    ------>   CR  i + 1/2
c                CC( i, j, k)    ------>   CC  j + 1/2
c                CV( i, j, k)    ------>   CV  k + 1/2
c      HY, BOT, TOP, SC1, SC2  are block centered values
c
c    Specify quantity to vary using the following keys ......
c      data  keys/'X-??','Y-??','Z-??','XY-?','YZ-?','XZ-?','XYZ-',
c    +           'HY??','BOT?','SC1?','SC2?','TOP?'/
c
c    Default assumption is to modify value by multiplication, unless the
c   identifier 'REPLACE'  is on the line..............
c
C        SPECIFICATIONS:
C     ------------------------------------------------------------------
      DIMENSION SC1(NCOL,NROW,NLAY),HY(NCOL,NROW,NLAY),
     +   CR(NCOL,NROW,NLAY),CC(NCOL,NROW,NLAY),CV(NCOL,NROW,NLAY),
     +   DELR(NCOL),DELC(NROW),BOT(NCOL,NROW,NLAY),TOP(NCOL,NROW,NLAY),
     +   SC2(NCOL,NROW,NLAY),IBOUND(NCOL,NROW,NLAY)
      dimension    nvkey(12)
      character*4   keys(12)
      character*10  action
      character*128 txt
C     ------------------------------------------------------------------
      data nvkey/2,2,2,3,3,3,4,2,3,3,3,3/
      data keys/'X-??','Y-??','Z-??','XY-?','XZ-?','YZ-?','XYZ-',
     +          'HY??','BOT?','SC1?','SC2?','TOP?'/
C
C1------READ ITMP(# OF HEAD updates OR FLAG TO REUSE DATA.)
      READ(IN,'(i10)') ITMP
C
C2------TEST ITMP
      IF(ITMP.lt.0) then
C
C2A-----IF ITMP<0 THEN REUSE DATA FROM LAST STRESS PERIOD
        WRITE(IOUT,7)
    7   FORMAT(1H0,'REUSING BCF-updates FROM LAST STRESS',
     1      ' PERIOD')
      else
C
```

```
C3------IF ITMP=>0 THEN IT IS THE # OF HYDRAULIC PROPERTIES
        Nvars = ITMP
C
C4------IF MAX NUMBER OF BCF values IS EXCEEDED THEN STOP
        if( nvars .gt. mxvar ) then
          WRITE(IOUT,99) Nvars,MXvar
   99     FORMAT(1H0,'NBOUND(',I4,') IS GREATER THAN MXvar(',I4,')')
C
C4A-----ABNORMAL STOP
          STOP'  Abnormal Stop!!!!!!!'
        endif
C
C5------PRINT # OF BCF Nodes altered THIS STRESS PERIOD
        WRITE(IOUT,1) nvars
    1   FORMAT(1H0,//1X,I6,' TIME-DEPENDENT BCF NODES')
C
C6------IF THERE ARE NO HYDRAULIC PROPERTIES THEN RETURN.
        IF(nvars.EQ.0) return
C
C7------READ, modify, & echo BCF info to main output file
        WRITE(IOUT,3)
    3   FORMAT(1H0,1X,'LAYER',5X,'ROW',5X
     1,'COL      OLD VAL      NEW       BOUND NO.'/1X,15X,60('-'))
        DO II = 1, nvars
          READ (IN,'(a128)') txt
          call caps( txt, 128 )
          ireplc = index(txt,'REPLACE')
          READ (txt,'(3I10,F10.0)') K,I,J,rmodfy
          icho = 0
c      data  keys/'X-??','Y-??','Z-??','XY-?','YZ-?','XZ-?','XYZ-',
c     +           'HY??','BOT?','SC1?','SC2?','TOP?'/
          action = txt(41:50)
          do nop = 1, 12
            if( index(action,keys(nop)(1:nvkey(nop))).gt.0 ) then
              icho = nop
            endif
          enddo
c
          if(     icho.eq.1 ) then
            varold = cr(j,i,k)
            varnew = varold * rmodfy
            if( ireplc.gt.0 )  varnew = rmodfy
              cr(j,i,k) = varnew
            elseif( icho.eq.2 ) then
              varold = cc(j,i,k)
              varnew = varold * rmodfy
              if( ireplc.gt.0 )  varnew = rmodfy
              cc(j,i,k) = varnew
            elseif( icho.eq.3 ) then
              varold = cv(j,i,k)
              varnew = varold * rmodfy
              if( ireplc.gt.0 )  varnew = rmodfy
              cv(j,i,k) = varnew
```

```
      elseif( icho.eq.4 ) then
        varold = cr(j,i,k)
        varnew = varold * rmodfy
        if( ireplc.gt.0 )  varnew = rmodfy
        cr(j,i,k) = varnew
        action(10:10) = 'X'
        WRITE (IOUT,'(1x,I4,I9,I8,G13.4,G14.4,I8,a10)')
     +       K,I,J,varold,varnew,II,action
        varold = cc(j,i,k)
        varnew = varold * rmodfy
        if( ireplc.gt.0 )  varnew = rmodfy
        cc(j,i,k) = varnew
        action(10:10) = 'Y'
      elseif( icho.eq.5 ) then
        varold = cr(j,i,k)
        varnew = varold * rmodfy
        if( ireplc.gt.0 )  varnew = rmodfy
        cr(j,i,k) = varnew
        action(10:10) = 'X'
        WRITE (IOUT,'(1x,I4,I9,I8,G13.4,G14.4,I8,a10)')
     +     K,I,J,varold,varnew,II,action
        varold = cv(j,i,k)
        varnew = varold * rmodfy
        if( ireplc.gt.0 )  varnew = rmodfy
        cv(j,i,k) = varnew
        action(10:10) = 'Z'
      elseif( icho.eq.6 ) then
        varold = cc(j,i,k)
        varnew = varold * rmodfy
        if( ireplc.gt.0 )  varnew = rmodfy
        cc(j,i,k) = varnew
        action(10:10) = 'Y'
        WRITE (IOUT,'(1x,I4,I9,I8,G13.4,G14.4,I8,a10)')
     +     K,I,J,varold,varnew,II,action
        varold = cv(j,i,k)
        varnew = varold * rmodfy
        if( ireplc.gt.0 )  varnew = rmodfy
        cv(j,i,k) = varnew
        action(10:10) = 'Z'
      elseif( icho.eq.7 ) then
        varold = cr(j,i,k)
        varnew = varold * rmodfy
        if( ireplc.gt.0 )  varnew = rmodfy
        cr(j,i,k) = varnew
        action(10:10) = 'X'
        WRITE (IOUT,'(1x,I4,I9,I8,G13.4,G14.4,I8,a10)')
     +     K,I,J,varold,varnew,II,action
        varold = cc(j,i,k)
        varnew = varold * rmodfy
        if( ireplc.gt.0 )  varnew = rmodfy
        cc(j,i,k) = varnew
        action(10:10) = 'Y'
        WRITE (IOUT,'(1x,I4,I9,I8,G13.4,G14.4,I8,a10)')
```

```
     +           K,I,J,varold,varnew,II,action
                 varold = cv(j,i,k)
                 varnew = varold * rmodfy
                 if( ireplc.gt.0 )  varnew = rmodfy
                 cv(j,i,k) = varnew
                 action(10:10) = 'Z'
               elseif( icho.eq.8 ) then
                 varold = hy(j,i,k)
                 varnew = varold * rmodfy
                 if( ireplc.gt.0 )  varnew = rmodfy
                 hy(j,i,k) = varnew
               elseif( icho.eq.9 ) then
                 varold = bot(j,i,k)
                 varnew = varold * rmodfy
                 if( ireplc.gt.0 )  varnew = rmodfy
                 bot(j,i,k) = varnew

               elseif( icho.eq.10 .and. iss.eq.0 ) then
                 varold = sc1(j,i,k)
                 varnew = varold * rmodfy
                 if( ireplc.gt.0 )  varnew = rmodfy
                 sc1(j,i,k) = varnew
               elseif( icho.eq.11 .and. iss.eq.0 ) then
                 varold = sc2(j,i,k)
                 varnew = varold * rmodfy
                 if( ireplc.gt.0 )  varnew = rmodfy
                 sc2(j,i,k) = varnew
               elseif( icho.eq.12) then
                 varold = top(j,i,k)
                 varnew = varold * rmodfy
                 if( ireplc.gt.0 )  varnew = rmodfy
                 top(j,i,k) = varnew
               else
               endif
            WRITE (IOUT,'(1x,I4,I9,I8,G13.4,G14.4,I8,a10)')
     +           K,I,J,varold,varnew,II,action
          enddo
        endif
c
C8------RETURN
        RETURN
        END
```

Program Listing for Module CAPS

```
      subroutine caps(a1,n)
      character*1 lc(26), uc(26)
      character*128  a1
      data lc /'a','b','c','d','e','f','g','h','i','j','k','l','m','n',
     .         'o','p','q','r','s','t','u','v','w','x','y','z'/
      data uc /'A','B','C','D','E','F','G','H','I','J','K','L','M','N',
     .         'O','P','Q','R','S','T','U','V','W','X','Y','Z'/
      do 10 i=1,n
        do 20 j=1,26
        if(a1(i:i).ne.lc(j)) goto 20
          a1(i:i)=uc(j)
          goto 10
20      continue
10    continue
      return
      end
```

Appendix D. Example of Main Program to Use with the Time-Variant Hydraulic-Property Package

The following main program has been modified to allow use of the Time-Variant Hydraulic-Property Package. The additions to the code specify that input data for the Time-Variant Hydraulic-Property Package are to be read from the unit number stored in element 21 of the IUNIT array. In the following program listing, records added to access the Time-Variant Hydraulic-Property Package are identified with the characters “VAR1” in rightmost columns. This identifier is not necessary but can only be added after column 72.

Program Listing

```
C     ****************************************************************
C     MAIN CODE FOR MODULAR MODEL --    6/1/83
C          BY MICHAEL G. MCDONALD AND ARLEN W. HARBAUGH
C-----VERSION 1116 28DEC1983 MAIN1
C     ****************************************************************
C
C        SPECIFICATIONS:
C     ----------------------------------------------------------------
      parameter (LENX=2000000)
      COMMON X(lenx)
      DIMENSION HEADNG(32),VBNM(4,20),VBVL(4,20),IUNIT(24)
      DOUBLE PRECISION DUMMY
      EQUIVALENCE (DUMMY,X(1))
c
C     ----------------------------------------------------------------
C
C1------SET SIZE OF X ARRAY. REMEMBER TO REDIMENSION X.
C
C2------ASSIGN BASIC INPUT UNIT AND PRINTER UNIT.
      INBAS=5
      IOUT=6
C
C3------DEFINE PROBLEM__ROWS,COLUMNS,LAYERS,STRESS PERIODS,PACKAGES
      CALL BAS1DF(ISUM,HEADNG,NPER,ITMUNI,TOTIM,NCOL,NROW,NLAY,
     1             NODES,INBAS,IOUT,IUNIT)
C
C4------ALLOCATE SPACE IN "X" ARRAY.
      CALL BAS1AL(ISUM,LENX,LCHNEW,LCHOLD,LCIBOU,LCCR,LCCC,LCCV,
     1              LCHCOF,LCRHS,LCDELR,LCDELC,LCSTRT,LCBUFF,LCIOFL,
     2              INBAS,ISTRT,NCOL,NROW,NLAY,IOUT)
      IF(IUNIT(1).GT.0) CALL BCF1AL(ISUM,LENX,LCSC1,LCHY,
     1     LCBOT,LCTOP,LCSC2,LCTRPY,IUNIT(1),ISS,
     2     NCOL,NROW,NLAY,IOUT,IBCFCB)
      IF(IUNIT(2).GT.0) CALL WEL1AL(ISUM,LENX,LCWELL,MXWELL,NWEL,
     1                 IUNIT(2),IOUT,IWELCB)
      IF(IUNIT(3).GT.0) CALL DRN1AL(ISUM,LENX,LCDRAI,NDRAIN,MXDRN,
     1                 IUNIT(3),IOUT,IDRNCB)
      IF(IUNIT(8).GT.0) CALL RCH1AL(ISUM,LENX,LCIRCH,LCRECH,NRCHOP,
     1            NCOL,NROW,IUNIT(8),IOUT,IRCHCB)
      IF(IUNIT(5).GT.0) CALL EVT1AL(ISUM,LENX,LCIEVT,LCEVTR,LCEXDP,
```

```
     1            LCSURF,NCOL,NROW,NEVTOP,IUNIT(5),IOUT,IEVTCB)
      IF(IUNIT(4).GT.0) CALL RIV1AL(ISUM,LENX,LCRIVR,MXRIVR,NRIVER,
     1            IUNIT(4),IOUT,IRIVCB)
      IF(IUNIT(14).GT.0) CALL STR1AL(ISUM,LENX,LCSTRM,ICSTRM,MXSTRM,
     1                 NSTREM,IUNIT(14),IOUT,ISTCB1,ISTCB2,NSS,NTRIB,
     2                  NDIV,ICALC,CONST,LCTBAR,LCTRIB,LCIVAR,LCFGAR)
      IF(IUNIT(7).GT.0) CALL GHB1AL(ISUM,LENX,LCBNDS,NBOUND,MXBND,
     1            IUNIT(7),IOUT,IGHBCB)
      IF(IUNIT(9).GT.0) CALL SIP1AL(ISUM,LENX,LCEL,LCFL,LCGL,LCV,
     1          LCHDCG,LCLRCH,LCW,MXITER,NPARM,NCOL,NROW,NLAY,
     2          IUNIT(9),IOUT)
      IF(IUNIT(13).GT.0) CALL PCG2AL(ISUM,LENX,LCV,LCSS,LCP,LCCD,
     1       LCHCHG,LCLHCH,LCRCHG,LCLRCH,MXITER,ITER1,NCOL,NROW,NLAY,
     2       IUNIT(13),IOUT,NPCOND)
      IF(IUNIT(20).GT.0) CALL CHD1AL(ISUM,LENX,LCCHDS,NCHDS,MXCHD,
     1                               IUNIT(20),IOUT)
      IF(IUNIT(21).GT.0) CALL var1AL(ISUM,LENX,MXvar,Iunit(21), IOUT )    VAR1
C
C5------IF THE "X" ARRAY IS NOT BIG ENOUGH THEN STOP.
      IF(ISUM-1.GT.LENX) STOP
C
C6------READ AND PREPARE INFORMATION FOR ENTIRE SIMULATION.
      CALL BAS1RP(X(LCIBOU),X(LCHNEW),X(LCSTRT),X(LCHOLD),
     1       ISTRT,INBAS,HEADNG,NCOL,NROW,NLAY,NODES,VBVL,X(LCIOFL),
     2       IUNIT(12),IHEDFM,IDDNFM,IHEDUN,IDDNUN,IOUT)
      IF(IUNIT(1).GT.0) CALL BCF1RP(X(LCIBOU),X(LCHNEW),X(LCSC1),
     1          X(LCHY),X(LCCR),X(LCCC),X(LCCV),X(LCDELR),
     2           X(LCDELC),X(LCBOT),X(LCTOP),X(LCSC2),X(LCTRPY),
     3           IUNIT(1),ISS,NCOL,NROW,NLAY,NODES,IOUT)
      IF(IUNIT(9).GT.0) CALL SIP1RP(NPARM,MXITER,ACCL,HCLOSE,X(LCW),
     1          IUNIT(9),IPCALC,IPRSIP,IOUT)
      IF(IUNIT(13).GT.0) CALL PCG2RP(MXITER,ITER1,HCLOSE,RCLOSE,
     1         NPCOND,NBPOL,RELAX,IPRPCG,IUNIT(13),IOUT,MUTPCG,IPCGCD)
C
C7------SIMULATE EACH STRESS PERIOD.
      DO 300 KPER=1,NPER
C
C7A-----READ STRESS PERIOD TIMING INFORMATION.
      CALL BAS1ST(NSTP,DELT,TSMULT,PERTIM,KPER,INBAS,IOUT)
C
C7B-----READ AND PREPARE INFORMATION FOR STRESS PERIOD.
      IF(IUNIT(2).GT.0) CALL WEL1RP(X(LCWELL),NWEL,MXWELL,IUNIT(2),
     1             IOUT)
      IF(IUNIT(3).GT.0) CALL DRN1RP(X(LCDRAI),NDRAIN,MXDRN,IUNIT(3),
     1                 IOUT)
      IF(IUNIT(8).GT.0) CALL RCH1RP(NRCHOP,X(LCIRCH),X(LCRECH),
     1            X(LCDELR),X(LCDELC),NROW,NCOL,NLAY,IUNIT(8),IOUT)
      IF(IUNIT(5).GT.0) CALL EVT1RP(NEVTOP,X(LCIEVT),X(LCEVTR),
     1            X(LCEXDP),X(LCSURF),X(LCDELR),X(LCDELC),NCOL,NROW,
     1            NLAY,IUNIT(5),IOUT)
      IF(IUNIT(4).GT.0) CALL RIV1RP(X(LCRIVR),NRIVER,MXRIVR,IUNIT(4),
     1            IOUT)
      IF(IUNIT(14).GT.0) CALL STR1RP(X(LCSTRM),X(ICSTRM),NSTREM,
```

```
     1                    MXSTRM,IUNIT(14),IOUT,X(LCTBAR),NDIV,NSS,
     1                    NTRIB,X(LCIVAR),ICALC,IPTFLG)
      IF(IUNIT(7).GT.0) CALL GHB1RP(X(LCBNDS),NBOUND,MXBND,IUNIT(7),
     1              IOUT)
      IF(IUNIT(20).GT.0) CALL CHD1RP(X(LCCHDS),NCHDS,MXCHD,CHDEXP,
     +  x(lcibou),ncol,nrow,nlay,perlen,delt,nstp,tsmult,IUNIT(20),iout)
      IF(IUNIT(21).GT.0) CALL VAR1RP(mxvar,X(LCIBOU),X(LCSC1),X(LCHY),             VAR1
     +   X(LCCR),X(LCCC),X(LCCV),X(LCDELR),X(LCDELC),X(LCBOT),X(LCTOP),           VAR1
     +   X(LCSC2),ISS,NCOL,NROW,NLAY,IUNIT(21),iout)                              VAR1
C
C7C-----SIMULATE EACH TIME STEP.
      DO 200 KSTP=1,NSTP
C
C7C1----CALCULATE TIME STEP LENGTH. SET HOLD=HNEW..
      CALL BAS1AD(DELT,TSMULT,TOTIM,PERTIM,X(LCHNEW),X(LCHOLD),KSTP,
     1             NCOL,NROW,NLAY)
      IF(IUNIT(20).GT.0)
     .   CALL CHD1FM(NCHDS,MXCHD,CHDEXP,X(LCCHDS), x(lcibou),x(lchnew),
     .        x(lchold),perlen,pertim,delt,ncol,nrow,nlay,iout)
C7C2----ITERATIVELY FORMULATE AND SOLVE THE EQUATIONS.
      DO 100 KITER=1,MXITER
C
C7C2A---FORMULATE THE FINITE DIFFERENCE EQUATIONS.
      CALL BAS1FM(X(LCHCOF),X(LCRHS),NCOL,NROW,NLAY,NODES)
      IF(IUNIT(1).GT.0) CALL BCF1FM(X(LCHCOF),X(LCRHS),X(LCHOLD),
     1          X(LCSC1),X(LCHNEW),X(LCIBOU),X(LCCR),X(LCCC),X(LCCV),
     2          X(LCHY),X(LCTRPY),X(LCBOT),X(LCTOP),X(LCSC2),
     3          X(LCDELR),X(LCDELC),DELT,ISS,KITER,KSTP,KPER,NCOL,
     4          NROW,NLAY,IOUT)
      IF(IUNIT(2).GT.0) CALL WEL1FM(NWEL,MXWELL,X(LCRHS),X(LCWELL),
     1           X(LCIBOU),NCOL,NROW,NLAY,iout)
      IF(IUNIT(3).GT.0) CALL DRN1FM(NDRAIN,MXDRN,X(LCDRAI),X(LCHNEW),
     1         X(LCHCOF),X(LCRHS),X(LCIBOU),NCOL,NROW,NLAY,iout)
      IF(IUNIT(8).GT.0) CALL RCH1FM(NRCHOP,X(LCIRCH),X(LCRECH),
     1            X(LCRHS),X(LCIBOU),NCOL,NROW,NLAY,iout)
      IF(IUNIT(5).GT.0) CALL EVT1FM(NEVTOP,X(LCIEVT),X(LCEVTR),
     1            X(LCEXDP),X(LCSURF),X(LCRHS),X(LCHCOF),X(LCIBOU),
     1            X(LCHNEW),NCOL,NROW,NLAY,iout)
      IF(IUNIT(4).GT.0) CALL RIV1FM(NRIVER,MXRIVR,X(LCRIVR),X(LCHNEW),
     1            X(LCHCOF),X(LCRHS),X(LCIBOU),NCOL,NROW,NLAY)
      IF(IUNIT(14).GT.0) CALL STR1FM(NSTREM,X(LCSTRM),X(ICSTRM),
     1                    X(LCHNEW),X(LCHCOF),X(LCRHS),X(LCIBOU),
     2              MXSTRM,NCOL,NROW,NLAY,IOUT,NSS,X(LCTBAR),
     3              NTRIB,X(LCTRIB),X(LCIVAR),X(LCFGAR),ICALC,CONST)
      IF(IUNIT(7).GT.0) CALL GHB1FM(NBOUND,MXBND,X(LCBNDS),X(LCHCOF),
     1            X(LCRHS),X(LCIBOU),NCOL,NROW,NLAY,iout)
C
C7C2B---MAKE ONE CUT AT AN APPROXIMATE SOLUTION.
      IF(IUNIT(9).GT.0) CALL SIP1AP(X(LCHNEW),X(LCIBOU),X(LCCR),X(LCCC),
     1     X(LCCV),X(LCHCOF),X(LCRHS),X(LCEL),X(LCFL),X(LCGL),X(LCV),
     2     X(LCW),X(LCHDCG),X(LCLRCH),NPARM,KITER,HCLOSE,ACCL,ICNVG,
     3     KSTP,KPER,IPCALC,IPRSIP,MXITER,NSTP,NCOL,NROW,NLAY,NODES,
     4     IOUT)
```

```
C
C    ADD AFTER CALL SOR1AP
C . . . . . . . . . . EXECUTE MULTIPLE INNER ITERATIONS OR . . .
      KPER1=KPER
      KSTP1=KSTP
      MX1=MXITER
      ITER11=ITER1
      IF(IUNIT(15).NE.0) THEN
        KPER1=IP
        KSTP1=KPER-1
      ENDIF
      IF(IUNIT(13).GT.0) CALL PCG2AP(X(LCHNEW),X(LCIBOU),X(LCCR),
     1      X(LCCC),X(LCCV),X(LCHCOF),X(LCRHS),X(LCV),X(LCSS),X(LCP),
     2      X(LCCD),X(LCHCHG),X(LCLHCH),X(LCRCHG),X(LCLRCH),
     3      KKITER,NITER,HCLOSE,RCLOSE,ICNVG,KSTP1,KPER1,IPRPCG,
     4      MX1,ITER11,NPCOND,NBPOL,NSTP,NCOL,NROW,NLAY,NODES,
     5      RELAX,IOUT,MUTPCG,IUNIT(15),IP,SN,SP,SR)
C
C7C2C---IF CONVERGENCE CRITERION HAS BEEN MET STOP ITERATING.
      IF(ICNVG.EQ.1) GO TO 110
  100 CONTINUE
      KITER=MXITER
  110 CONTINUE
C
C7C3----DETERMINE WHICH OUTPUT IS NEEDED.
      CALL BAS1OC(NSTP,KSTP,KPER,ISTRT,ICNVG,X(LCIOFL),NLAY,
     1  IBUDFL,ICBCFL,IHDDFL,IUNIT(12),IOUT)
C
C7C4----CALCULATE BUDGET TERMS. SAVE CELL-BY-CELL FLOW TERMS.
      MSUM=1
      IF(IUNIT(1).GT.0) CALL BCF1BD(VBNM,VBVL,MSUM,X(LCHNEW),
     1     X(LCIBOU),X(LCHOLD),X(LCSC1),X(LCCR),X(LCCC),X(LCCV),
     2     X(LCTOP),X(LCSC2),DELT,ISS,NCOL,NROW,NLAY,KSTP,KPER,
     3     IBCFCB,ICBCFL,X(LCBUFF),IOUT)
      IF(IUNIT(2).GT.0) CALL WEL1BD(NWEL,NWELL,VBNM,VBVL,MSUM,X(LCWELL),
     1     X(LCIBOU),DELT,NCOL,NROW,NLAY,KSTP,KPER,IWELCB,ICBCFL,
     1     X(LCBUFF),IOUT)
      IF(IUNIT(3).GT.0) CALL DRN1BD(NDRAIN,MXDRN,VBNM,VBVL,MSUM,
     1     X(LCDRAI),DELT,X(LCHNEW),NCOL,NROW,NLAY,X(LCIBOU),KSTP,KPER,
     2     IDRNCB,ICBCFL,X(LCBUFF),IOUT)
      IF(IUNIT(8).GT.0) CALL RCH1BD(NRCHOP,X(LCIRCH),X(LCRECH),
     1     X(LCIBOU),NROW,NCOL,NLAY,DELT,VBVL,VBNM,MSUM,KSTP,KPER,
     2     IRCHCB,ICBCFL,X(LCBUFF),IOUT)
      IF(IUNIT(5).GT.0) CALL EVT1BD(NEVTOP,X(LCIEVT),X(LCEVTR),
     1     X(LCEXDP),X(LCSURF),X(LCIBOU),X(LCHNEW),NCOL,NROW,NLAY,
     2     DELT,VBVL,VBNM,MSUM,KSTP,KPER,IEVTCB,ICBCFL,X(LCBUFF),IOUT)
      IF(IUNIT(4).GT.0) CALL RIV1BD(NRIVER,MXRIVR,X(LCRIVR),X(LCIBOU),
     1     X(LCHNEW),NCOL,NROW,NLAY,DELT,VBVL,VBNM,MSUM,
     2     KSTP,KPER,IRIVCB,ICBCFL,X(LCBUFF),IOUT)
      IF(IUNIT(14).GT.0) CALL STR1BD(NSTREM,X(LCSTRM),X(ICSTRM),
     1   X(LCIBOU),MXSTRM,X(LCHNEW),NCOL,NROW,NLAY,DELT,VBVL,VBNM,MSUM,
     2   KKSTP,KKPER,ISTCB1,ISTCB2,ICBCFL,X(LCBUFF),IOUT,NTRIB,NSS,
     3   X(LCTRIB),X(LCTBAR),X(LCIVAR),X(LCFGAR),ICALC,CONST,IPTFLG)
```

```
      IF(IUNIT(7).GT.0) CALL GHB1BD(NBOUND,MXBND,VBNM,VBVL,MSUM,
     1     X(LCBNDS),DELT,X(LCHNEW),NCOL,NROW,NLAY,X(LCIBOU),KSTP,KPER,
     2     IGHBCB,ICBCFL,X(LCBUFF),IOUT)
C
C------SAVE CELL-BY-CELL FLOW TERMS FOR USE IN MT3D
                                                                      IMT3D=IUNIT(22)
      IF(IMT3D.ne.0) then
        CALL BAS1MT(X(LCHNEW),X(LCIBOU),
     2     NCOL,NROW,NLAY,KSTP,KPER,X(LCBUFF),IMT3D)
        IF(IUNIT(1).GT.0) CALL BCF1MT(X(LCHNEW),X(LCIBOU),X(LCCR),
     1     X(LCCC),X(LCCV),X(LCTOP),NCOL,NROW,NLAY,KSTP,KPER,
     3     X(LCBUFF),IMT3D)
        IF(IUNIT(2).GT.0) CALL WEL1MT(NWELLS,MXWELL,
     1     X(LCWELL),X(LCIBOU),NCOL,NROW,NLAY,KSTP,KPER,IMT3D)
        IF(IUNIT(3).GT.0) CALL DRN1MT(NDRAIN,MXDRN,
     1     X(LCDRAI),X(LCHNEW),NCOL,NROW,NLAY,X(LCIBOU),KSTP,
     2     KPER,IMT3D)
        IF(IUNIT(8).GT.0) CALL RCH1MT(NRCHOP,X(LCIRCH),X(LCRECH),
     1     X(LCIBOU),NROW,NCOL,NLAY,KSTP,KPER,X(LCBUFF),IMT3D)
        IF(IUNIT(5).GT.0) CALL EVT1MT(NEVTOP,X(LCIEVT),X(LCEVTR),
     1     X(LCEXDP),X(LCSURF),X(LCIBOU),X(LCHNEW),NCOL,NROW,NLAY,
     2     KSTP,KPER,X(LCBUFF),IMT3D)
        IF(IUNIT(4).GT.0) CALL RIV1MT(NRIVER,MXRIVR,X(LCRIVR),X(LCIBOU),
     1     X(LCHNEW),NCOL,NROW,NLAY,KSTP,KPER,IMT3D)
        IF(IUNIT(7).GT.0) CALL GHB1MT(NBOUND,MXBND,
     1     X(LCBNDS),X(LCHNEW),NCOL,NROW,NLAY,X(LCIBOU),KSTP,
     2     KPER,IMT3D)
      endif
C
C7C5---PRINT AND OR SAVE HEADS AND DRAWDOWNS. PRINT OVERALL BUDGET.
      CALL BAS1OT(X(LCHNEW),X(LCSTRT),ISTRT,X(LCBUFF),X(LCIOFL),
     1        MSUM,X(LCIBOU),VBNM,VBVL,KSTP,KPER,DELT,
     2        PERTIM,TOTIM,ITMUNI,NCOL,NROW,NLAY,ICNVG,
     3     IHDDFL,IBUDFL,IHEDFM,IHEDUN,IDDNFM,IDDNUN,IOUT)
C
  200 CONTINUE
  300 CONTINUE
C
C8------END PROGRAM
c     ENDFILE (UNIT=IOUT)
      STOP
C
      END
C
```